FORSCHUNGSZENTRUM JÜLICH GmbH
Institut für Festkörperforschung

H and D in Niobium, Tantalum and Vanadium

by

T. Schober

Jül-2347
February 1990
ISSN 0366-0885

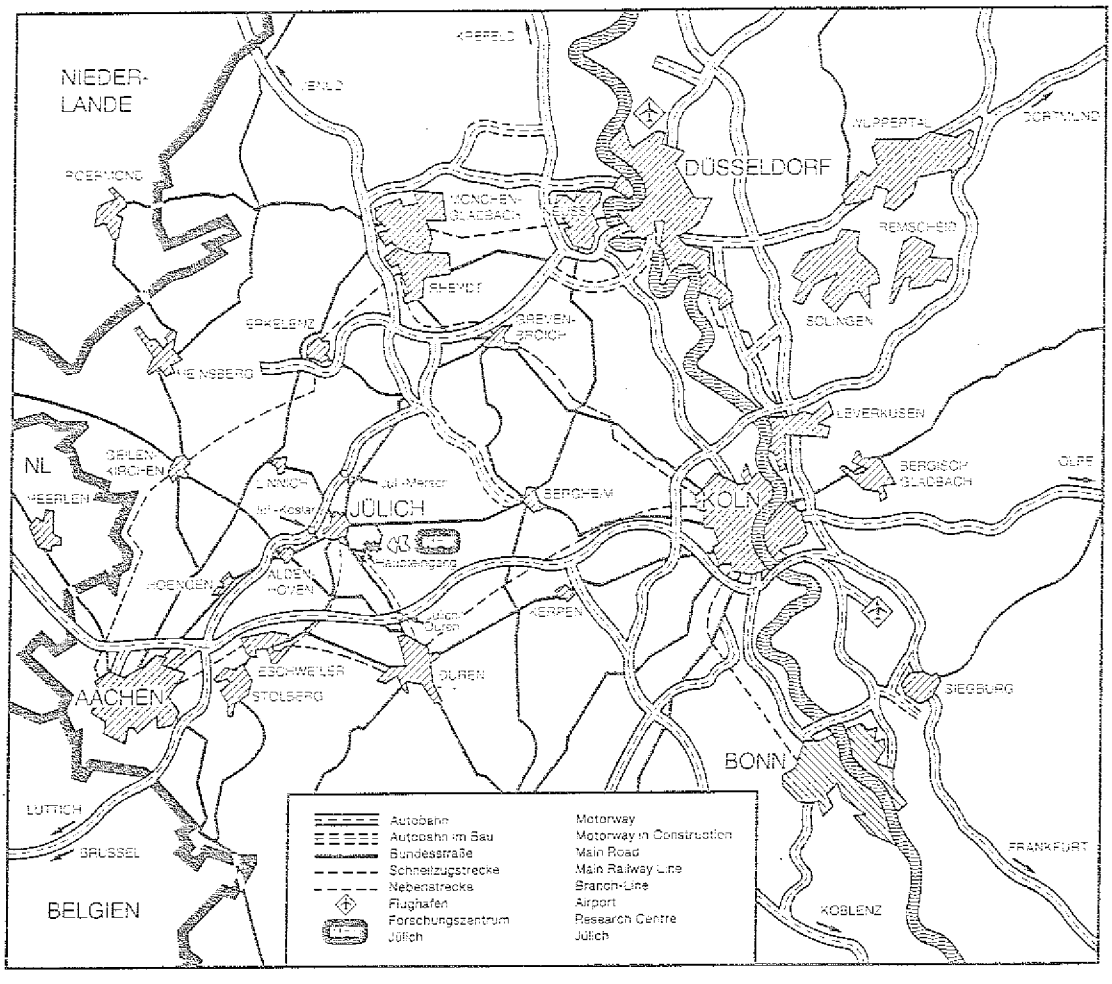

Als Manuskript gedruckt

Forschungszentrum Jülich: Berichte Nr. 2347
Institut für Festkörperforschung Jül-2347

Zu beziehen durch: ZENTRALBIBLIOTHEK · Forschungszentrum Jülich GmbH
Postfach 1913 · D-5170 Jülich (Bundesrepublik Deutschland)
Telefon: 02461/61-0 · Telex: 833556-70 kfad · Telefax: 02461/61-6103

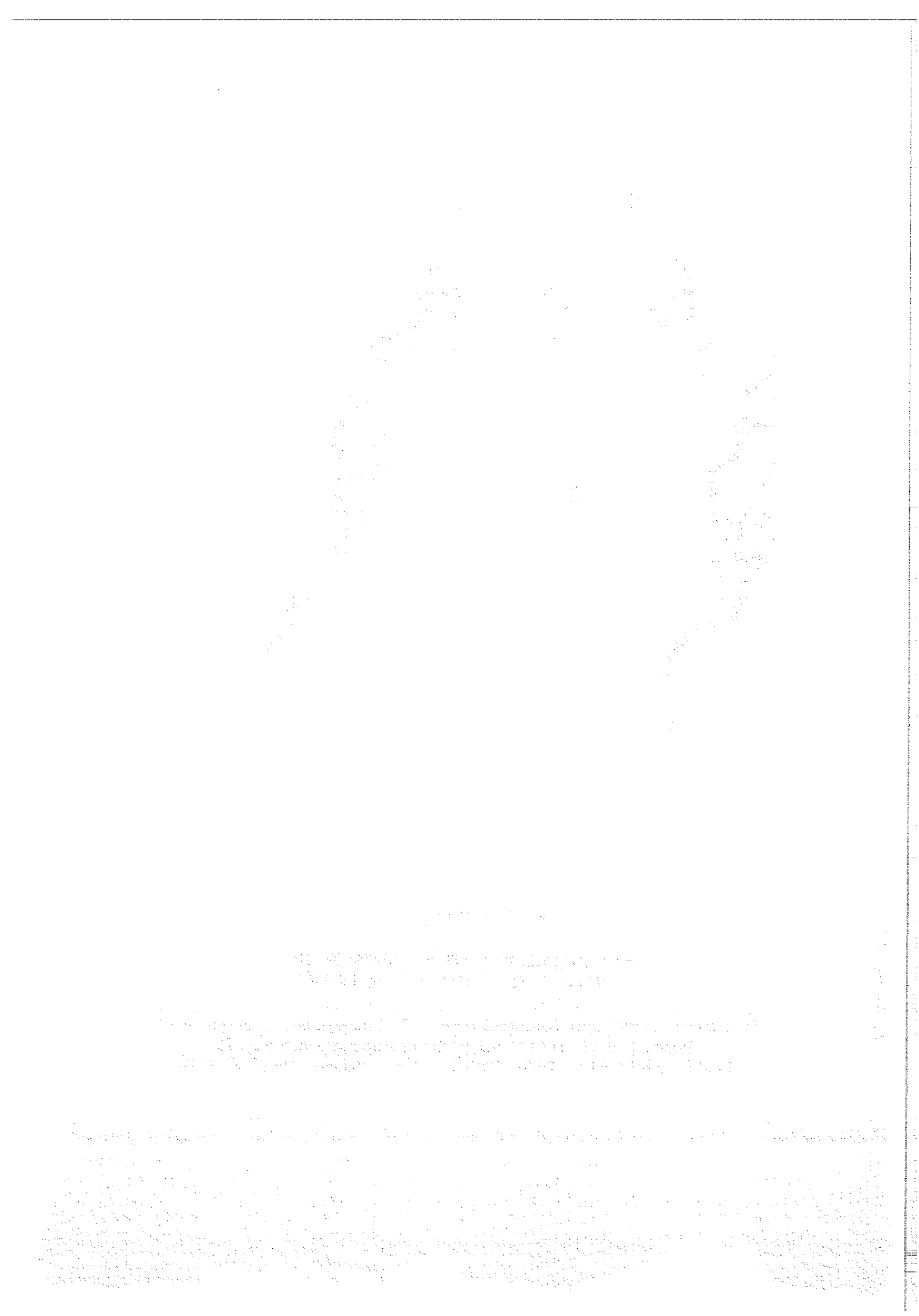

H and D in Niobium, Tantalum and Vanadium

by

T. Schober

H and D in Niobium, Tantalum and Vanadium

T. Schober

Abstract

After a general introduction the hydride and deuteride phases of Nb, Ta and V are discussed. Recent phase diagrams of the systems Nb-H(D), Ta-H(D), and V-H(D) are presented. The key diffusivities of H and D in the above metals are also covered. The basic thermodynamic relations required for an understanding of p-c-T data are given. Sieverts and various p-c-T curves pertaining to H and D in Nb, Ta and V are presented. Selected thermodynamic quantities and heats of phase transformations are included. Further topics include a discussion of localized vibrations, hydride morphologies, permeation, resistivity and property changes.

Contents

1 Introduction

Historically, Pd and then Nb, Ta and V were at the focus of research on M-H systems. It is estimated that there are far more than 1000 publications on the subject of Nb, Ta and V-H(D) alone. For recent reviews of this topic see [1, 2, 3, 4, 5, 6]. Nb, Ta and V dissolve large quantities of the three isotopes on interstitial sites. These metals are exothermic occluders of molecular hydrogen: hydriding at low temperatures produces heat and can result in high hydrogen concentrations (expressed in this Chapter as the atom ratio, c= H/M). Phase diagrams and thermodynamics provide a suitable description of which phases arise under specific circumstances. Many of the high concentration phases are ordered as are the low temperature ones. For most of the hydrides considered here , the metal atom arrangement is typically not changed dramatically upon hydriding. Diffusion of H and D occurs orders of magnitude faster than that of other light elements in these metals. Another characteristic feature is that loading and degassing is a rather reversible procedure and normally only increases the oxygen content, and the dislocation and crack density.

A few selected industrial applications of the hydrogen free metals or alloys are listed below.

(a) Nb and its alloys

- superconducting cavities in accelerator technology

- NbTi superconductors
- NbZr alloys in high pressure sodium lamps
- Alloying additions in steels

(b) Ta and its alloys

- tubing in chemical industry
- containers for corrosive fluids
- heaters and heat exchangers; bellows

(c) V and its alloys

- alloying additions in steels
- Ti-Al-V alloys in aircraft industry
- reactor or fusion reactor components from various V-Ti alloys(V-20Ti, V-15Cr-5Ti, for instance). These are corrosion resistant at high temperatures in molten Li and Na. Also, they are not readily activated by fast neutrons.

We emphasize that this review represents a rather biased, personal view of the results in this area in the last 15 - 20 years. It is by no means a complete account or an accurate historical document of the development of M-H research in this area. Only a small number of the many hundreds of references can be incorporated in this work.

1.1 H and D in Niobium

1.1.1 Hydride Phases

Phases α and α'. These phases are a disordered solution of bcc Nb with low and high hydrogen content, respectively. Hydrogen occupies the tetrahedral sites. The lattice parameter increases linearly with concentration [7]:

$$(1/a)(\Delta a/\Delta c) = 0.054 \pm 0.003 \tag{1}$$

Alternatively, we could consider the volume change upon hydriding:

$$(\Delta V/V) = c_H(\Delta v/\Omega) \tag{2}$$

where $(\Delta v/\Omega)$ is the specific volume change when one hydrogen atom is added. Ω is the atomic volume. Precision density measurements give the following values for $(\Delta v/\Omega)$: 0.172 ± 0.003 for H and 0.1695 ± 0.001 for D [8].

The β-phase is an ordered interstitial solution of hydrogen. It exists from $\sim$0.70 to 1.0 H/Nb. The definitive structural investigation of its structure is still the work by Somenkov et al. [9, 10]. As seen in Fig. 1, β is face centered orthorhombic and is described by the base vectors a, b, c where $a \approx b \approx a_o\sqrt{2}$ and $c \approx a_o$. The deviations from cubic symmetry as a function of concentration are described in [11]; for accurate x-ray measurements of the magnitudes of a, b and c, see [12]. TEM studies [2] confirmed the reciprocal lattice of β as derived from the neutron scattering work [9, 10]. There are 6 different possible orientations of β. All of them can be made visible by optical metallography [13] using polarized light. By the same technique the transformation $\beta \longrightarrow \alpha'$ was studied [14]. This reaction corresponds in the lattice gas picture to the melting of the interstitial crystal structure

Fig. 1

formed by the hydrogen. β decomposes peritectically near 145 °C by a first order reaction. In theoretical calculations, it has been demonstrated that it is necessary to include both long-range electronic interactions and many-body elastic interactions in order to predict the ordered phases β and ϵ [15].

Phase ζ. This phase has not been unambiguously established. There are TEM reports of the existence of a new ordered phase in the temperature range between -66°C and -45°C [2], supported by internal friction results [16]. However, further TEM results [17] do not provide any evidence for the existence of phase ζ. If it does exist, there are presumably only minor changes in the hydrogen atom configuration when compared with phase ϵ.

Phase ϵ *(*Nb_4H_3*).* It is firmly established by neutron scattering [10] and TEM [2, 17]. It is produced by a further ordering of vacancies in the hydrogen sublattice of phase β. ϵ is described (Fig. 2) by a cell with unit vectors $a \approx b \approx 2a_o\sqrt{2}$, $c \approx a_o$. In Fig. 3 we see a {001}-pattern of ϵ as observable by TEM [2]. We note that there is no change in the metal atom arrangement when going from β to ϵ. Even the domain structure of β remains unchanged when the sample is cooled to the ϵ phase region. Fig. 2 Fig. 3

Phase η. Evidence for this hydride was first obtained in [18, 19]. It was then corroborated by TEM work [20]. η has the same composition as ϵ but exists only in the narrow temperature range from -68°C to -66°C. It decays into phase ζ. A tentative model of the reciprocal lattice of η is given in [20].

The cubic γ *phase.* It was first described in [11]. γ is a high-concentration, low-temperature phase of approximate composition $NbH_{0.9}$. It is stable below 200 K and is visible in X-ray diffraction through the disappearance of the orthorhombic reflections of the metal atoms. Clear evidence for γ has been obtained by cold-stage light microscopy [21]. In a TEM study [18] the

disappearance of domain boundaries was observed when cooling a β phase sample below 200 K. It is important to note that superlattice reflections were observed in γ [22]. This should encourage future research on the crystal structure of γ.

The dihydride δ phase (NbH_2). δ is fcc and has the CaF_2-structure as shown in Fig. 4. The metal lattice parameter has a value of 0.4554 nm for pure Nb [23]. Alloying with Ta and V leads to somewhat different values [23]. A dihydride is formed up to about 50 at.% Ta. The lattice parameters of the fcc and orthorhombic phases decrease linearly with increasing Ta content [24]. Fig. 4

If the mean concentration of a sample exceeds H/M=1 , thin plates of phase δ are observed in the microstructure [21]. There are no domain boundaries visible in δ. Referring to the cubic reference state, δ precipitates on $\{210\}_c$-planes of the matrix. δ is extremely brittle and the introduction of δ plates into the brittle β-matrix often causes cracks in the latter. Fig. 5 depicts schematically how the microstructure of Nb changes when the hydrogen concentration is raised continously to from c=0 to 2.-There is no evidence of phases with an even higher hydrogen concentration than δ, i.e. of possible trihydrides. There is no reason to believe that these could not be prepared at very high H fugacities. Fig. 5

The λ-phases. Beyond the stoichiometry of Nb_4H_3 several further ordered phases have been observed. Since two basically independent groups have worked on the λ-phases with some conflicting results, we will present both views.

The λ-phases: results by Köbler and Welter [18]. From susceptibility and DTA data a detailed phase diagram was proposed featuring distinct phases

at the concentrations of 0.73, 0.78, 0.83, 0.85, 0.9 and 1.0 . (See also the discussion below).

The λ-phases: results by Birnbaum's group [17] and Brun et al. [25]. There are at least three λ-phases in the concentration ranges 0.72-0.77, 0.85-0.90 and 0.91-0.96. The lattice periodicities in the $[100]_c$ and $[010]_c$ directions are unaltered by the $\beta \rightarrow \lambda$ transition. The $[001]_c$ periodicity, however, is increased. Since there are no β-type superlattice reflections in the λ- phases, the structures cannot be explained by multiple arrangements of the β unit cells. The λ-phases have long period superlattices as outlined schematically in Fig. 6. Two variants β_1 and β_2 are introduced, related by a $(1/2, 1/2, 0)_c$ translation. The long period superlattice in $[001]_c$ is formed by 14 β-cells with alternating β_1 and β_2 cells in the sequence 2-3-2-2-3-2. In addition, a hydrogen density wave is superimposed on this structure removing some nearest neighbor H atoms. Fig. 6

1.1.2 Phase Diagrams

In Fig. 7 and 8 we present uptodate phase diagrams for the Nb-H and Nb-D systems, respectively. Obviously, there is much less detail available for the deuterium diagram [7]. Only the three main phases above room temperature are covered. The concentrations in Fig. 8 are readily obtained by using the conversion [7] : Fig. 7 Fig. 8

$$(1/a)(\Delta a/c_{H,D}) = 0.058 \qquad (3)$$

A few solvus studies of the NbH system are listed in Ref. [2]. We still consider the results by Whitton et al. most reliable [26] (see Fig. 9). The temperature Fig. 9

dependence of the terminal solubility may be given in the usual way as

$$c_\alpha = c_o \exp(-\Delta H/kT) \tag{4}$$

The parameters describing best the solvus are $c_o = 5.35$ and $\Delta H = 0.12$ eV. In view of the considerable scatter of the data an isotope effect, if present, is not discernible.

In the case of the α-α' *phase transition*, which may be understood in terms of the elastic interaction of hydrogen atoms via their long range elastic displacement field (Alefeld [27]), we have to distinguish:

- *The coherent state* [28, 29]. It is characterized by an inhomogeneous macroscopic density distribution. Also, the amplitude of density fluctuations grow continously with $(T - T_c)$. (Here, T_c denotes the critical temperature). The macroscopic modes depend on the shape of the sample. Usually, the samples become elastically deformed. Upon reheating to $(T - T_c)$ there is a reversible change of state with a homogeneous density distribution. A perfect crystal would still be a perfect crystal.

- *The incoherent state* [7, 28]. There are 2 distinct densities given by the incoherent phase boundary. Within the single phases the density is uniform. The phase separation grows continously with $(T - T_c)$. The phase separation is independent of the shape of the crystal. Precipitation of α' or β produces plastic deformation. Upon reheating above the critical temperature we thus have an irreversible change of state and an inhomogeneous density distribution.

The incoherent phase diagram after Zabel and Peisl [7] focussing on the α-α' transition is shown in Fig. 10. The "λ-phase region" shown in Fig. 11 [18] contains several phases. It is reasonable to assume that there are 3-4 different phases higher in concentration than ϵ. The diagram should, however, not be taken too literally. Without full justification, all phase transitions in Fig. 11 are, nonetheless, drawn as first order transitions. A few of them are expected to be of second order. Examples of genuine transformations of first order are the $\beta \rightarrow \lambda$ transition and the one leading to the pseudo-cubic γ-phase. Fig. 10 Fig. 11

Comments on the Köbler-Welter Diagram [18]. Fig. 2 of that work shows two low temperature phases (η and ϑ)in the concentration range from 0 to 0.70. In our opinion there is no sound basis for the introduction of these phases. There has been no evidence from other authors that there are hydride phases with concentrations lower than $\sim$0.7. Thus, in the present Fig. 7 we only draw the established phase ϵ and its decomposition products. The difficulties introduced in Fig. 2 of [18] are immediately obvious if one considers the relative proportions of the α-phase and the ordered phase upon raising the temperature in a sample with $\sim$ 0.2 of hydrogen. This fraction would vary dramatically with temperature which, physically, would be rather unreasonable. On the other hand, there is almost no temperature dependence of the relative proportions of α-areas versus hydride areas in the traditional NbH diagrams. Thus, basically, ϵ and its decomposition products are in equilibrium with α along the solvus.

1.1.3 Diffusion

A number of experimental techniques may be used to measure the dynamic properties of H and D in metals(see, for example,[30]):

- Quasi-elastic neutron scattering (QENS). It may be used to measure the tracer diffusivity D_t. Coherent QENS can yield D_t and the chemical diffusion coefficient, D_c
- Gorsky effect (GE). It allows to determine the long- range or chemical diffusion coefficients. It also yields the thermodynamic factor f_{ther}
- Nuclear magnetic resonance (NMR). It is used to determine D_t

We note that we need to consider a *tracer correlation factor*, f_t, which enters into the expression for the tracer diffusivity, and a *mobility correlation factor*, f_M, associated with Fick's diffusion coefficient, D_c [30].

Below we discuss Gorsky effect measurements of the diffusion in the temperature range from -140°C to 100°C [31, 32]. Fig. 12 shows the diffusivities for all the systems which are the concern of this review in a comprehensive form. We present the temperature dependence in the usual Arrhenius form Fig. 12

$$D = D_o \exp(-U/k_B T) \tag{5}$$

where the activation energy U and the pre-exponential factor D_o are constant over the upper temperature ranges considered. For Nb and Ta there are changes in the slopes of the curves. Therefore, we specify the above values in Table 1 taken from [32] for the linear segments. The results in Fig. 12 and Table 1 refer to the limit of infinite dilution. The diffusivities measured at finite concentrations were extrapolated to $c \approx 0$ using Table 1

$$D(c \to 0) = D(c) \frac{T}{T - T_s} \tag{6}$$

Here, T_s is the concentration dependent spinodal temperature which for small concentrations is given by:

$$T_s = uc/k_b \tag{7}$$

where u is the H-H interaction energy (u_{Nb}=0.21 eV; u_{Ta}=0.17 eV and u_V=0.17 eV). The relaxation strength in Gorsky experiments, Δ_E, its temperature and its concentration dependence are also given in [32]. Δ_E is found to be isotope independent. The trace of the dipole force tensor, 3P, was determined to be 11.1±1.5 eV for Nb-H, D, T; 9.3±0.9 eV for Ta-H, D, T and 7.5±0.9 eV for V-H, D, T [32]. Also, it is pointed out that neutron scattering and Gorsky effect results on the diffusion and spatial fluctuations of D interstitials in NbD_x reveal striking differences [33]. It is shown in that work that these discrepancies are caused by coherency stresses raising the elastic energy of the short-wavelength fluctuations as studied by coherent neutron scattering [33]. The pressure dependence of the diffusivity up to a pressure of 2 GPa has been investigated for dilute NbH alloys. No significant effect was observed [34]. Similarly, the effects of lattice parameter changes as induced by an applied pressure on D has been studied in the case of dilute NbH alloys and a 1.5% increase at 5000 bars was claimed [35]. Quantum diffusion of hydrogen in Nb is discussed in [36]. In the same Conference Proceedings, further articles on that subject may be found. Diffusivities of H in Nb at very low temperatures are available in [37]. In that work, diffusivities were determined by resistivity techniques after experimentally very challenging, ultra-fast quenches. As expected, the diffusion constants derived in that study are orders of magnitude higher than the extrapolation of the Gorsky values.

Recently, a simple technique became available for measuring diffusivities via the Gorsky effect [38]. Strain gauges are attached to thin metal plates. Resistivity changes in the strain gauges are registered using a Wheatstone bridge. The experimental set-up is illustrated in Fig. 13. Fig. 13

1.1.4 Thermodynamic Data, Solubilities

Basic Thermodynamic Concepts [39] In very basic experiments on M-H systems the hydrogen pressure, concentration and temperature (p, c, T) of a sample are recorded at equilibrium. If this is done for a variety of temperatures , one can extract from these data the essential thermodynamic parameters of the system [39, 40, 41, 42]. One generally tries to curve fit the data with either of the following two representations: depending on the representation chosen one obtains different entropy but identical enthalpy values. : *Ansatz A*

$$\Delta\mu_{\mathrm{H}} = \mathrm{RTln}\sqrt{\mathrm{p_{H_2}}} = \Delta\mu^{\circ}_{\mathrm{H}} + \mathrm{RTln}\frac{\mathrm{c}}{\beta - \mathrm{c}} + \mu^{\mathrm{E}}_{\mathrm{H}} \qquad (8)$$

The term μ^{E}_{H} (the excess chemical potential) describes all deviations from non-ideality. It is zero for c$\rightarrow$0. Usually, μ^{E}_{H} is modeled as a polynomial in c:

$$\mu^{\mathrm{E}}_{\mathrm{H}}(\mathrm{c},\mathrm{T}) = \mathrm{Bc} + \mathrm{Cc}^2 + \cdot\cdot \qquad (9)$$

where B and C , in general, depend on temperature. For c$\rightarrow$0 we obtain the approximation known as Sieverts' law:

$$\mathrm{c} = \sqrt{\mathrm{p_{H_2}}}\exp(-\frac{\Delta\mu^{\circ}_{\mathrm{H}} - \mathrm{RTln}\beta}{\mathrm{RT}}) = \sqrt{\mathrm{p_{H_2}}}\exp(-\frac{\Delta\mathrm{H}^{\circ}_{\mathrm{H}} - \mathrm{T}\Delta\mathrm{S}^{\circ}_{\mathrm{H}} - \mathrm{RTln}\beta}{\mathrm{RT}}) \qquad (10)$$

In the case of Nb, Ta and V Ansatz A often leads to unnecessary complications during fitting of the results to $\mu^{\mathrm{E}}_{\mathrm{H}}$.

Ansatz B produces a more acceptable analytical form for the excess potential:

$$\Delta\mu_H = RTln\sqrt{p_{H_2}} = \Delta\mu_H^{\circ} + RTln\frac{c}{1-c} + \mu_H^{\circ E} \tag{11}$$

Here also the excess term disappears for $c \to 0$. At low c, $(1 - c) \approx 1$ and we obtain Sieverts' law in the form

$$c = \sqrt{p_{H_2}} exp(-\frac{\Delta H_H^{\circ} - T\Delta S_H^{\circ}}{RT}) \tag{12}$$

Comparison of the two expressions in Eqn(8) and (11) for $\Delta\mu_H$ yields the following relations between the differently defined quantities:

$$\Delta H_H^{\circ} = \Delta H_H^{\circ}; \ \Delta S_H^{\circ} = \Delta S_H^{\circ} + Rln\beta \tag{13}$$

$$\mu_H^E = \mu_H^{\circ E} + RTln\frac{\beta(1-c)}{\beta - c} \tag{14}$$

We see that the enthalpies do not depend on the ansatz but the entropies and excess hydrogen potentials do.

The β-phases. The pressure rises sharply in the single phase concentration range. In most cases the chemical potential is best represented in the form

$$\Delta\mu_H = A + Bc + Cc^2 + \cdot\cdot \tag{15}$$

A, B and C are functions of the temperature.

Thermodynamics of Plateaus. Suppose a β-phase with composition $c = x$ is formed from Nb according to the following relation

$$Nb + \frac{x}{2}H_2(g, 1atm) \to NbH_x \tag{16}$$

The standard free energy change for this formation reaction is

$$\Delta G_f^{\circ}(NbH_2) = -RTlnK$$

$$= -RTln\alpha_{NbH_x} + RTln\alpha_{Nb} + \frac{x}{2}RTlnp_{H_2}(plat)$$
$$= -RTln\frac{\alpha_{NbH_x}}{\alpha_{Nb}} + \frac{x}{2}\Delta\mu_{H_2}(plat) \quad (17)$$

Here, the α's denote activities of the dilute and concentrated phases. K is the equilibrium constant. At low temperatures, we are concerned with almost pure Nb and the β-phase. Thus, one obtains

$$\Delta G_f^\circ(NbH_2) = \frac{x}{2}\Delta\mu_{H_2}(plat) = \frac{x}{2}(\Delta H_{H_2}(plat) - T\Delta S_{H_2}(plat)) \quad (18)$$

The plateau pressure is related to the thermodynamic quantities by

$$RTlnp_{H_2}(plat) = \Delta\mu_{H_2}(plat) = \Delta H_{H_2}(plat) - T\Delta S_{H_2}(plat) \quad (19)$$

$$= \frac{2}{x}\Delta G_f^\circ(NbH_2) \quad (20)$$

Experimentally, it is found that the plateau enthalpies and entropies are temperature independent. These values provide a suitable description of plateau thermodynamics.

Thermodynamics of the $\beta \rightarrow \delta$ transformation. Consider the reaction

$$NbH_x + \frac{1}{2}(y-x)H_2 \rightarrow NbH_y \quad (21)$$

Here, x and y correspond with the stoichiometries of β and δ. As before, the standard free energy change for this reaction is

$$\Delta G^\circ = \frac{1}{2}(y-x)\Delta\mu_{H_2}(plat) - RTln\frac{\alpha_{NbH_y}}{\alpha_{NbH_x}} \quad (22)$$

At low temperatures, where the two hydrides are approximately in their refence states, the plateau pressure properties are related to ΔG°:

$$RTlnp_{H_2}(plat) = \Delta H_{H_2}(plat) - T\Delta S_{H_2}(plat) \approx \frac{2}{y-x}\Delta G^\circ \quad (23)$$

Thus, it suffices to describe the experimental results by indicating the free energy change of the reaction and the enthalpies and entropies of the plateau pressure.

Numerical Values for the α-phase. A rather complete compilation of α-phase data was given in [5]. More recent values have been given by Kuji and Oates [40] who have obtained the following data for $c \rightarrow 0$:

$\Delta H_H^\circ = -33.868$ kJ/mol H and $\Delta S_H^\circ = -71.28$ J/K mol H

In a recent electrochemical determination the value of $\Delta H_H^\circ = -27.8$ kJ/mol H was obtained [43] Thus, in considering the above values and Ref. [5] an enthalpy value in the vicinity of -34 kJ/mol H seems most reasonable. As the hydrogen concentration increases, ΔH_H becomes increasingly more negative [40, 5].

The α/β-plateau. Smith [5] gives the following relation for the $\alpha+\beta$ two-phase field:

$\frac{1}{2}\Delta\mu_{H_2}(plat) = -38.48 + 0.0422T$ kJ/mol H.

Direct vapor pressure measurements [44] are in agreement with these values.

The β-phase. For further thermodynamic data of β see [5]. Kuji and Oates obtain for β at c=0.7:

$\mu_H^{\circ\beta}(c = 0.7) - \frac{1}{2}\mu_{H_2}^\circ = -56105 + 92.52T$ J/mol H [41, 42]

The β/δ-plateau. Vapor pressure measurements over the $\beta + \delta$ two-phase field yield [45]:

$\frac{1}{2}\Delta\mu_{H_2}(plat) = -20.00 + 0.06569T$ kJ/mol H

The δ-phase. From Kuji and Oates [41] we take the expressions for the δ-phase:

$\mu_H^\delta(c = 1.7) - \frac{1}{2}\mu_{H_2}^\circ = -21168.3 + 53.91T$ J/mol H

$\mu_H^\delta - \mu_H^{\circ\delta}(c = 1.7) = RT\ln(\frac{c}{2-c}\frac{0.3}{1.7}) - 9466.7(c-1.7) + 74666.67(c-1.7)^2$

J/mol H.

Some heats of phase transitions in the NbH- system are available from recent Russian work [46]:

$\beta - NbH_{0.86} \rightarrow \alpha' - NbH_{0.86} : \Delta H = 14.0 \pm 0.5$ kJ/atom H

$\beta - NbH_{0.95} \rightarrow 0.95\alpha' - NbH_{0.90} + 0.05\,\delta - NbH_{1.82} : \Delta H = 20.9 \pm 1.3$ kJ/atom H.,

$\delta - NbH_{1.75} \rightarrow \alpha' - NbH_{0.83} + 0.46H_2 : \Delta H = 62.0 \pm 6.3$ kJ/mol H_2,

$\alpha' - NbH_{0.83} \rightarrow \alpha - NbH_{0.07} + 0.38H_2 : \Delta H = 84.0 \pm 5.3$ kJ/mol H_2.

The last two reactions are no solid/solid phase transitions.

Some reaction heats from Craft et al. [47] determined indirectly from differential scanning calorimetry (DSC) are given below:

$\frac{1}{2}H(D)_2(g) + \alpha \rightarrow \beta : \Delta H = -48.7$ kJ/mol H

$\frac{1}{2}H(D)_2(g) + \alpha \rightarrow \alpha' : \Delta H = -52.2$ kJ/mol D

Selected p-c-T curves. Sieverts type curves for Nb are shown at relatively low temperatures in Fig. 14 (a) [48] while Fig. 14 (b) shows p-c-T-curves over a wider range of contents for the isotope protium [49]. Complementary curves are seen in Fig. 15 a) for H and in Fig. 15 (b) for D. A log p versus 1/T plot is provided in Fig. 16 [50]. We also note other extensive p-c-T- work [51]. Further curves are available in [49] for $Nb_{90}V_{10}, Nb_{75}V_{25}, Nb_{50}V_{50}, Nb_{25}V_{75}, Nb_{10}V_{90}$, and $Nb_{97}Mo_3$. In Fig. 17 p-c-T-curves of the $\beta + \delta$-plateau region are shown [41].

Fig. 14

Fig. 15

Fig. 16

Fig. 17

1.1.5 Miscellaneous

Energies of localized vibrations. Hydrogen atoms perform oscillations about their equilibrium positions in the interstices. These vibrations are relatively uncoupled from the phonons of the heavy metal atoms. The energies

of such localized vibrations are determined by inelastic neutron scattering. Since these energies are important for many thermodynamic calculations we provide in Table 2 a compilation of recent values based on work in [52, 53, 54, 55, 56, 57]. Table 2

Hydride Morphologies. We summarize the essential results given in [2]. β-phase plates precipitate as thick plates on {100}-planes upon slow cooling. The β-phase itself consists of thin plate-like domains the habit plane of which are low index planes of the matrix. Phase δ, however, is found to precipitate on $\{210\}_c$-planes. As to the phase α', it also precipitates on {100}-planes. At the triple point temperature, plates of β are formed in regions where the α'-phase was originally located. Rapid cooling of NbH-alloys produces a dendritic pattern of β-precipitation. If the concentration is sufficiently low precipitation will occur only below room temperature. It is generally accompanied by punching of prismatic loops along $< 111 >$ directions. Dissolution of such hydrides by subsequent reheating dramatically increases the dislocation density in the former hydride area and may even lead to crack formation.

Permeation. The total flux J of hydrogen atoms through a membrane of thickness L and area A is given by

$$J = PA(\sqrt{p_1} - \sqrt{p_2})/L \tag{24}$$

Here, P is the permeability and p_1, p_2 denote the upstream and downstream pressures. P itself is given by the product of diffusivity D and solubility S. For Nb the following temperature dependence of P was given in recent reviews [58] for $1223 < T < 1338K$:

$$P = 5.58 \times 10^{-2} \exp(-\frac{2621 \pm 70}{T}) cm^3(STP)/(cm\,s\,atm^{\frac{1}{2}}) \tag{25}$$

Resistivity. As rather accurate values for the resistivity increase produced by c=0.01 H/M in the α-phase , expressed in $\mu\Omega$ cm, we quote [59]: $\Delta\rho$: 0.63 ± 0.01 (H); 0.62 ± 0.01 (D).

Isotope effects in the resistivity variations caused by H and D in Nb are discussed in [60].

Property Changes. For the change in hardness, other mechanical properties and susceptibility upon hydriding, Fromm and Hörz provide a good review of the relevant data [1].

1.2 H and D in Tantalum

1.2.1 Hydride and Deuteride Phases

Since there is no evidence that the structures of the various phases are isotope dependent, we assume below that the coresponding H and D phases are isomorphic. The phase diagrams , however, will be seen to depend somewhat on the isotope.

The α-phase is a disordered solution of H in bcc Ta. At room temperature Ta may even contain as much as $c \approx 0.17$ of H or D without precipitation of the β- phase. As with Nb, H is located on tetrahedral sites. Consider the lattice expansion with increasing hydrogen concentration in the α- phase. The length change of a sample is given by

$$\frac{\Delta L}{L} = \frac{1}{3}\Delta V/V = c_H \frac{\Delta v}{\Omega} \tag{26}$$

Using for the lattice parameter $a_o = 0.330285 \pm 0.000002$ nm and for $(\Delta v/\Omega)$ the values of 0.154 ± 0.001 for hydrogen (or 0.152 ± 0.001 for deuterium) [8], we can readily calculate the lattice parameter or length change of a sample with hydrogen concentration. The above coefficients $(\Delta v/\Omega)$ were deter-

mined by precision density measurements. Fig. 18 illustrates the results from such measurements of the density which can be performed with a precision in the low 10^{-5} region. The normalized density decreases with c according to [8]: Fig. 18

$$\rho/\rho_o \approx 1 - (\frac{\Delta v}{\Omega} - A_H/A_M)c \qquad (27)$$

Here the A's denote the relative atomic masses. An important parameter for the characterization of the α- phase is the anelastic relaxation. For H and D the common value of $\Delta_E = (1.3 \pm 0.1) \times 10^{-2}$ for c= 0.01 was obtained [32].

The β-phase is an ordered hydride phase centered around the composition Ta_2H. It may be hypo- or hyperstoichiometric to a considerable extent. The metal atom structure is orthorhombic [61]. Including the hydrogen sublattice, β has an orthorhombic unit cell as depicted in Fig. 19 a. It is described by: [62, 63, 64, 65] Fig. 19

$A = a\sqrt{2(1+\cos\gamma)}$

$B = c$

$C = a\sqrt{2(1-\cos\gamma)}$

The space group is C222 with the following atomic coordinates:
$(0,0,0;\frac{1}{2},\frac{1}{2},0)$ + fourTa in 4(k) : $\frac{1}{4},\frac{1}{4},z;\frac{1}{4},\frac{3}{4},\bar{z}$ with $z = \frac{3}{4} - \delta$, two H in 2(a):0, 0, 0.δ was determined to be 0.016 [66]. The lattice parameters are:A=0.4738, B=0.3398 and C=0.4763 nm [65]. The reciprocal lattice of β is seen in Fig. 19 (b). The reflections on (100) arise from both the metal atom distortions and the ordering of hydrogen. Obviously, if c<0.50, the vertical plane containing the H-atoms in Fig. 19 (a) is depopulated. If c exceeds 0.5, the equivalent adjacent planes are gradually filled [63] until there is equal occupancy on both planes.

The δ-phase is a high concentration phase beyond c=0.65 to 0.70. It is isomorphic with β-NbH in Fig. 1. It is obtained, as pointed out above, by equal filling of both hydrogen planes in hyperstoichiometric $\beta - Ta_2H$. There are no superlattice reflections on (100). A gradual transition from β to δ seems possible without going through a two- phase field for which there is no experimental evidence. Thus, presumably, we have the following two possibilities:

- the transition $\beta \rightarrow \delta$ is a second order phase transformation with no two phase field.
- β and δ are essentially the same phase and we could designate both as β.

We cannot as yet differentiate between these two cases and will use β and δ rather interchangeably in this section.

The η-phase has a composition near Ta_3H_2. It has a pseudo-orthorhombic unit cell defined by [67, 68]:

$A = 4\sqrt{2}a$; $B = 3\sqrt{2}a$ and $C = a$

The structure (Fig. 20 (a)) may be described by a hydrogen concentration wave with the wave vector parallel $[3\bar{1}0]$ where the wavelength is $2\sqrt{2}a$ [67]. 20

The ζ-phase(see Fig. 20 (b)) has a fully ordered structure with a pseudo-orthorhombic unit cell with $A = 2\sqrt{2}a, B = \sqrt{2}a, C = a$ [67, 68, 69]. It is also described by a hydrogen concentration wave with the wave vector parallel to $[3\bar{1}0]$. Here, the wavelength is $4\sqrt{10}a/9$.

The γ-phase of composition Ta_5H_4 was postulated from DTA results only [18, 70] . There is no diffraction evidence as yet.

The ϵ-phase(also designated as β_2) is a high temperature modification of β.

As pointed out in [71] , the unit cell of ϵ is orthorhombic and identical with the one of β. It contains four Ta and two H(D) atoms in a volume that is about $\sqrt{2} \times 1 \times \sqrt{2}$ larger than that of the bcc lattice. Fig.19 (c) depicts the H(D) superlattice of β and ϵ. Open circles denote positions that are fully occupied in β but are only filled with the probability p_1 in ϵ. Full circles denote positions that are filled with the probability p_2 in ϵ. From the experiment, p_1 and p_2 were determined to be 0.6 and 0.4, respectively.

The θ-phase is a cubic, low temperature phase analoguous to the γ-NbH phase. Presumably, it also has a stoichiometry where c >0.80. θ was found in recent TEM work [22] where it was observed that domain boundaries of selected TaH alloys suddenly disappear below -150°C, resulting in a cubic phase which still displayed superlattice reflections.

1.2.2 Phase Diagram-Ta-H

Again we divide the overall phase diagram into one for temperatures above room temperature - as seen in Fig. 21- and into another for low temperatures. The diagram in Fig. 21 first presented in [72] is based on DTA data and is widely accepted. Fig. 21

The solvus as seen in Fig. 22 is a simple exponential function up to about c=0.1. There is no isotope effect[4, 73]. This solvus was analyzed in more detail in [74]. The solvus free energy is written as Fig. 22

$$\Delta G_{solv} = \Delta H^{z,o}_{solv} - T\Delta S^{z,o}_{solv} + H_{HH}x \qquad (28)$$

where H_{HH} is an interaction energy and is negative. The following results were obtained by computer fitting of the raw solvus data:

$\Delta H^{z,o}_{solv} = 10.19\,kJ/mol\,H$;
$\Delta S^{z,o}_{solv} = -3.6\,J\,K^{-1}mol^{-1}$,
$H_{HH} = -18.18$ kJ/molH. The above parameter describes the solvus best in the limit of infinite dilution. In a recent NMR study, the TaH solvus was determined again with rather similar numerical values [75].

Fig. 23 depicts the high temperature/high concentration region of the TaH diagram in more detail. Finally, the low temperature phase diagram as seen in Fig. 24 should only be considered tentative. With regard to a recently published version of this diagram [18] we have made the following changes: Fig. 23 Fig. 24

- the phase ϑ has been dropped since the evidence for it is weak at best.
- the cubic θ-phase has been inserted.

1.2.3 Phase Diagram-Ta-D

Recently, a Ta-D diagram has been established (Fig. 25) [73] which covers mainly the "high"-temperature phases α, β, δ and ϵ. No difference was made in that work between β and δ. We list below the main features of the hydrogen and deuterium diagrams: Fig. 25

- There is no measurable isotope effect in the solvus
- The lower limit of β is shifted to lower c values going from hydrogen to deuterium.
- The $\beta/\beta+\alpha'$ and the $\beta+\alpha'/\alpha'$ boundaries are shifted slightly upward when going from H to D.
- In Ta-D, the ϵ-phase covers a larger stoichiometric range.

A few low temperature transitions are also covered in [73]. It was observed that ζ and γ may exist to higher stoichiometric compositions as compared with the Ta-H system.

1.2.4 Diffusion

We refer here to the introductory remarks in the Nb Section. In Fig. 12, the Gorsky data for Ta- H alloys are depicted. Numerical values are found in Table 1. Diffusivities derived from NMR data for more concentrated alloys are shown in Fig. 26 [76]. Similarly, the chemical and tracer diffusion coefficients of H in α and α'-phase of TaH_x were obtained from Gorsky and neutron spectroscopic measurements [77]. The considerable differences between these two diffusivities are due to the thermodynamic factor which is best derived from Gorsky experiments [77]. The hydrogen diffusivity at very low temperatures (<30K) as obtained by perturbed- angular-correlation measurements [78] is presented in Fig. 27. Finally, we briefly mention Gorsky-type data in the disordered α-phase and in the ordered phases β and ϵ of the alloy $TaH_{0.52}$ (Fig. 28) [79]. Some evidence was obtained in that work for rapid diffusion along the domain boundaries of the ordered phases.

Fig. 26
Fig. 27
Fig. 28

1.2.5 Thermodynamic Data, Solubilities

Reference is made first to the introductory equations in the equivalent Section on Nb. A good overview over the p-c-T-behavior of Ta is provided in Fig. 29 for protium and in Fig. 30 for deuterium [49]. As for Nb, we also present Sieverts and other p-c-T data by Fujita et al. [50] in Figs. 31 (a) for H, in Fig. 31 (b) for D, and in Fig. 32 for H in a different representation. Sieverts curves for the case of deuterium and very low temperatures

Fig. 29
Fig. 30
Fig. 31
Fig. 32

are provided in Fig. 33 [80]. From the same work of the authors the $\alpha + \beta$ plateau p-c-T-data for deuterium are given in Fig. 34 [80]. Ref. [81] provides Sieverts curves in the temperature range from 917-1213 K (Fig. 35). We also note further, general p-c-T-work on Ta [51]. Fig. 33 Fig. 34 Fig. 35

Numerical values. The α-phase. Pryde and Tsong listed the following values: $\Delta H^{\circ}_{D} = -39.6\,\mathrm{kJ/mol\,D}$ and $\Delta S^{\circ}_{D} = -28.4\,\mathrm{J/K\,mol\,D}$ [80]. Franzen et al. [81] obtained $\Delta H^{\circ}_{H} = -34.3\,\mathrm{kJ/mol\,H}$ and $\Delta S^{\circ}_{H} = 28.5\,\mathrm{JK^{-1}mol^{-1}}$. On the other hand, Dantzer and Kleppa [82] list: $\Delta H^{\circ}_{H} = -32.37\,\mathrm{kJ/mol\,H}$ and $\Delta H^{\circ}_{D} = -32.956\,\mathrm{kJ/mol\,D}$ at 717 K. Finally, we cite electrochemical work on Ta [83] in which the TaH properties were determined from electrode potential measurements. Similar p-c-T curves were obtained as in gas-phase equilibration work. Other electrochemical work [43] on Ta produced enthalpies and entropies that are somewhat at variance with the gas phase values.

The α-β plateau. In the mixed phase region Pryde and Tsong obtained for the plateau enthalpies [80]:
$\Delta H_{H_2}(\mathrm{plat}) = (-96.21 \pm 5.0)\,\mathrm{kJ/mol\,H_2}$ and $\Delta H_{D_2}(\mathrm{plat}) = -(100 \pm 6)\,\mathrm{kJ/mol\,D_2}$.

On heats of phase transitions. In [84] heat capacity data for various Ta-H alloys are reported. Observed entropy changes in the transitions are found to correlate with the configurational entropy change of the H atoms evaluated from the structural models.

1.2.6 Miscellaneous

Hydride Morphologies. At room temperature, the ϵ phase precipitates first as the concentration is increased in form of thin plates on {100} [2]. The $\epsilon \rightarrow \beta$ transition is clearly visible in polarized light as can be seen in Fig. 36. Patches Fig. 36

of ϵ are much brighter than the β-phase areas. Since ϵ and β are seen to coexist in Fig. 36 we can safely conclude that this transition is of first order. Hydride precipitation also leads to typical surface corrugations [13] which are readily detected by Nomarski interference contrast. As to TEM results, precipitation of β at low concentrations and temperatures leads again to spherical or platelike morphologies. Loop punching occurs frequently. Going to concentrations somewhat below 0.5 and to low temperatures, leads to the formation of thin plates of α on $\{100\}$ in the β-matrix. Both, coherent and incoherent morphologies have been observed [2]. As mentionned before, cooling of alloys with c> 0.8 below -155°C leads to the disappearance of the domain boundaries when the pseudocubic θ-phase is formed.

Permeation. Writing the permeability in the form

$$P = P_o \exp(-E_p/kT) \tag{29}$$

we quote the following calculated values for H in Ta cited in [85]:

$P_o = 5.8 \times 10^{-9}\,\mathrm{mol/m\,s\,Pa^{\frac{1}{2}}}; E_p = -0.209\,\mathrm{eV}$

Alternatively, one could use the values for V or Ti given by Maroni and van Deventer if only the order of magnitude is important [58].

Resistivity. As rather accurate values for the resistivity increase in the α-phase for c= 0.01 , expressed in $\mu\Omega\,\mathrm{cm}$, we quote [59]: $\Delta\rho$: 0.71 ± 0.01 (H); 0.71 ± 0.01 (D).

Isotope effects in the resistivity variations caused by H and D in Ta are discussed in [60].

Changes in selected properties such as hardness, other mechanical properties and susceptibility are reviewed in [1, 86].

1.3 H in Vanadium

1.3.1 Hydride Phases

The α-phase. It is a disordered solution of H in bcc V. For low concentrations, an equation of the form given in eqn. (25) gives the increase in length or lattice parameter with hydrogen content c. The pertinent parameters in this case are [8]:

$(\frac{\Delta v}{\Omega})_H = 0.196 \pm 0.003$, $a_o = 0.302694 \pm 0.000002\,nm$

The regular H site is the tetrahedral site. There have been recent claims that the H-atoms become delocalized under applied stress [87]. Furthermore, it was suggested in [87] that diffusion occurs much faster in the case of the delocalized states. This alleged "superdiffusion" could, however, not be repeated in recent control experiments.

The β_H-phase. It is isomorphic with β_D [88]. Its structure is seen in Figs. 37, 38 and will be discussed in the V-D Section. It has a composition near V_2H. The effects of pressure on the structure of V_2H are discussed in [89]. The bct metal atom structure of β is conserved up to 60 GPa with gradually decreasing lattice parameters. Interestingly, it was found that the volume increase due to hydrogen, Δv_H, is practically pressure independent.

Fig. 37
Fig. 38

The structure of β as arising under applied stress was analyzed by neutron diffraction in [90]. A tetragonal superstructure of space group I41/amd was identified. Isotopic differences between the H and D β-phases are presented. Similar results on stressed β crystals were obtained by X-ray diffraction [91]. The latter results were re-interpreted in [92]; in that work the space group of β is given as C2/m. L. Pauling [93] describes the β -structure as containing linear VHV-complexes, with V-H half-bonds with a length of about

0.176 nm.

The ϵ-phase. It is a high temperature modification of the β-phase. The hydrogen atoms (see Fig. 37) are distributed in the 4 o_z sites ($\frac{3}{4}0\frac{1}{4}$; $\frac{1}{4}\frac{1}{2}\frac{1}{4}$; $\frac{1}{4}0\frac{3}{4}$; $\frac{3}{4}\frac{1}{2}\frac{3}{4}$) with equal probability [94]. Fig. 37

The low temperature phase δ_H. It has the composition V_3H_2 [95]. Octahedral interstices are occupied. The structure is also depicted in Fig. 37. Every third layer of $(0\bar{1}1)$ is vacant while the other two layers are fully occupied. The β to δ transition may also be described as the freezing of the hydrogen concentration wave with the k-vector parallel to the <011> direction. δ is described by the unit vectors:

$A = \sqrt{a_o^2 + c_o^2}$; $B = a_o$; $C = \sqrt{4a_o^2 + c_o^2}$; $\beta = 77°$

Here, a_o and c_o are the lattice constants of the bct metal lattice [95]. The β to δ transition is of first order.

The γ-phase. It has the composition VH_2 and has an fcc structure (a_o = 0.424 nm) [45]. It is isomorphic with NbH_2 and has a CaF_2 structure.

1.3.2 Phase Diagrams

The α/β solvus. Fig. 39 depicts the solvus for VH,VD and a mixed system [96]. It was determined with bulk chips of uniform concentration using precision DTA techniques. The numerical values characterizing the solvus are found in the figure caption. We note that the solubilities at 20°C differ by almost a factor of 2 when going from H to D. Fig. 39

The V-H phase diagram is shown in a more recent version [4] in Fig. 40. The $\beta \rightarrow \epsilon$ transition is of second order [67, 68]. TEM work of this author showed that phases β and δ coexist. Thus, the transformation $\beta \rightarrow \delta$ must be of first order. An open area is still the concentration range from Fig. 40

c=0.8 to 1.0. Conceivably, there could be further ordered phase with octahedral occupancy.

Partial high-concentration diagram. Phase relationships from c=0.8 to 2.0 are shown in Fig. 41 [97]. It is based on DTA experiments with samples between c=1.0 and 2.0. Such samples produce strong DTA peaks at 102°C. These were attributed to the peritectoid reaction at 102°C, Fig. 41

$\gamma \rightarrow \epsilon + \alpha'$.

Effects of substitutional impurities on the V-H diagram are considerable. For details, see [98].

1.3.3 Hydrogen Diffusion in V

The diffusivities at low concentrations are given in Fig. 12 previously referred to in the Nb Section. The influence of N impurities is discussed in [99] and O impurities are covered in [100]. Tracer diffusion coefficients for H in V as a function of concentration may be found in [101].

1.3.4 Thermodynamic Data, Solubilities

Selected p-c-T-curves. Recent, rather accurate p-c- T-curves are presented in Fig. 42 [102]. From Fujita et al. [50] we show data in Fig. 43 (a),(b) also covering a different range. Sieverts type curves and two- phase plateaus are shown in Fig. 44 and Fig. 45 [103]. Finally, Fig. 46 shows quite precise measurements of the VH – VH_2 plateaus [104]. As to selected V-alloys, p-c-T data are available in [49, 105]. Fig. 42 Fig. 43 Fig. 44 Fig. 45 Fig. 46

Numerical values-α-phase. From Meuffels [102] we cite the following values for the extrapolated case of infinite dilution:

$\Delta H^{\circ}_{H} = -30.2\,\mathrm{kJ/(mol\,H)^{-1}}$, $200 < T < 550°C$

$\Delta S^{\circ}_{H} = -72.7 \pm 0.4\,\mathrm{J\,(mol\,H\,K)^{-1}}$

Similar values were reported in [106]:

$\Delta H^{\circ}_{H} = -31.7 \pm 1.6\,\mathrm{kJ/(mol\,H)}, \Delta S^{\circ}_{H} = -74.5 \pm 3.7\,\mathrm{J\,(mol\,H\,K)^{-1}}, 150 < T < 550°C$

Other but possibly less precise values may be found in [103, 51, 5].

The β and ϵ phase. The Gibbs energy of phase formation near c=0.50 for ϵ is [5]:

$\Delta G^{\circ}_{f} == -12550 + 18.06\,T\ \mathrm{J/mol}$

For the β phase the same workers obtained:

$\Delta G^{\circ}_{f} = -13750 + 20.66\,T\,\mathrm{J/mol}$

The following estimates of the Gibbs energies of formation for c=0.66 were also given in [5]

phase α : $\Delta G^{\circ}_{f} = -14000 + 20.8T\ \mathrm{J/mol}$

phase ϵ : $\Delta G^{0}_{f} = -14600 + 22.0T\ \mathrm{J/mol}$

phase β : $\Delta G^{\circ}_{f} = -15100 + 23.0T\ \mathrm{J/mol}$

phase δ : $\Delta G^{\circ}_{f} = -15600 + 25.0T\ \mathrm{J/mol}$

For the reaction $2VH + H_2 \rightarrow 2VH_2$ the plateau free energy in $\mathrm{J/(mol\,H_2)}$ is given by [5]:

$\Delta G_{H2}(\mathrm{plat}) = -40250 + 141T\ \mathrm{J/mol\ H_2}$

Heat capacities are listed in the same work. *Calorimetry* of V hydrides was carried out by Luo et al. [107].It was found necessary to heat up the sample somewhat before adding new hydrogen.In this way, a reproducible, stress-free state was achieved.

1.3.5 Miscellaneous

Hydride Morphologies. The β-phase precipitates in the form of thin plates on (10 3 3)-planes [2]. The phenomenological theory of martensitic transformations was successfully applied to β precipitation in the α-phase [108]. The habit plane and orientation relationship are correctly predicted. Cursory data on VH_2 precipitation in VH are reported in [2].

Permeation. We can only report the calculated values listed below [85]: $P_o = 4 \times 10^{-9}\,\mathrm{mol/m\,s\,Pa^{1/2}}$, $E_p = -0.258\,\mathrm{eV}$

Electrical Resistivity. A recent, reliable value for the resistivity increase for c= 0.01 is $0.85 \pm 0.02\,(\mathrm{H}), 0.83 \pm 0.02\,(\mathrm{D})\,\mu\Omega\,\mathrm{cm}$ [59]. Isotope effects in the resistivity variations caused by H and D in V are discussed in [60].

The twist effect. Wires of V are known to become twisted on the onset of hydride precipitation upon cooling [109]. This twist occurs as a result of the stress-assisted preferential precipitation of one or more variants of the hydrides. Also,the movement of dislocations punched out from the hydrides contributes to the effect. Obviously, internal stresses must be responsible for the twisting [109].

Property Changes. A variety of data on mechanical properties are summarized in [1].

1.4 D in Vanadium

1.4.1 Deuteride Phases

The α-phase again is a disordered solution of D in V. As to length or lattice parameter changes at rather low concentrations, the pertinent parameters for Eqn. 25 are :

$(\Delta v/\Omega)_D = 0.191 \pm 0.003$; and $a_o = 0.302694 \pm 0.000002$ nm

For c=0.5, it was found by early neutron diffraction [110] that 90% of the D atoms occupy tetrahedral, but 10 % occupy octahedral positions in the α-phase. a_o is 0.313 nm at 400 K. The redistribution of deuterium atoms to certain octahedral interstices in the α-phase under applied stress was investigated in [111]. In diffuse X-ray scattering work [112] the force dipole tensor was deduced for D in the α-phase. The tensor has cubic symmetry with $|A - B| \leq 0.3$ eV, and $\mathrm{Tr}\, P_{ij} = 3A = 7.6 \pm 0.2$ eV.

The β-phase has a composition near c=0.5 . Fig. 38 shows its structure (after [110, 113, 114]). The structure is monoclinic, space group Cm. The unit cell is described by the vectors:

$A = \sqrt{a_o^2 + c_o^2}$; $B = b_o$; $C = \sqrt{a_o^2 + c_o^2}, \beta = 95.5^o, A \approx C = 0.4466$ nm, $B = 0.302$ nm

At c=0.50 there are two D atoms in the shaded unit cell. Above c=0.50 the excess sites become filled. 95% of the D's occupy octahedral, the rest tetrahedral sites. The c_o/a_o ratio is approximately 1.1. Ordering produces also a modulation of the metal atom lattice [114] resulting in X-ray peaks at the positions of the D superlattice reflections. Deuterium atoms repel two neighboring V atoms along the metal atom c-axis. The displacement was estimated to be 0.014 nm. For β the following equations describe the variation of the lattice parameters with the deuterium content in o_z sites, n_o, and in tetrahedral sites, n_t, where $n_o + n_t = 0.5$[113]:

$$c = a_v(1 + 0.195\, n_o + 0.0548\, n_t);\ a_v = 0.3032\,\text{nm} \qquad (30)$$

$$a = a_v(1 - 0.0256\, n_o + 0.0548\, n_t) \qquad (31)$$

The order parameter of phase β decreases gradually upon heating and becomes zero at 403 K [113]. The β to α transition is of first order.

The γ-phase has a composition near V_4D_3 and is produced by cooling of α-phase regions of suitable concentration. Its structure is depicted in Fig. 47 [113, 115, 116, 117]. The unit cell can be described by: Fig. 47

$A = C = \sqrt{2}a_o$; $B = 2a_o$; $(a_o = 0.3143\text{nm})$

The space group is P_{cc2}. Entin [117], however, reported that even γ is unstable against prolonged storage at low temperatures and decays to a different superstructure.

In further TEM work on the γ-phase [118] superlattice reflections of type $\frac{1}{4}(004)$ were observed for stoichiometric V_4D_3. In the hyperstoichiometric region, however, small systematic shifts of these spots were found which correlate with concentration. This effect was in excellent agreement with a model of *incommensurate deuterium density modulations*. An illustration of this effect is provided in Fig. 48 (a),(b) (for details, see Figure Caption). Fig. 48

The δ-phase is a partially ordered low temperature phase with a concentration between 0.75 and 1.0 [113, 115, 116]. It is isomorphic with β-NbH and thus has an orthorhombic structure with space group P_{nnn}. The unit vectors are [113, 115, 116]:

$A = B = \sqrt{2}\,a_o$; $C = c_o$; $a_o = 0.3156\,\text{nm}$

The D's occupy tetrahedral sites.

The ζ-phase is a transitory phase when going from α to δ. Presumably, it is also orthorhombic with predominantly tetragonal occupancy [2]. It exists between c=0.75 and 0.83 in the temperature range from -62°C to - 39°C [2].

The di-deuteride phase VD_2 is isomorphic with the corresponding protium

phase. a_o was determined to 0.42555 nm [2].

1.4.2 VD Phase Diagrams

The VD solvus was shown in Fig. 39. Note the strong isotope effect. (Details in the Figure Caption). Fig. 39

The VD phase diagram is depicted in Fig. 49 [4]. The transition γ to δ was found to be of second order. γ transforms into an incommensurate phase when c exceeds 0.75. -It is conceivable that there exists also a cubic low temperature phase as in Nb-H and Ta-H. In Fig. 50 a rather conjectural extension of the present diagram to c=2.0 is shown [97]. Fig. 49 Fig. 50

Effects of substitutional impurities on the phase diagrams V-H and V-D are discussed in [119]. Similarly,the phase stability and structural changes in β upon replacing 10 % of the V atoms by Cr and Ta was studied in [120].An ϵ-type phase was observed in the system with Cr. When Ta was added, the O site occupation by deuterium becomes unstable.

1.4.3 Deuterium Diffusion in V

The reader is referred to Fig. 12 in the Section on Nb.

1.4.4 Thermodynamic Data, Solubilities

Selected p-c-T-curves are shown in Fig. 51 (a) for c<0.5 [102] and in Fig.51 (b) for a somewhat wider temperature and concentration range[50].Further p-c-T data are shown in Fig. 52 for the $VD - VD_2$ equilibrium [104]. Fig. 51 Fig. 52

Numerical values - the α-phase. We cite for the extrapolated case of infinite dilution:

$\Delta H^{\circ}_{D} = -31.6 \pm 0.3$ kJ/mol D [102]; $\Delta H^{\circ}_{D} = -32.8 \pm 1.6$ kJ/mol D [106]

$\Delta S^{\circ}_{D} = -75.1 \pm 0.4$ J/(mol K) [102], $\Delta S^{\circ}_{D} = -76.3 \pm 3.7$ J/(mol K) [106].
Excess quantities are cited in [5].

The β-phase. The Gibbs energy function for the formation of the β-phase is given by [5]:

$\Delta G^{\circ}_{f} = -14225 + 22.5T$ J/mol alloy.

Calorimetry results of a few selected transitions in the V-D system are analyzed in [5].

1.4.5 Miscellaneous

We refer here to the hydride section.

Acknowledgement

The author appreciates very helpful discussions with W. A. Oates, T. B. Flanagan, R. Hempelmann, R. Lässer, H. Wenzl and P. Meuffels. Technical assistance was provided by C. Dieker .

References

[1] Fromm E., Hörz G., Int. Metals Rev. 1980, 5, 6, 269-311.

[2] Schober T., Wenzl H., in: Topics in Applied Physics, Hydrogen in Metals II: Alefeld G., Völkl J. (eds.) Berlin: Springer Verlag, 1978;Vol. 29, pp. 11-71.

[3] Wenzl H., Welter J.-M., in Current Topics in Materials Science: Kaldis E. (editor)Amsterdam North-Holland Publ. Co., 1978; Vol. 1, pp. 603-656.

[4] Schober T. in : Electronic Structure and Properties of Hydrogen in Metals: Jena P., Satterthwaite C. B. (eds), New York Plenum Press, 1983, pp. 1-10.

[5] Smith J. F., Bulletin of Alloy Phase Diagrams 1983, 4, 39-46.
Smith J. F., Peterson D. T., *ibide* 1982, 3, 49-54.
Smith J. F., Peterson D. T., *ibide* 1982, 3, 55-59.
San-Martin A., Manchester F. D. *ibide*, in press.

[6] Somenkov V. A., Shil'shtein S. Sh. ,Progr. Mater. Sc. ,1980 24, 267-335.

[7] Zabel H., Peisl J., J. Phys. F: Metal Phys. 1979, 9, 1461-1476.

[8] Schober T., Dieker C., Feenstra R., J. Phys. F: Metal Phys. 1988 18, 1119-1125.

[9] Somenkov V. A., Gurskaya A. V., Zemlyanov M. G., Kost M. E., Chernoplekov N. A., Chertkov A. A., Sov. Physics-Sol. State 1968, 10, 1076-1082.

[10] Somenkov V.A., Petrunin V.F., Shil'shtein S.Sh., Chertkov A.A., Sov.Phys.-Cryst.1970, 14, 522-530.

[11] Pick M.A., Bausch R., J.Phys F: Metal Phys.1976 6, 1751-1763.

[12] Mair G., Bickmann K., Wenzl H., Z.Phys.Chem.NF 1979, 114, 29-35.

[13] Schober T., Linke U., Metallography 1976, 9, 309-320.

[14] Schober T., Wenzl H., phys.stat.sol.(a) 1976, 33, 673-681.

[15] Hall C.K., Soteros C., Macgillivray I., Shirley A.I., J.Less-Comm.Met. 1987, 130, 319-327.

[16] Buck O., Thompson D.O., Wert C., Sripta Met.1974, 8, 1061-1066.

[17] Makenas B.J., Birnbaum H.K., Acta Met.1982 30, 469-481.

[18] Köbler U., Welter J.-M., J.Less-Comm.Metals 1982, 84, 225-235.

[19] Welter J.-M., Schöndube F., J.Phys.F:Metal Phys. 1983, 13, 529-538.

[20] Pesch W., Schober T., Wenzl H., Scripta Met.1978 12, 815-820.

[21] Schober T., Linke U., J.Less- Comm.Met.1976, 44, 77-86.

[22] Schober T., Proc.Ninth Int.Congr.Electron Micr.(Toronto) 1978, 1, 644-645.

[23] Weymann K., Müller H., J.Less-Comm.Metals 1986, 119, 127-139.

[24] Müller H., Weymann K., Hartwig P., J.Less-Comm.Met.1980, 74, 17-22.

[25] Brun T.O., Kajitani T., Mueller M.H., Westlake D.G., Makenas B.J., Birnbaum H.K., Proc.Modulated Structures Meeting 1979, Kailua-kona, Hawaii, AIP Conf.Proc.No.53, 397-399.

[26] Whitton J.L., Mitchell J.B., Schober T., Wenzl H., Acta Met.1976, 24, 483-490.

[27] Alefeld G., phys.stat.sol.1969 32 67-72.

[28] Zabel H., Peisl H.,Acta Met.1980, 28, 589-599.
Burkel E., Fenzl W., Peisl J., Phil.Mag.A 1986, 54, 317-323.

[29] Steyrer G.,Peisl J., J.Less-Comm.Met.,1987 , 130, 147-153.

[30] Faux D.A., Ross D.K., J.Phys.C:Solid State Phys.1987 20, 1441-1457.

[31] Völkl J., Alefeld G., Z.Phys.Chem.NF 1979, 114, 123-139.

[32] Qi Zh, Völkl J., Lässer R., Wenzl H., J.Phys.F:Met.Phys.1983, 13, 2053-2062.

[33] Wipf H., Völkl J., Alefeld G., Z.f.Physik B (Cond.Matter) 1989, 76, 353-358.

[34] Pusch A. ,Fenzl W. ,Peisl J. , Z.Phys. Chem.NF 1989, 163, 497-502.

[35] Steinbinder D.,Wipf H.,Schober H.R.,Blank H.,Kearley G.,Vettier C., Magerl A., Z.Phys.Chem.NF 1989, 163, 503-508.

[36] Schober H.R., Stoneham A.M., Z.Phys.Chem. 1989, 164, 757-762.

[37] Staiger
W., Blocher R., Plachke D., Carstanjen H.D., Z.Phys.Chem.NF, 1989, 164, 991-998.

[38] Schober T., J.Phys.E:Sci.Instr.1984, 17, 196-198.

[39] Oates W.A, Flanagan T.B., Wenzl H. "Thermodynamics of Metal Hydrogen Systems"(to be published)

[40] Kuji T., Oates W.A. , J.Less- Comm.Met.1984, 102, 251-260.

[41] Kuji T., Oates W.A. , J.Less- Comm.Met.1984, 102, 261-271.

[42] Kuji T., Oates W.A., J., Less- Comm.Met.1984, 102, 273-279.

[43] Harada S., Trans.Jap.Inst.Metals 1988, 29, 939-946.

[44] Pryde J.A., Titcomb C.G., Trans.Faraday Soc.1969, 65, 2758-2765.

[45] Reilly J.J., Wiswall R.H., Inorg.Chem.1970, 9, 1678-1682.

[46] Padurets L.N., Shilov A.L., Kost M.E., Kuznetsov N.T., Russian J.Phys.Chem. 1987, 61, 417-419.

[47] Craft A., Kuji T., Flanagan T.B., J.Phys.F:Met.Phys.1988, 18, 1149-1163.

[48] Pryde J.A.,Titcomb C.G., J.Phys.C:Sol.State Phys.1972, 5, 1293-1299.

[49] Lässer R., Meuffels P., Feenstra R. 1988, KFA Jülich Report # Jül-2183.

[50] Fujita K., Huang Y.C., Tada M., Nippon Kinzoku Gakkaishi, 1979, 43, 601-610; 611-617.

[51] Veleckis E., Edwards R.K., J.Phys.Chem. 1969, 73, 683-692.

[52] Magerl A., Rush J.J., Rowe J.M., Phys.Rev.B.1986, 33, 2093-2097.

[53] Richter D., Shapiro S.M., Phys.Rev.B.1980, 22, 599-603.

[54] Rush J.J., Magerl A., Rowe J.M., Harris J.M., Provo J.L., Phys.Rev.B., 1981, 24 , 4903-4908.

[55] Hempelmann R., Richter D., Kollmar A., Z.Phys.B 1981, 44, 159-165.

[56] Hempelmann R., Richter D., Price D.L., Phys.Rev.Lett. 1987, 58, 1016-1019.
Hempelmann R., Z.f.Phys.Chem.N.F.1987, 154, 221-249.

[57] Rush J.J., Berk N.F., Magerl A., Rowe J.M., Provo J.L., Phys.Rev.B 1988, 37, 7901-7904.

[58] Burger L.L., Morgan L.G., Battelle Pacific Northwest Report, "Permeation, Solubility and Diffusion of Hydrogen Isotopes", 1980.
Maroni V.A., Van Deventer E.H., J.Nucl.Mat. 1979, 85, 86, 257-269.

[59] Watanabe K., Fukai Y., J.Phys.F:Met.Phys. 1980, 10 , 1795-1801.

[60] Maier W.,Wipf H., Scripta Met.1977, 11, 695-698.

[61] Ducastelle F., Caudron R., Costa P., J.Phys.Chem.Solids 1970, 31, 1247-1256.

[62] Petrunin V.F., Somenkov V.A., Shil'shtein S.Sh., Chertkov A.A., Sov.Phys.-Cryst. 1970, 15, 137- 139.

[63] Asano H., Ishino Y., Yamada R., Hirabayashi M., J.Sol.State Chem.1975, 15, 45-53.

[64] Schober T., Wenzl H., Scripta Met.1976, 10, 819-822.

[65] Asano H., Ishikawa Y., Hirabayashi M., J.Appl.Cryst.1978, 11, 681-683.

[66] Asano H., Kishi K., Hirabayashi M., Proc. Second JIM International Symposium Hydrogen in Metals, Minakami, Japan. Supplement to: Trans.Jap.Inst.Met.1980, 21, 93-96.

[67] Hirabayashi M., Asano H., in: "Metal Hydrides", Bambakidis G.(ed.), New York: Plenum Press, 1981, pp.53- 80.

[68] Asano H., Hirabayashi M., in: "Metal Hydrides", Bambakidis G.(ed.), New York: Plenum Press 1981, pp.81- 104.

[69] Somenkov V.A., Chervyakov A.Y., Shil'shtein S.S., Chertkov A.A., Sov.Phys.-Cryst.1972, 17, 274- 280.

[70] Köbler U., Schober T., J.Less-Comm.Met. 1978, 60, 101-107.

[71] Kaneko H.,Kajitani T., Hirabayashi M. ,Nimura N., Schultz A.J., Leung P.,J.Less-Comm.Met. 1984, 103, 45-51.

[72] Schober T., Carl A., Scripta Met.1977, 11, 397-400.

[73] Condon J.B., Schober T., Lässer R., J.Nucl.Mat.1990, 170, 24-30.

[74] Flanagan T.B., Schober T., Wenzl H., Acta Met., 1983, 31, 483-487.

[75] Majer G., Messer R., Seeger A., Z.Phys. Chem.NF, 1989, 164, 873-878.

[76] Mauger P.E., Williams W.D., Cotts R.M., J.Phys.Chem.Sol., 1981, 42, 821-826.

[77] Potzel U., Völkl J., Wipf H., Magerl A., phys.stat.sol.(b) 1984, 123, 85-92.

[78] Weidinger A., Peichl R., Phys.Rev.Lett. 1985, 54, 1683-1685.

[79] Papathanassopoulos K., Schober T., Wenzl H., Sol.State Comm.1984, 52, 575-577.

[80] Pryde J.A., Tsong I.S.T., Trans.Far.Soc. 1971, 67, 297-304.

[81] Franzen H.F., Khan A.S., Peterson D.T., J.Less- Comm.Met.1977, 55, 143-147.

[82] Dantzer P.G., Kleppa O.J., J.Sol.State Chem. 1978, 24, 1-9.

[83] Lewis F.A., Obermann A., J.Less-Comm.Met. 1976, 49, 349-356.

[84] Asano H., Yamada R., Hirabayashi M., Trans.Jap.Inst.Met. 1977 , 18, 155-160.

[85] Lässer R., "Tritium and Helium-3 in Metals", 1989, Berlin: Springer, p. 39.

[86] Hörz G., Metall 1977, 31, 1- 6.

[87] Suzuki T., Namazue H., Koike S., Hayakawa H., Phys. Rev. Lett. 1983 , 51, 798-800.

[88] Asano H., Abe Y., Hirabayashi M., J. Phys. Soc. Japan 1976, 41, 974-976.

[89] Fukizawa A., Fukai Y., J. Phys. Soc. Jap. 1983, 52, 2102-2107.

[90] Kajitani T., Hirabayashi M., Z. Phys. Chem. NF 1985, 145, 27-42.

[91] Noda Y., Masumoto K., Koike S., Suzuki T., Sato S., Acta Cryst. 1986, B42 , 529-533.

[92] Marsh R. E., Acta Cryst. 1987, B43 , 415-416.

[93] Pauling L. , J. Sol. St. Chem. 1989, 79, 63-64.

[94] Asano H., Abe Y., Hirabayashi M., Acta Met. 1976, 24, 95-99.

[95] Asano H., Hirabayashi M., phys. stat. sol. (a) 1973, 16, 69-72.

[96] Schober T., Scripta Met. 1978, 12, 549-554.

[97] Schober T. ,Pesch W., Z. Phys. Chem. NF, 1979, 114 , 21-28.

[98] Saito Y., Fukai Y., J. Less-Comm. Met. 1988, 138, 161-172.

[99] Freudenberg U., Völkl J., Bressers J., Alefeld G., Scripta Met. 1978, 12, 165-167.

[100] Peterson D. T., Schlader B. J., Met. Trans. A 1988, 19A, 67-72.

[101] Kleiner J. E., Sevilla E. H., Cotts R. M., Phys. Rev. B, 1986, 33, 6662-6667.

[102] Meuffels P., KFA-Jülich Report # 2081, 1986.

[103] Griffiths R., Pryde J.A., Righini-Brand A., Trans.Far.Soc. 1972, 68, 2234-2341.

[104] Rummel W., Siemens Forsch. Entw. Ber. 1981, 10 , 371-378.

[105] Nelson S. O., Jager W. S., J. Less-Comm. Met. 1989, 146 , 167-178.

[106] Bleichert H., Wenzl H., phys. stat. sol. (b) 1987, 144, 361-373.

[107] Luo W., Clewley J. D. , Flanagan T. B . , Scripta Met. 1989, 23, 1225-1230.

[108] Bowles J. S., Muddle B. C., Wayman C. M., Acta Met. 1977, 25, 513-520.

Cassidy M. P., Muddle B. C., Scott T. E., Wayman C. M., Bowles J. S., Acta Met. 1977, 25, 829-838.

[109] Koiwa M., Yoshinari O., Acta Met. 1983, 31, 2073-2081.

[110] Somenkov V. A., Entin I. R., Chervyakov A. Yu., Shil'stein S. Sh., Chertkov A. A., Sov. Phys. Sol. State 1972, 13, 2178-2182.

[111] Takakusaki M., Kajitani T., Hirabayashi M.,

J. Less-Comm. Met. 1987, 129 , 47-55.

[112] Peisl J., Fischer H., Metzger T. H., Z. Phys. Chem. NF 1985, 145 , 189-198.

[113] Asano H., Hirabayashi M., Z. Phys. Chem. NF 1979, 114 , 1-19.

[114] Metzger H., Jo H., Moss S. C., Westlake D. G., phys. stat. sol. (a), 1978, 47, 631-638.
Jo H. S. U., Moss S. C., Westlake D. G., J. Appl. Cryst. 1980, 13, 486-493.

[115] Chervyakov A. Yu., Entin I. R., Somenkov V. A., Shil'shtein S. Sh., Chertkov A. A., Sov. Phys. Sol. State 1972, 13 ,2172-2177.

[116] Entin I. R., Somenkov V. A., Shil'shtein S. Sh., Sov. Phys. Sol. State, 1977, 19, 59-62.

[117] Entin I. R., Somenkov V. A., Shil'shtein S. Sh., Sov. Phys. Sol. State 1976, 18 , 1729-1732.

[118] Pesch W., Phil. Mag. A, 1982, 46 , 41-47.

[119] Watanabe K., Saito Y., Fukai Y., J. Less- Comm. Met. 1982, 88, 43-47.

[120] Kajitani T., Konno T., Hirabayashi M., J. Less-Comm. Met.,1982, 88, 51-55.

Figure Captions

Fig. 1. The structure of β-NbH. The metal atoms are not shown.

Fig. 2. The fully ordered structure of the ϵ-NbH phase. The metal atoms are not shown.

Fig. 3. (001)-SAD pattern of the ϵ-phase [2]. The strong spots are the metal reflections. The weaker spots are the hydrogen superlattice reflections.

Fig. 4. The δ-phase structure, CaF_2- type. Metal atoms form a fcc lattice and are omitted.

Fig. 5. Schematic diagram of the α, β and δ-phase morphology as observable on a (100)-oriented single crystal when the concentration is raised to c=2. 0.

Fig. 6. Schematic representation for the λ-phases [17, 25]. Nb atoms are not shown. (a) Long period superlattice in $[001]_c$ consisting of 14 β unit cells with alternating β_1 and β_2 cells. β_1, β_2 orientations correspond to two variants of β with reference to the α' orientation. (b) Same as above, with the presence of a hydrogen density wave having $q = (2\pi/a)(3/14)[001]_c$ removing the H interstitials at the nearest neighbor positions.

Fig. 7. Nb-H phase diagram [2]. Low temperature transitions are omitted (see Fig. 11). Note that there is a narrow two-phase region $(\alpha + \eta)$ between the two phase regions $(\alpha + \zeta)$, $(\alpha + \epsilon)$.

Fig. 8. Nb-D phase diagram after [7]. Only the "high- temperature" phases are shown.H: o; D:×

Fig. 9. Nb-H, Nb-D solvus [26] as determined with a channeling technique. There is no obvious isotope effect.

Fig. 10. The incoherent α- α'-phase diagram [28] as obtained from X-ray work. Full circles: X-ray data, open circles: DTA data [2].

Fig. 11. Partial low-temperature Nb-H diagram [18] depicting the λ-phase region.

Fig. 12. H, D, T diffusivities in Nb, Ta, V in the limit of very low concentrations as determined with the Gorsky technique [31, 32]. Note the break in the slope of the hydrogen diffusivities.

Fig. 13. Experimental set-up for the measurement of the diffusivity with strain gauges [38].

Fig. 14. p-c-T-curves for H in Nb.
(a) Sieverts type curves for relatively low temperatures. In this range, clean surfaces and reliable low pressure gauges are a necessity [48, 49].
(b) General p-c-T-curves for protium in Nb [49].

Fig. 15. p-c-T-curves for H and D in Nb including the high-temperature Sieverts regime [50]. (a) log p versus at.% - isotope H
(b) log p versus at.% - isotope D

Fig. 16. p-c-T-curves for H in Nb [50]. Plot of log p versus 1/T.

Fig. 17. p-c-T-curves in the $\beta+\delta$ two-phase region [41].

Fig. 18. Precision density data for H, D, T for low c's [8] as obtained with a buoyancy technique. Note quasi -linear decrease. It is fortuitous that the protium and tritium curves coincide.

Fig. 19. Crystal structure of the β-TaH phase [66].
(a) real lattice. The monoclinic metal lattice is shown by dashed lines.
(b) reciprocal lattice, small circles denote superlattice reflections.
(c) H(D) superlattice, open circles: full occupation in beta, occupation with probability 0.6 in phase ϵ, full circles: tetrahedral sites filled with probability 0.4 in phase ϵ.

Fig. 20. Crystal structure of two low-temperature hydrides adapted after [67, 68].
(a) Structure of η-Ta_3H_2. Hydrogen arrangement is projected on (001) plane. Open and full circles denote H atoms at the T-sites with z=1/4 and z=3/4, respectively. Broken lines denote concentration wave parallel to $[3\,\bar{1}\,0]$
(b) Structure of ζ.

Fig.21. The Ta-H-diagram [72]. Only transitions above room temperature are shown. For low temperature transformations,

see Fig. 24 [70]. Arbitrarily, we do not distinguish here between β and δ.

Fig.22. The Ta-H, Ta-D solvus after [4, 73]. There is no visible isotope effect. For a thermodynamic analysis see [74].

Fig.23. Partial Ta-H phase diagram [72] established with very low heating rates and precise temperature and concentration control.

Fig.24. Low temperature Ta-H phase diagram, adapted after [18, 70].

Fig.25. The Ta-D phase diagram [73]. Low temperature transitions are not shown. No difference is made between β and δ.

Fig.26 . NMR derived, concentration dependent diffusivities of H in Ta [76].

Fig. 27. Diffusivity of H in Ta for T<30 K as obtained with a nuclear technique after [78]. The extrapolation of the high-temperature data is depicted.

Fig. 28. Gorsky type diffusivities of H in the alloy $TaH_{0.52}$ [79]. Depending on temperature this alloy is in phase α, β or ϵ.

Fig.29. General p-c-T behavior of H in Ta [49].

Fig.30. General p-c-T behavior of D in Ta [49].

Fig. 31. p-c-T-curves for H and D in Ta [50].
(a) log p versus at.% - isotope H
(b) log p versus at.% - isotope D

Fig. 32. p-c-T-curves for H in Ta [50]. log p vs. 1/T representation.

Fig. 33. Sieverts type curves for D in Ta [80]. We do not expect a considerable isotope effect.

Fig. 34. p-c-T data in the two-phase region (α+ ordered phase) [80].

Fig. 35. Sieverts type curves for H in Ta extending to rather high temperatures [81].

Fig. 36. Series of optical micrographs depicting in polarized light the β to ϵ to α transformation [2]. Phase ϵ appears much brighter than β. Striped regions are domains of the ordered phases. These domains are not present in the α- phase.

Fig. 37. The structures of hyperstoichiometric β, ϵ and δ-VH after [67, 68] as projected on (100)-plane. Full and open triangles indicate partly filled o_z- sites at x=0 and 1/2, respectively. Full and open small circles denote hydrogen atoms on the o_z sites of x=0 and 1/2, respectively.

Fig.38. The monoclinic structure of the VH or VD β-phase. Most of the hydrogen atoms occupy octahedral sites. For more details, see deuteride Section.

Fig. 39. Solvus for the VH and VD and a mixed system [96].
VH-solvus: $\Delta H = 0.1413 \pm 0.005$ eV and $c_o = 5.10 \pm 0.50$.
VD-solvus: $\Delta H = 0.135 \pm 0.004$ eV and $c_o = 7.00 \pm 0.70$. These enthalpies are the energies required to transfer one H atom from the ordered to the α

phase.

Fig. 40. V-H phase diagram derived from DTA data [4].The β to ϵ transition is of second order; there is a $(\beta + \delta)$ two-phase region.

Fig. 41. Partial high-concentration diagram covering the range from c= 0.80 to 2.0 [97].

Fig. 42. General p-c-T-curves for H in V [102].

Fig. 43. p-c-T-curves for H in V [50].
(a)log p vs. at.%,
(b) log p versus 1/T.

Fig. 44. Sieverts curves for H in V [103].

Fig. 45. p-c-T-curves for the $(\alpha+\beta)$-phase region [103].

Fig. 46. p-c-T-curves for the $VH - VH_2$-equilibrium [104].

Fig. 47. The structure of γ-VD [115, 116].

Fig. 48. Incommensurate density modulations in hypostoichiometric γ-VD .
(a) sinusoidal deuterium density modulation. The indicated tetrahedral sites are occupied according to the sinusoidal distribution function P.
(b) calculated reciprocal lattice using model in (a). Excellent agreement with the experiment is obtained. Superlattice reflections are only observed at positions denoted by δ and γ.

Fig. 49 . V-D phase diagram [4].

Fig. 50. Schematic, rather hypothetical phase diagram for D in V up to c=2.0 [97].

Fig. 51. p-c-T-data for deuterium in V

(a) Data by Meuffels [102]

(b) Data by Fujita et al. [50]

Fig. 52. The VD – VD_2 equilibrium: p-c-T data after Rummel [104].

Table 1: Activation energies and pre-exponential factors for the diffusion of H, D and T in Nb, Ta and V

Element	Isotope	U(eV)	$D_o 10^4$ $cm^2 s^{-1}$
Nb	H (T > 250K)	0.106 ± 0.006	5.0 ± 1.0
	H (T < 250K)	0.068 ± 0.004	0.9 ± 0.2
	D	0.127 ± 0.006	5.2 ± 1.0
	T	0.133 ± 0.007	4.4 ± 1.4
Ta	H (T > 250K)	0.136 ± 0.009	4.2 ± 1.2
	H (T < 250K)	0.042 ± 0.006	0.028 ± 0.015
	D	0.153 ± 0.006	3.8 ± 1.0
	T	0.162 ± 0.007	3.7 ± 1.4
V	H	0.045 ± 0.004	3.1 ± 0.6
	D	0.073 ± 0.004	3.8 ± 0.8
	T	0.094 ± 0.007	5.6 ± 1.4

Table 2: Energies in meV of localized vibrations of H, D and T in the α- and β-phases in Nb, Ta and V

Element	Isotope	x	y	z	Reference
Nb α	H	107	163	163	[52]
Nb α	D				
Nb α	T				
Nb β	H	116±0.7	167±1.5	167±1.5	[53]
Nb β	D	86±1	120 ± 1.5	120±1.5	[53]
Nb β	T	72±1	101 ± 1	101±1	[54]
Ta α	H	114	154	154	[52]
Ta α	H	114.0 ±0.6	163.5±0.8	163.5±0.8	[55]
Ta α	D	84.4±0.6	116.0±0.6	116.0±0.6	[55]
Ta α	T				
Ta β	H	121.3±0.2	161.4±0.3	166.6± 0.3	[55]
Ta β	D	88.4±0.4	116.4 ±0.7	120.4±0.7	[55]
Ta β	T				
V α	H	106	170	170	[52]
V α	D				
V α	T				
V β	H	50.2±1.0	59.7±1.0	223±1	[56]
V β	D	39	39	164	[57]
V β	T	36	36	135	[57]

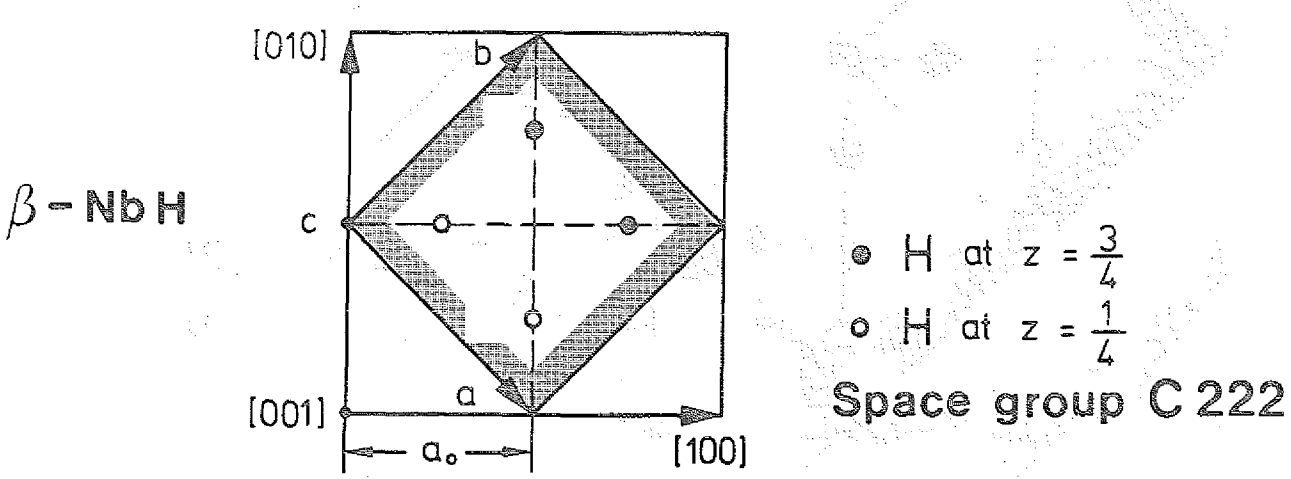

Fig. 1. The structure of β-NbH. The metal atoms are not shown.

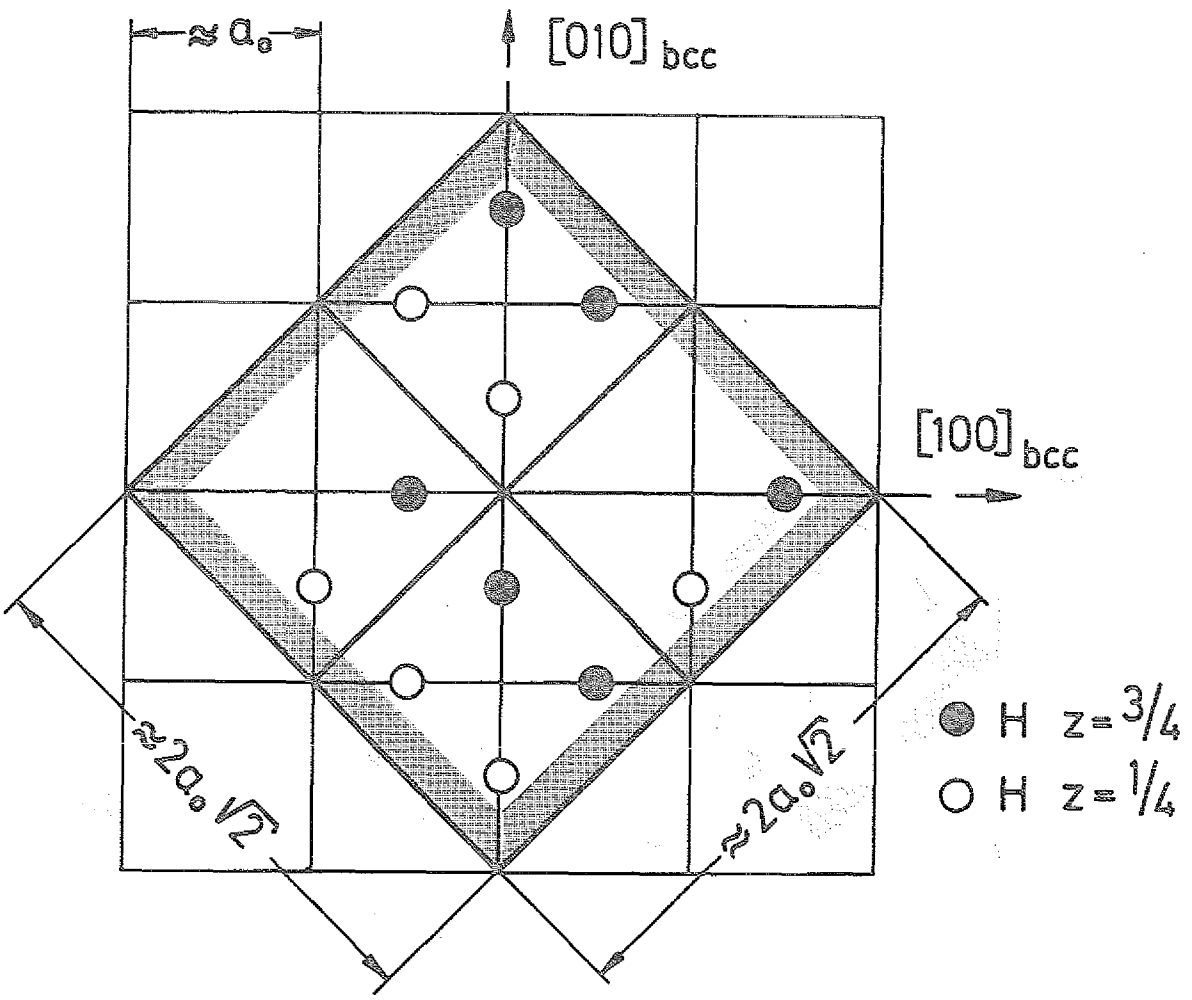

Fig. 2. The fully ordered structure of the ϵ-NbH phase. The metal atoms are not shown.

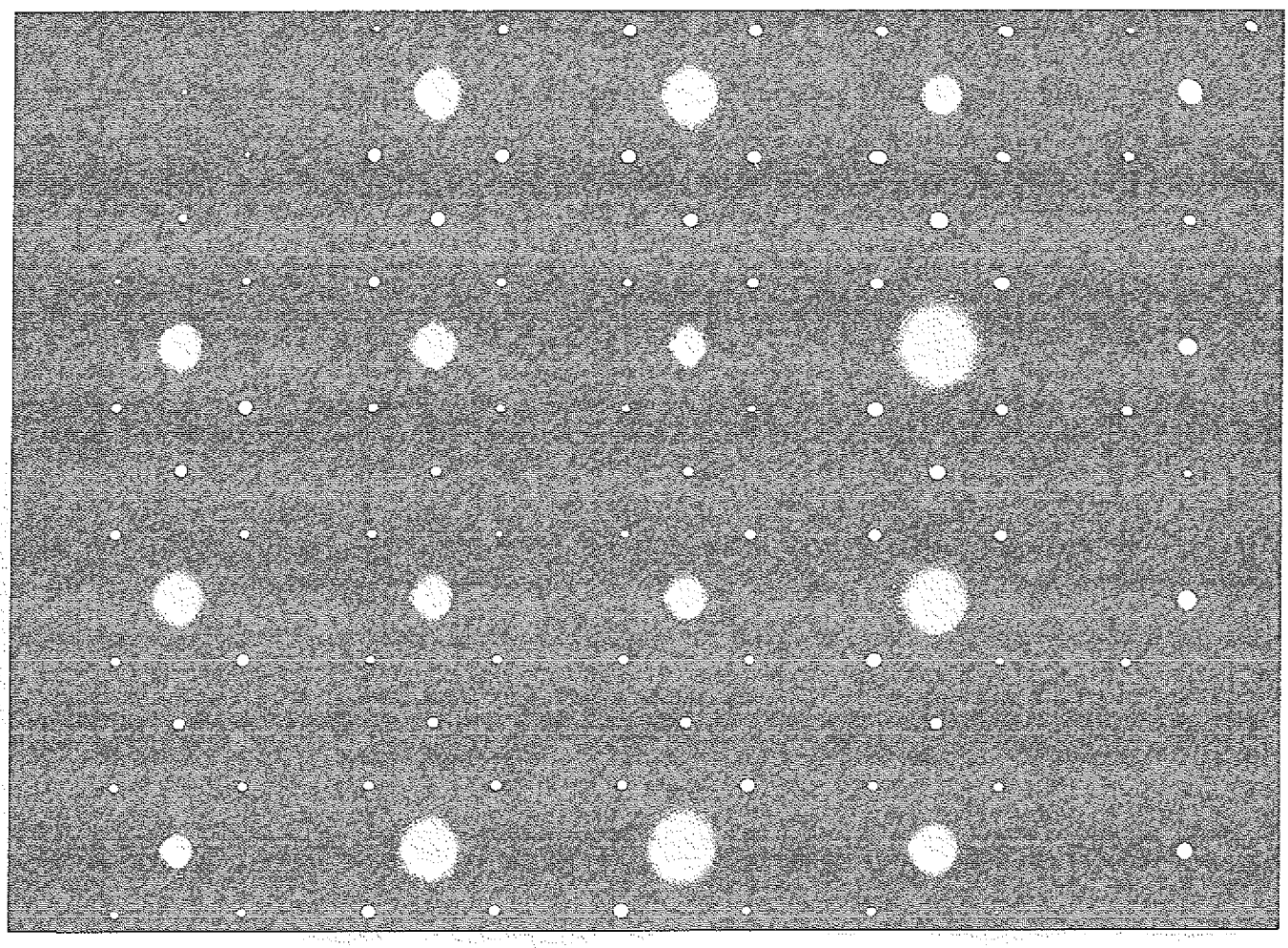

Fig. 3. (001)-SAD pattern of the ϵ-phase [2]. The strong spots are the metal reflections. The weaker spots are the hydrogen superlattice reflections.

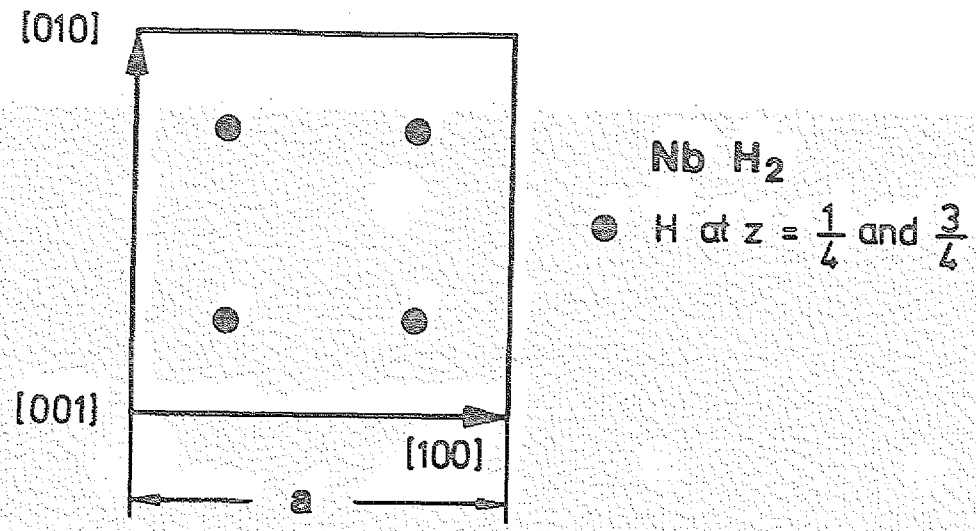

Fig. 4. The δ-phase structure, CaF_2- type. Metal atoms form a fcc lattice and are omitted.

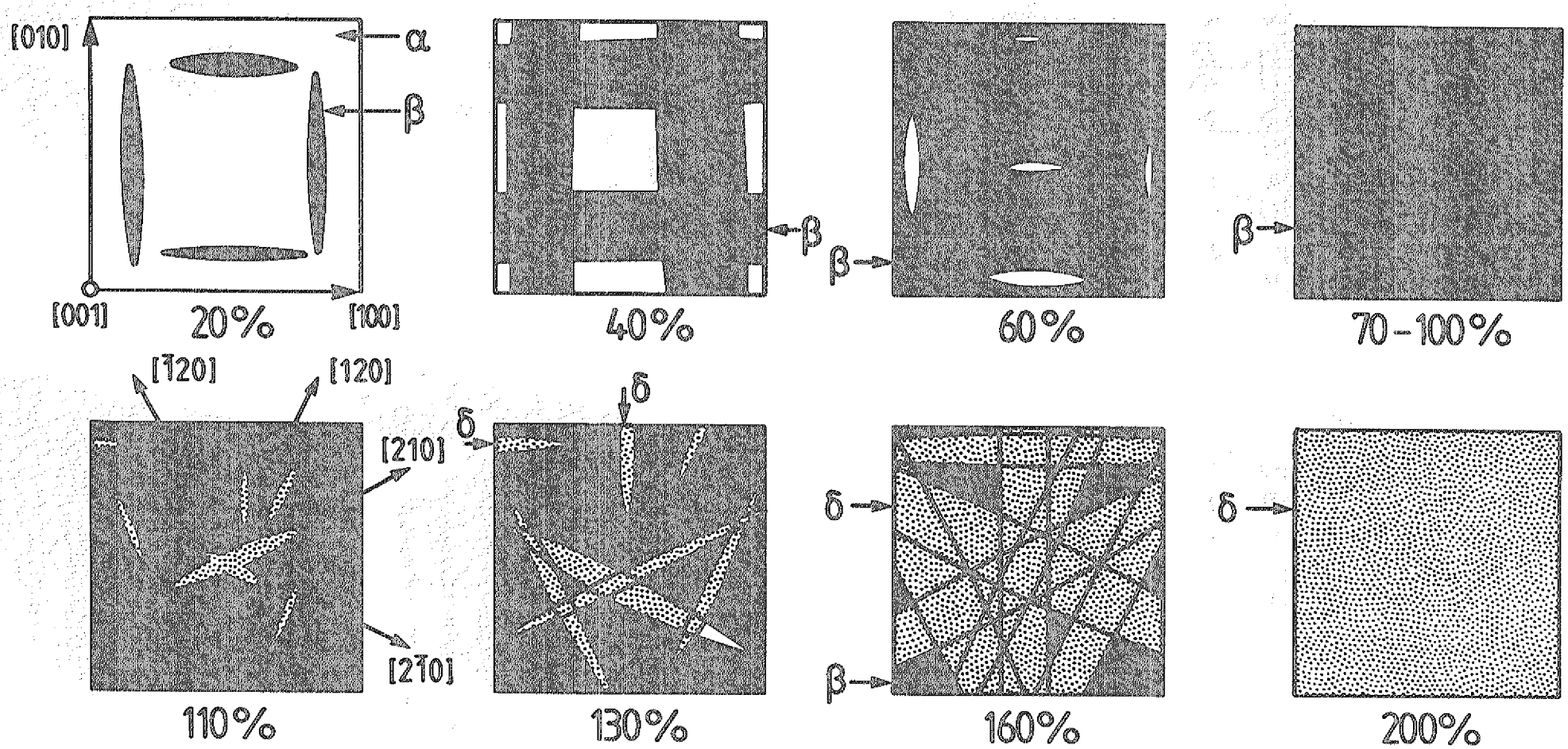

Fig. 5. Schematic diagram of the α, β and δ-phase morphology as observable on a (100)-oriented single crystal when the concentration is raised to c=2.0.

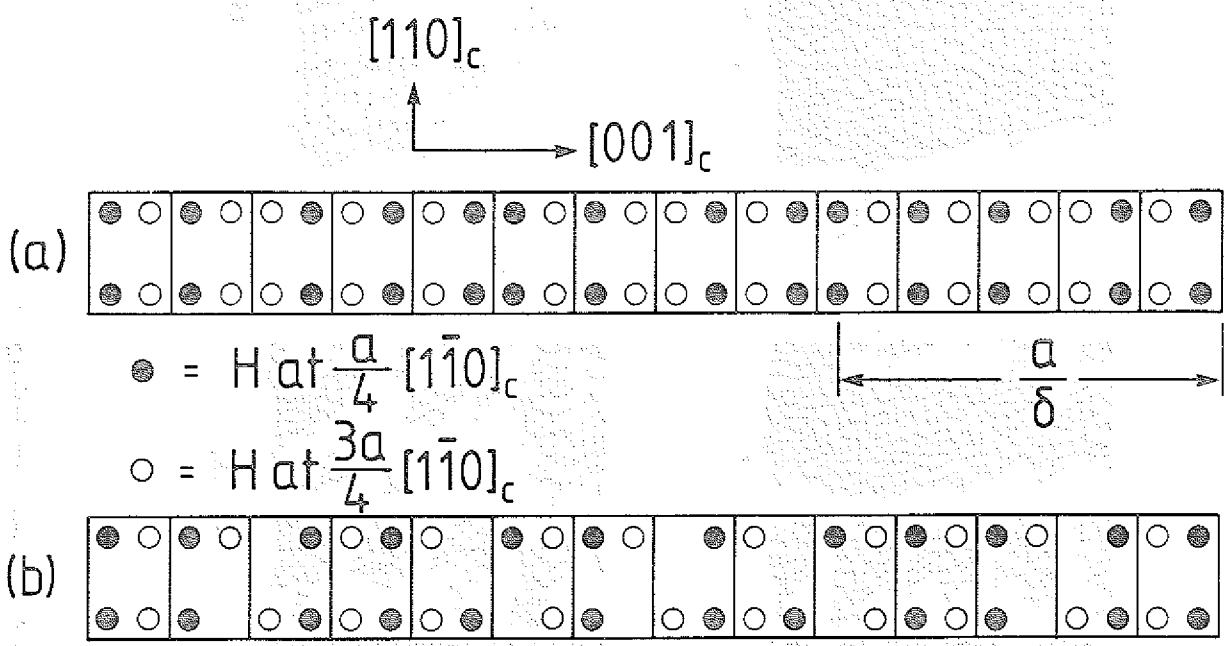

Fig. 6. Schematic representation for the λ-phases [17, 25]. Nb atoms are not shown. (a) Long period superlattice in $[001]_c$ consisting of 14 β unit cells with alternating β_1 and β_2 cells. β_1, β_2 orientations correspond to two variants of β with reference to the α' orientation. (b) Same as above, with the presence of a hydrogen density wave having $q = (2\pi/a)(3/14)[001]_c$ removing the H interstitials at the nearest neighbor positions.

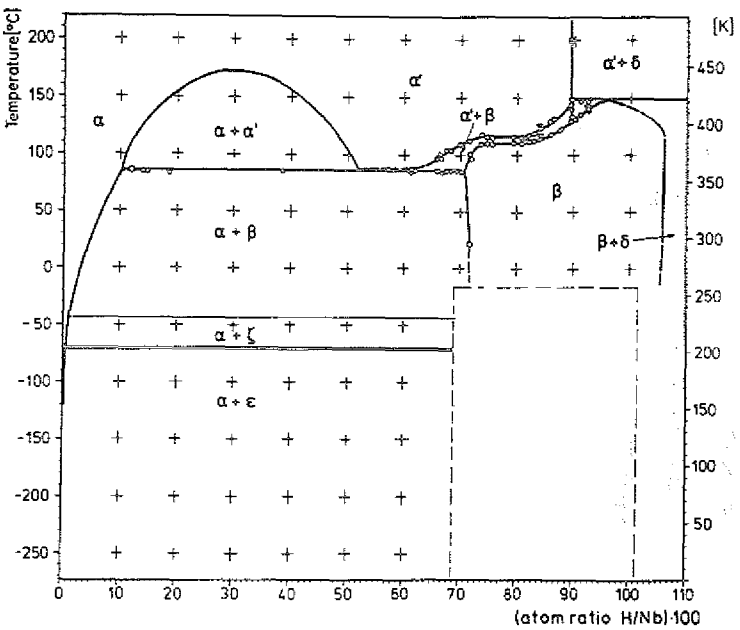

Fig. 7. Nb-H phase diagram [2]. Low temperature transitions are omitted (see Fig. 11). Note that there is a narrow two-phase region $(\alpha + \eta)$ between the two phase regions $(\alpha + \zeta)$, $(\alpha + \epsilon)$.

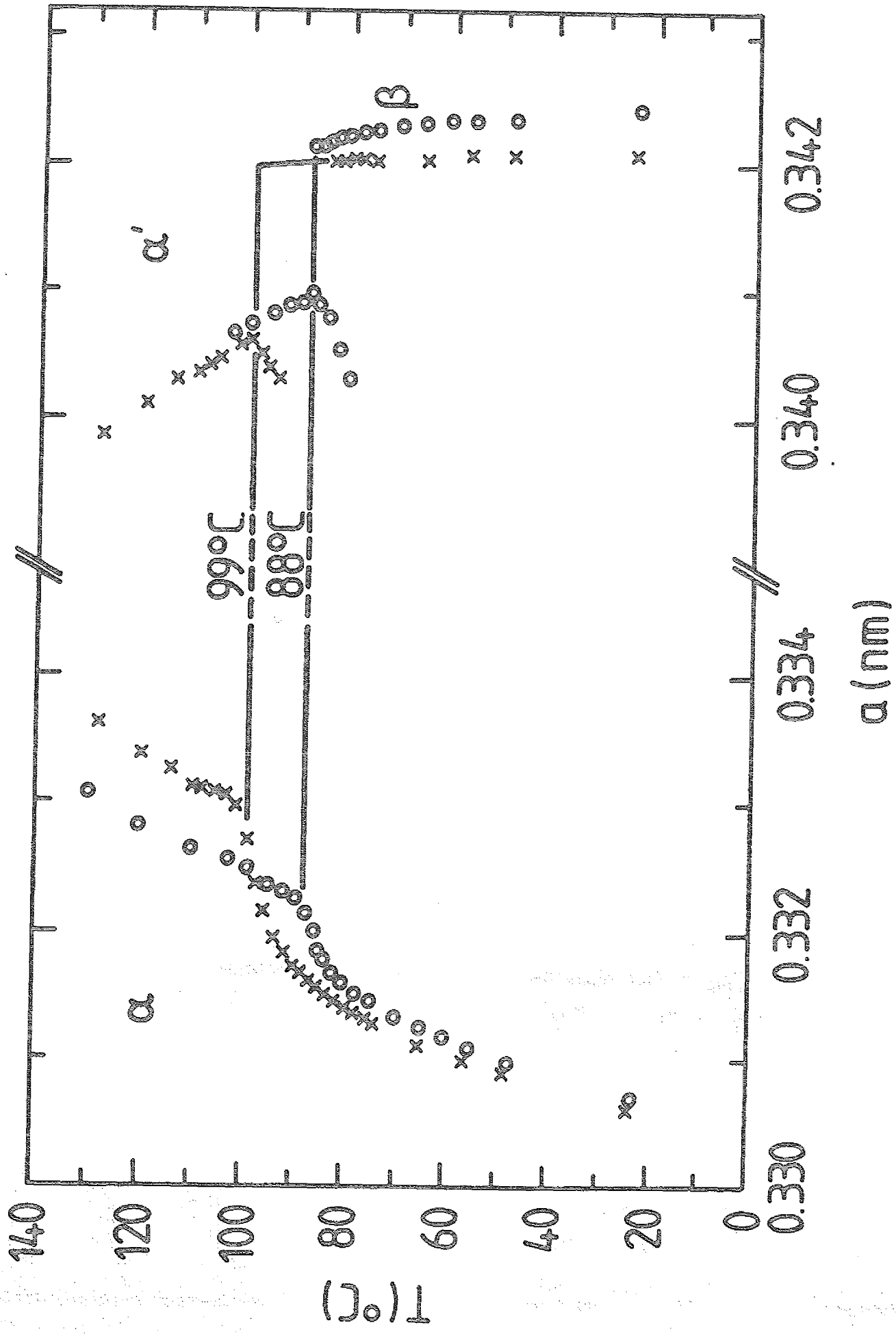

Fig. 8. Nb-D phase diagram after [7]. Only the "high- temperature" phases are shown.H: o; D:×

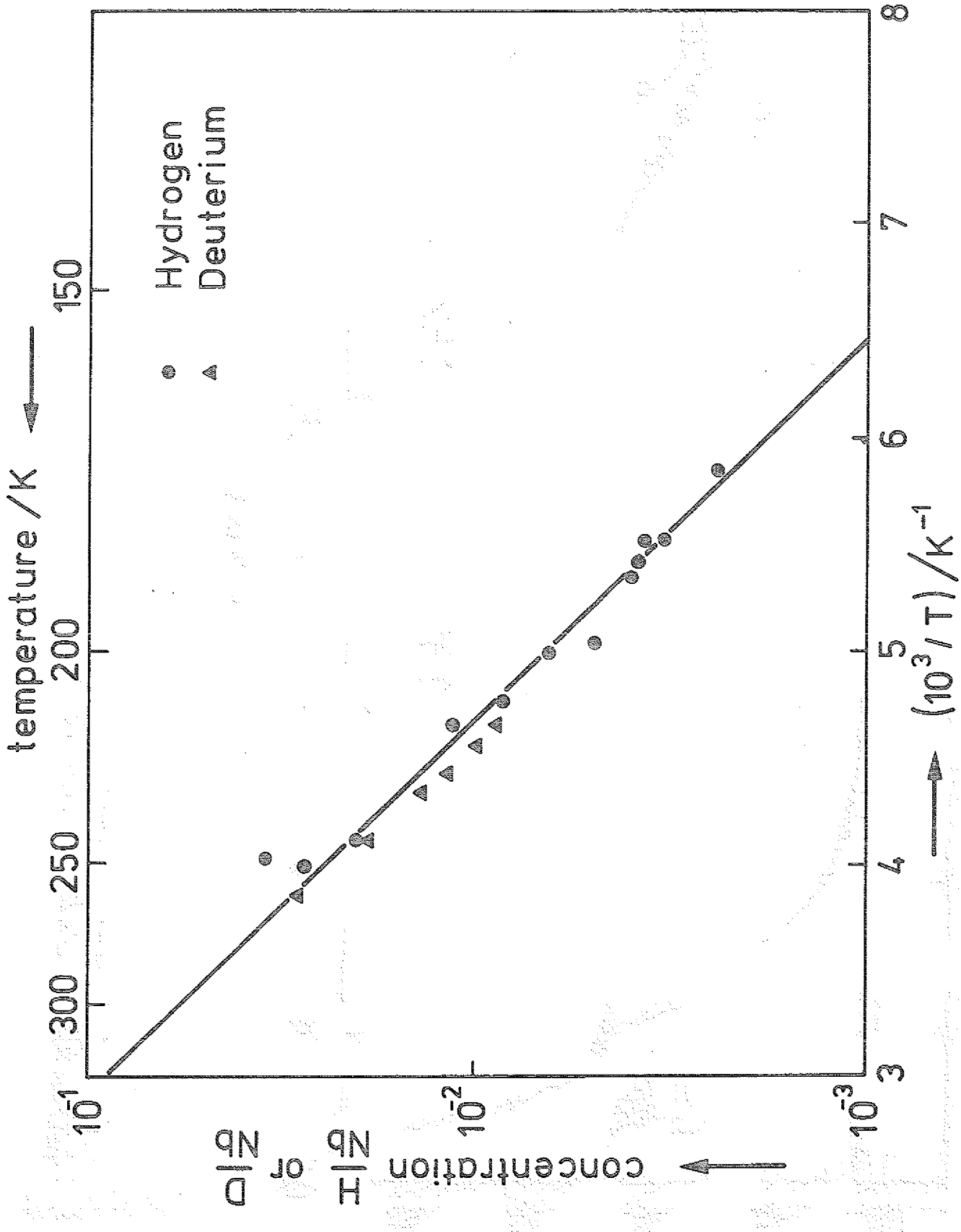

Fig. 9. Nb-H, Nb-D solvus [26] as determined with a channeling technique. There is no obvious isotope effect.

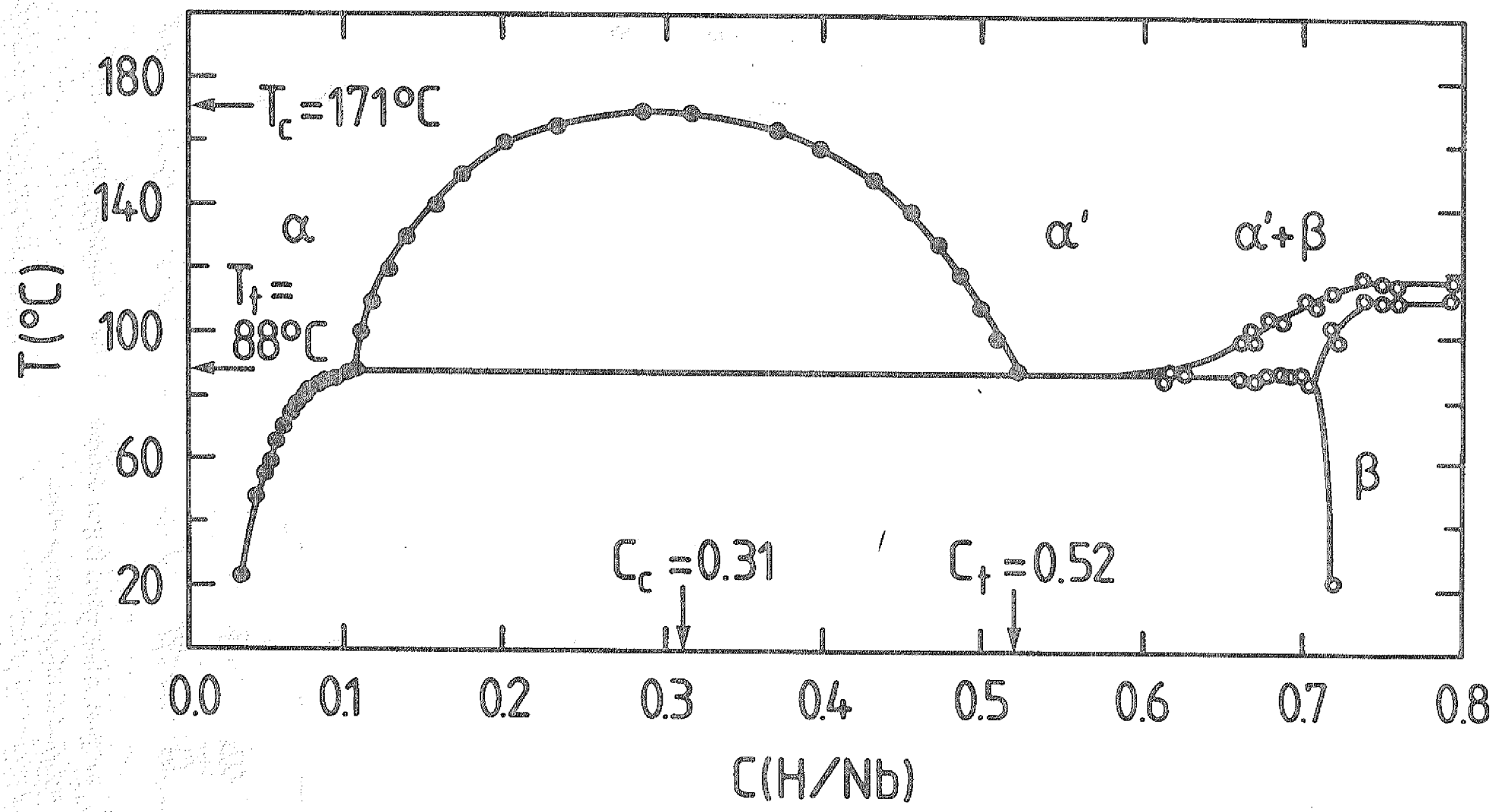

Fig. 10. The incoherent α- α'-phase diagram [28] as obtained from X-ray work. Full circles: X-ray data, open circles: DTA data [2].

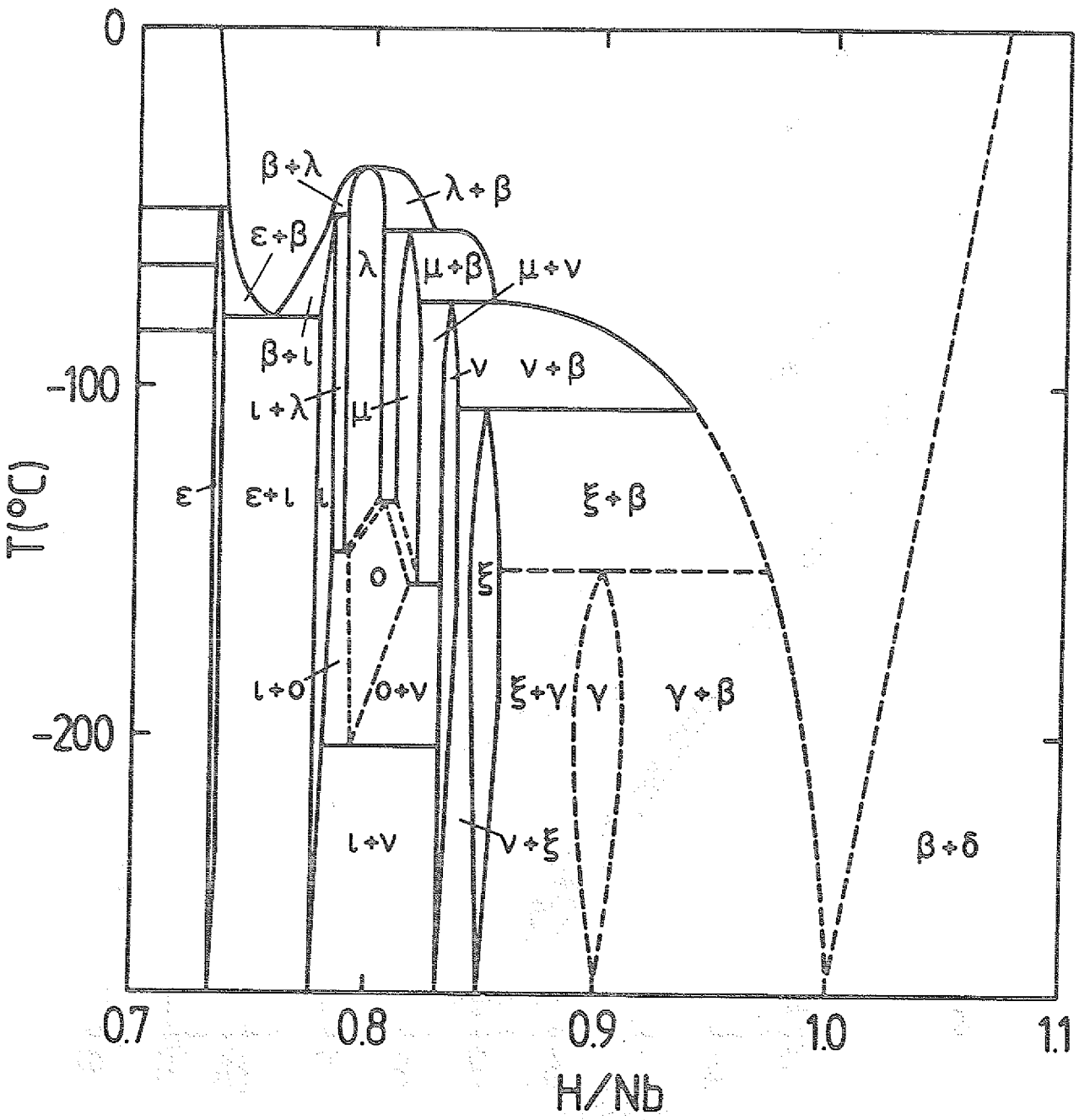

Fig. 11. Partial low-temperature Nb-H diagram [18] depicting the λ-phase region.

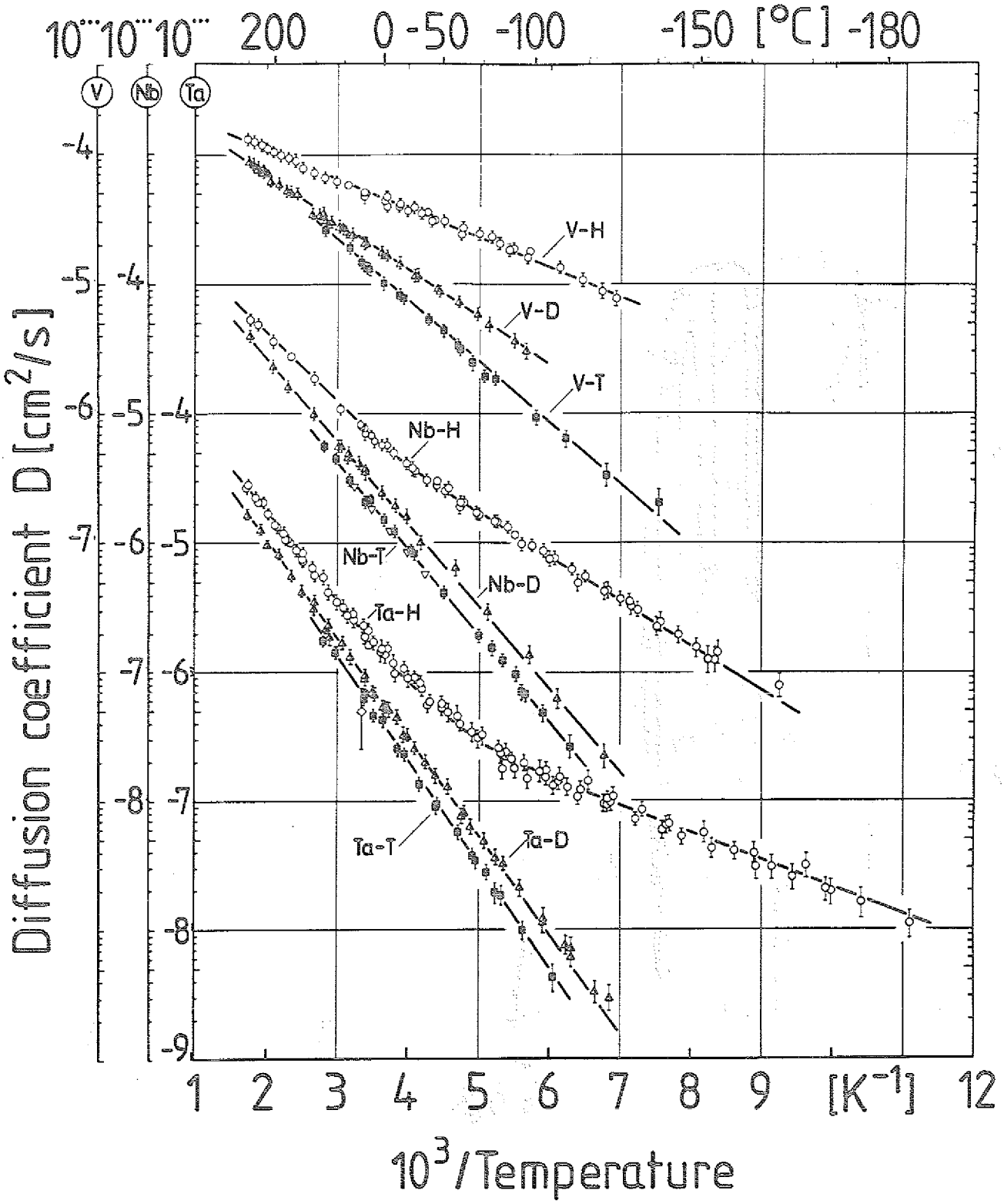

Fig. 12. H, D, T diffusivities in Nb, Ta, V in the limit of very low concentrations as determined with the Gorsky technique [31, 32]. Note the break in the slope of the hydrogen diffusivities.

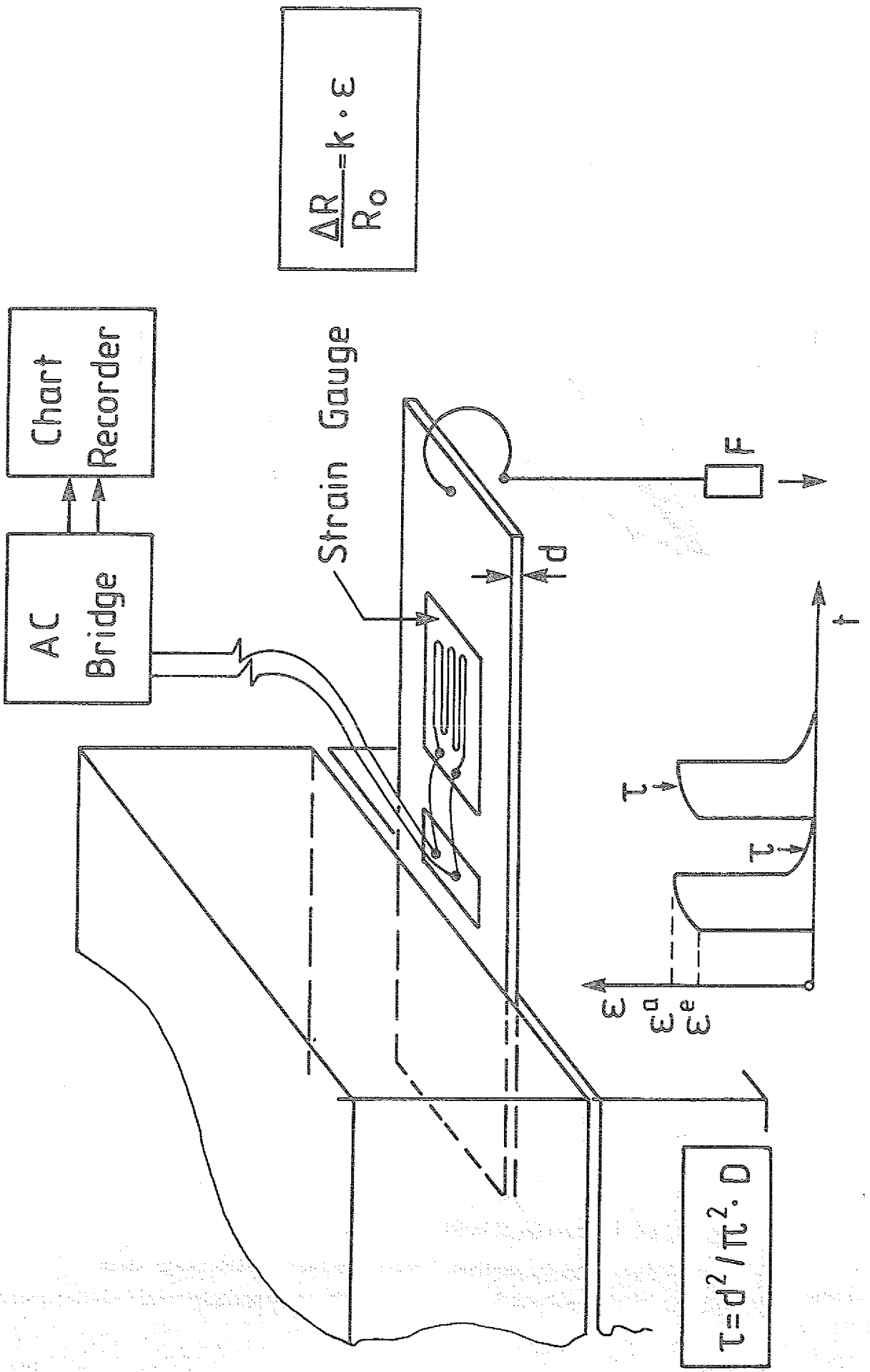

Fig. 13. Experimental set-up for the measurement of the diffusivity with strain gauges [38].

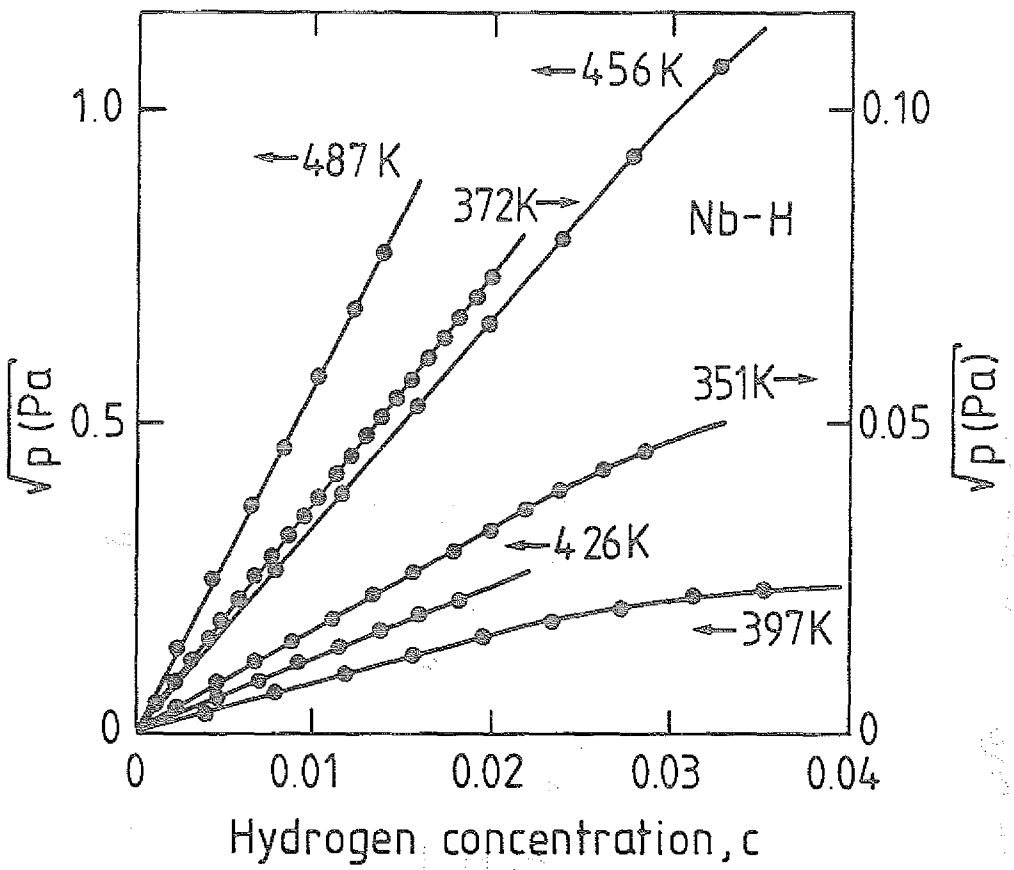

Fig. 14. p-c-T-curves for H in Nb.

(a) Sieverts type curves for relatively low temperatures. In this range, clean surfaces and reliable low pressure gauges are a necessity [48, 49].

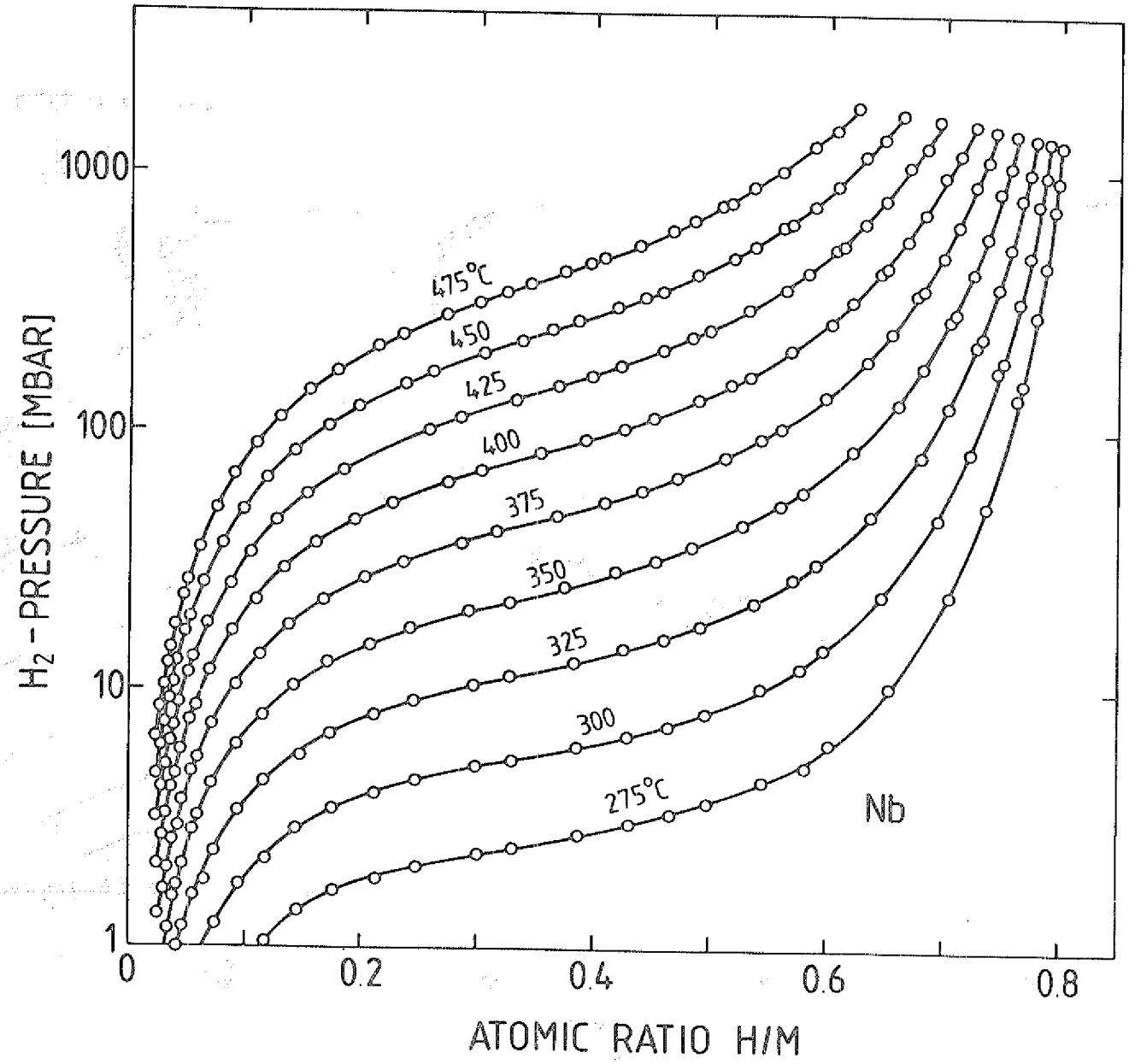

Fig. 14 (b) General p-c-T-curves for protium in Nb [49].

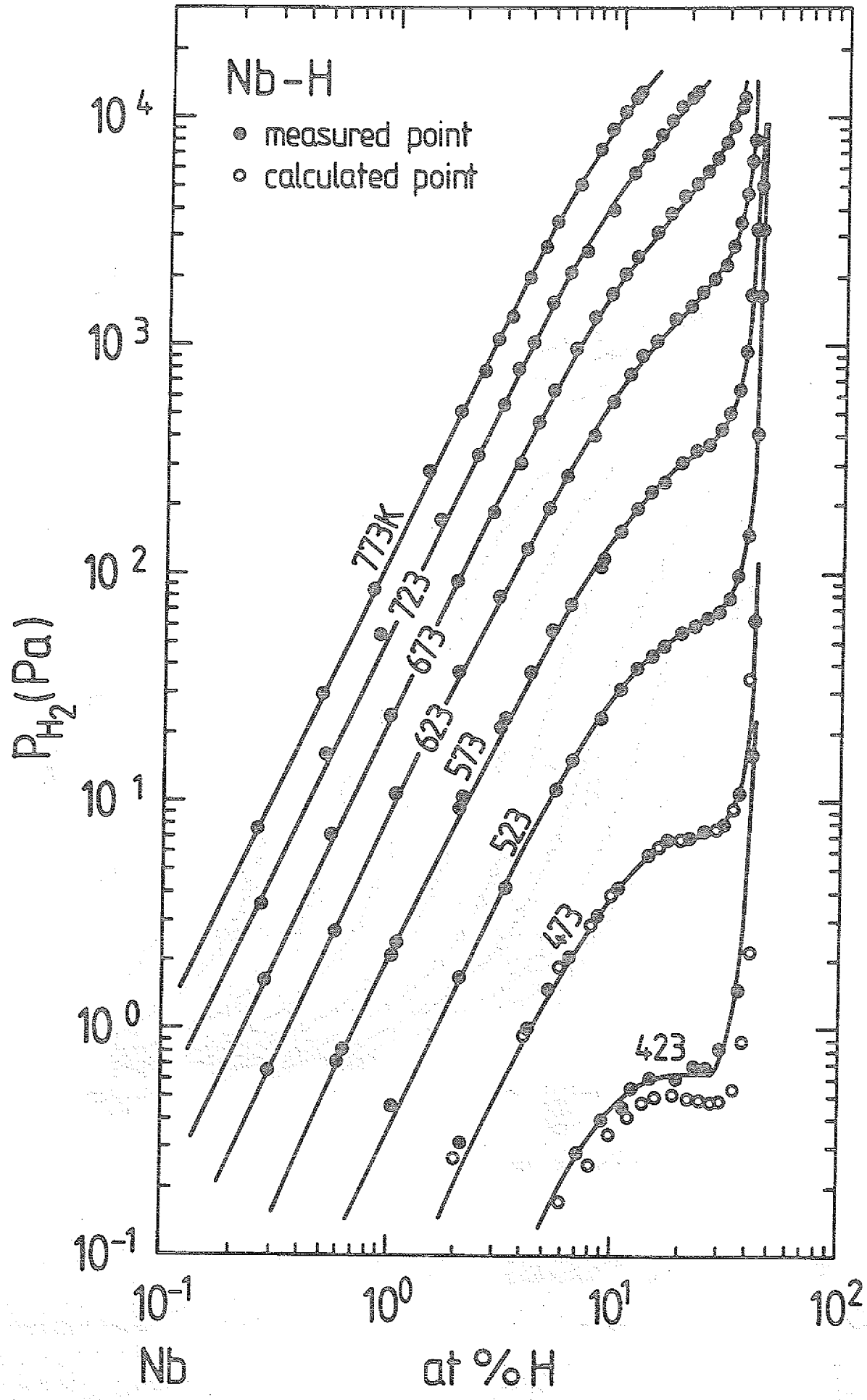

Fig. 15. p-c-T-curves for H and D in Nb including the high-temperature Sieverts regime [50]. (a) log p versus at.% - isotope H

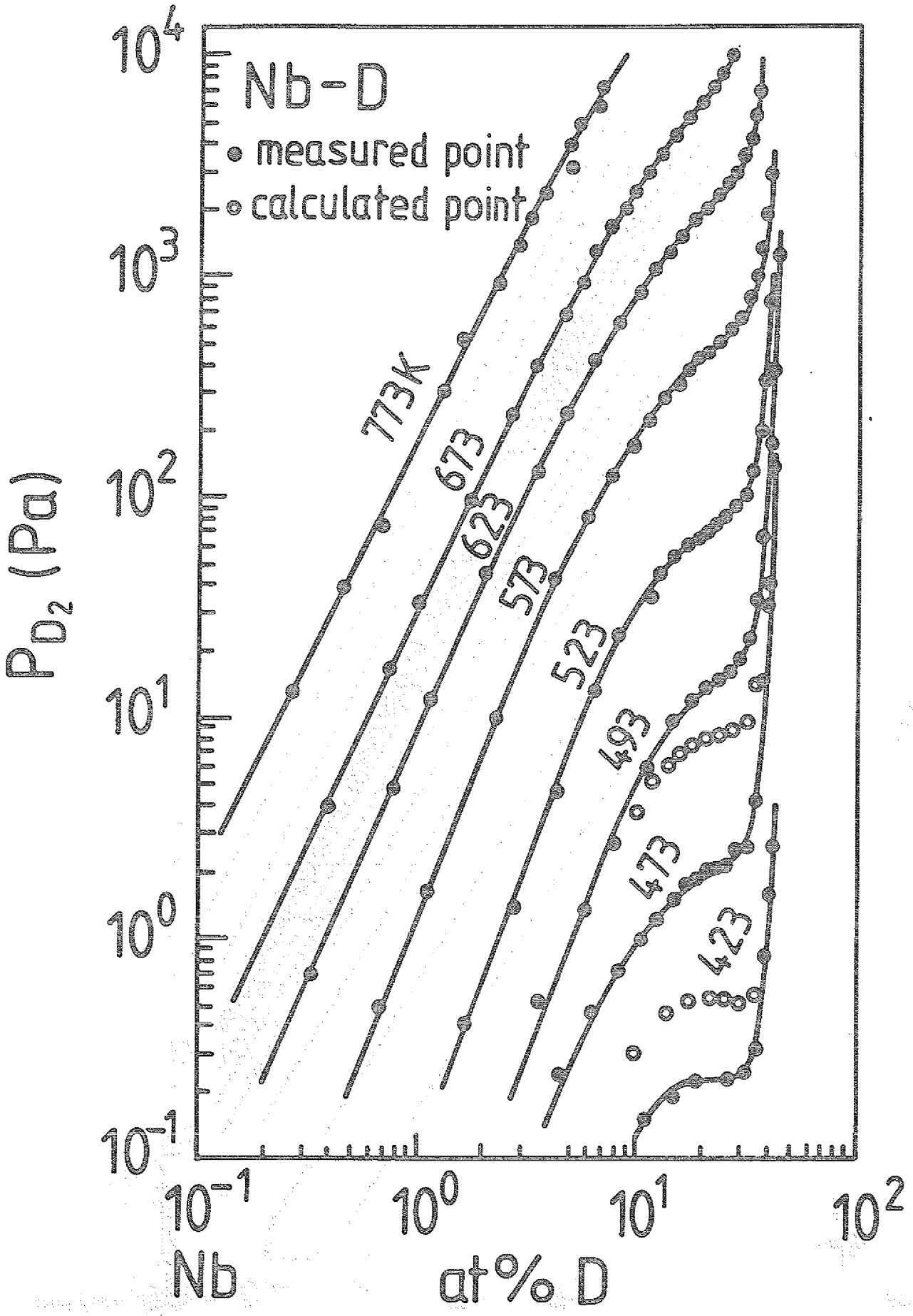

Fig. 15 (b) log p versus at.% - isotope D

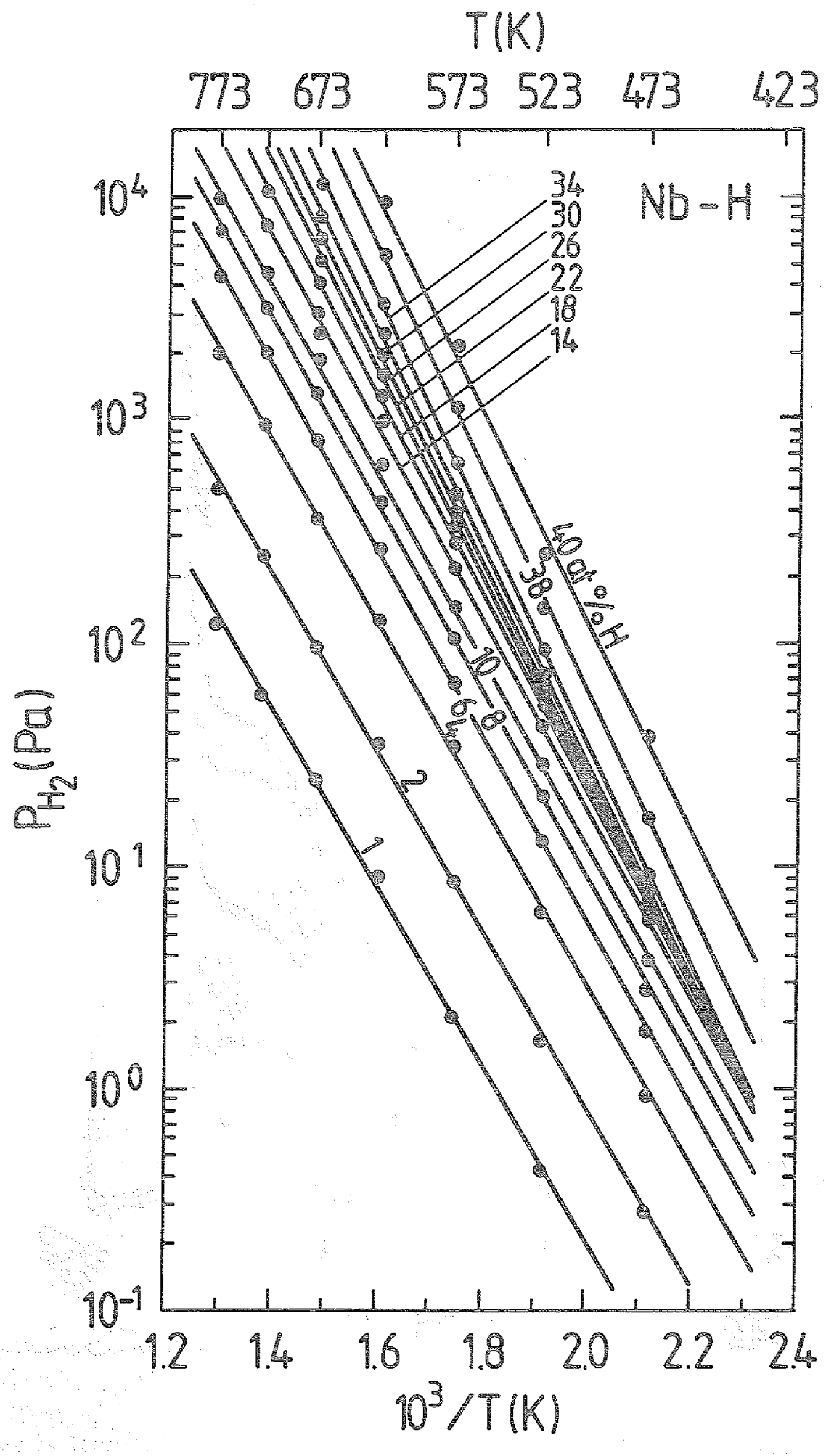

Fig. 16. p-c-T-curves for H in Nb [50]. Plot of log p versus 1/T.

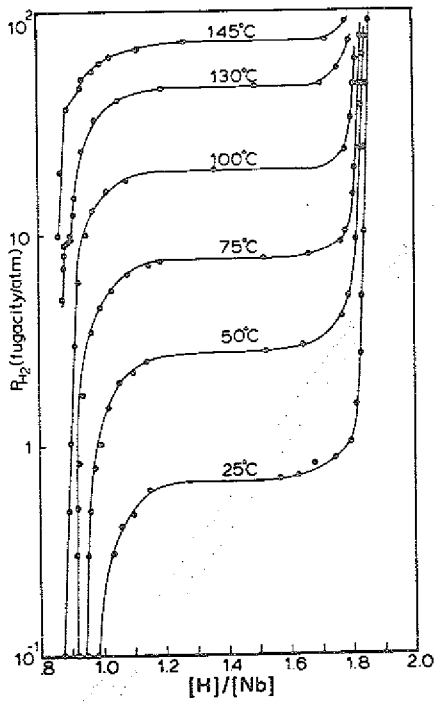

Fig. 17. p-c-T-curves in the $\beta+\delta$ two-phase region [41].

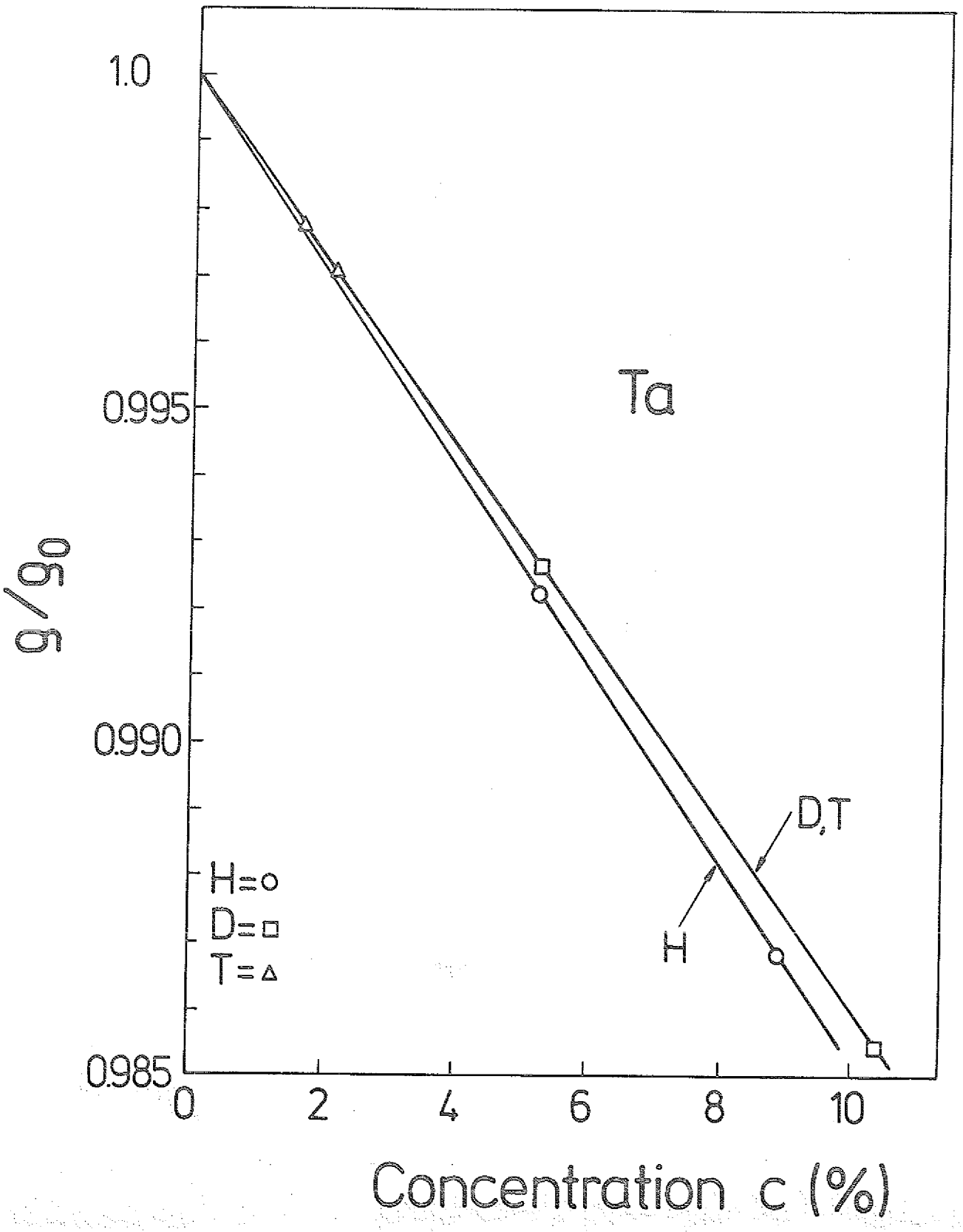

Fig. 18. Precision density data for H, D, T for low c's [8] as obtained with a buoyancy technique. Note quasi -linear decrease. It is fortuitous that the protium and tritium curves coincide.

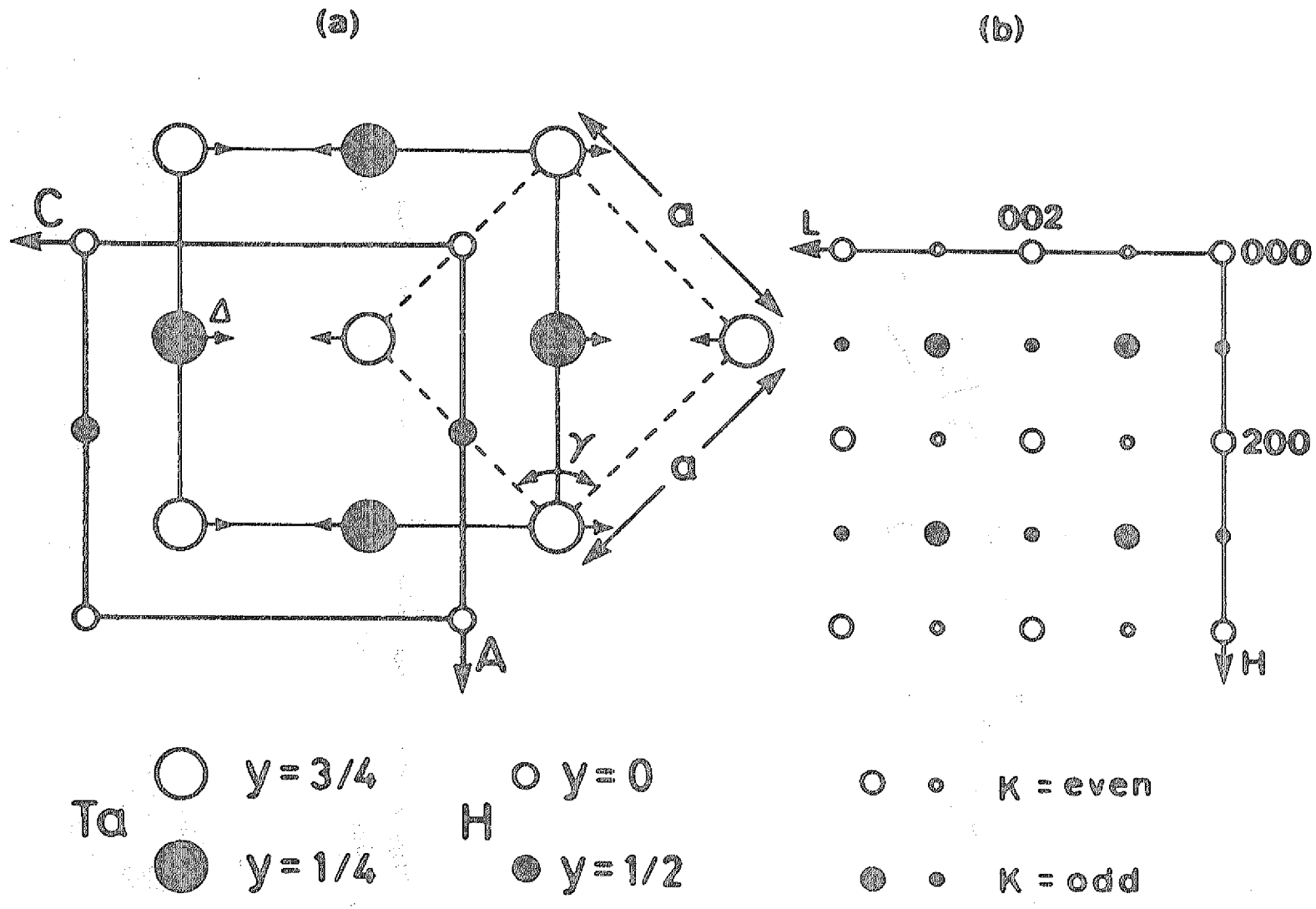

Fig. 19. Crystal structure of the β-TaH phase [66].

(a) real lattice. The monoclinic metal lattice is shown by dashed lines.

(b) reciprocal lattice, small circles denote superlattice reflections.

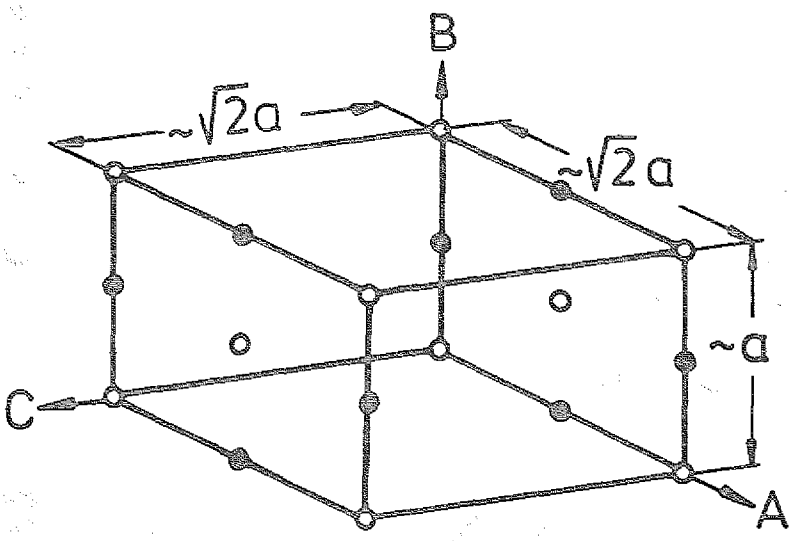

Fig. 19 (c) H(D) superlattice, open circles: full occupation in beta, occupation with probability 0.6 in phase ϵ, full circles: tetrahedral sites filled with probability 0.4 in phase ϵ.

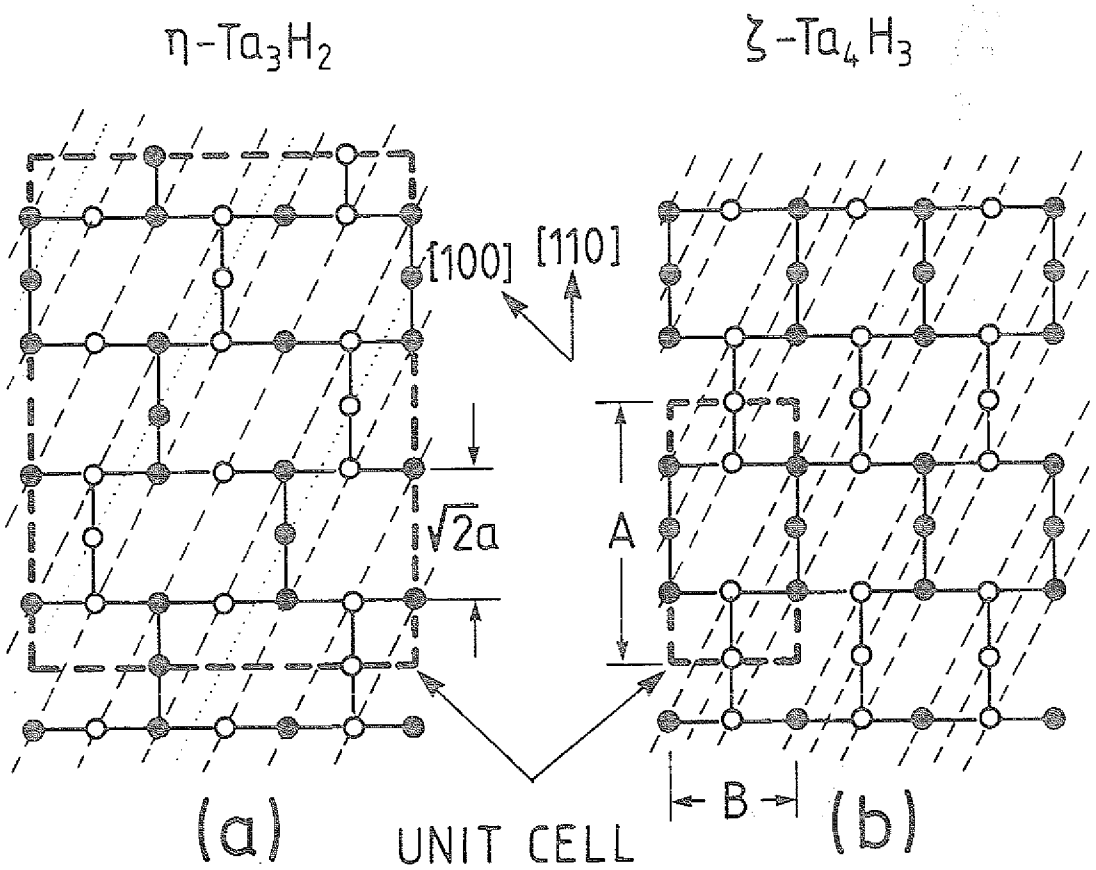

Fig. 20. Crystal structure of two low-temperature hydrides adapted after [67, 68].

(a) Structure of η-Ta_3H_2. Hydrogen arrangement is projected on (001) plane. Open and full circles denote H atoms at the T-sites with z=1/4 and z=3/4, respectively. Broken lines denote concentration wave parallel to $[3\bar{1}0]$

(b) Structure of ζ.

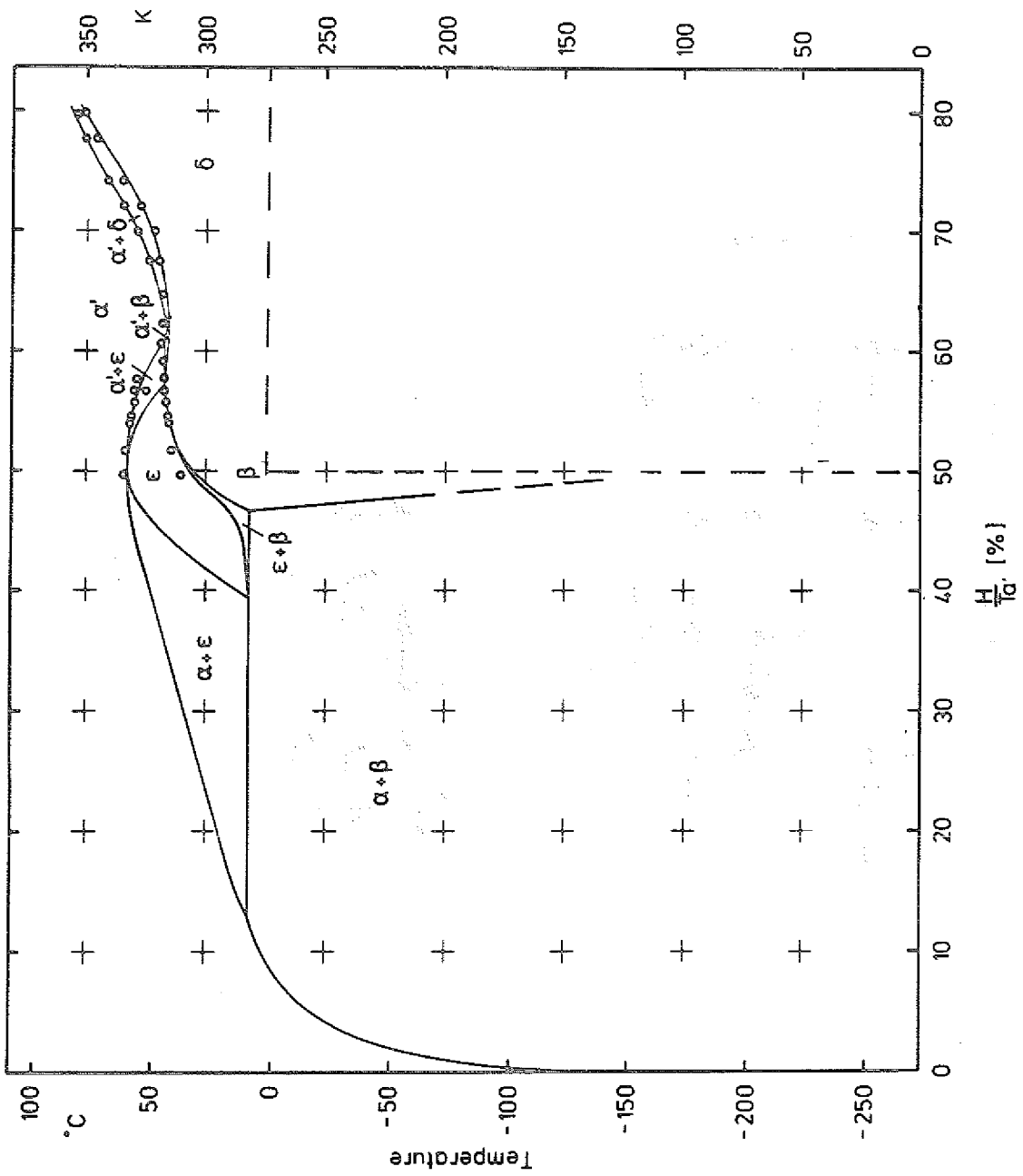

Fig.21. The Ta-H-diagram [72]. Only transitions above room temperature are shown. For low temperature transformations,

see Fig. 24 [70]. Arbitrarily, we do not distinguish here between β and δ.

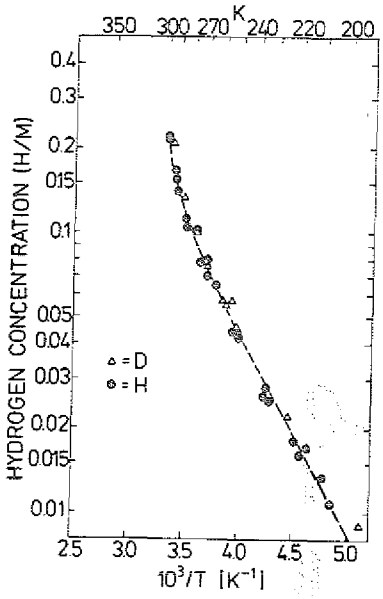

Fig.22. The Ta-H, Ta-D solvus after [4, 73]. There is no visible isotope effect. For a thermodynamic analysis see [74].

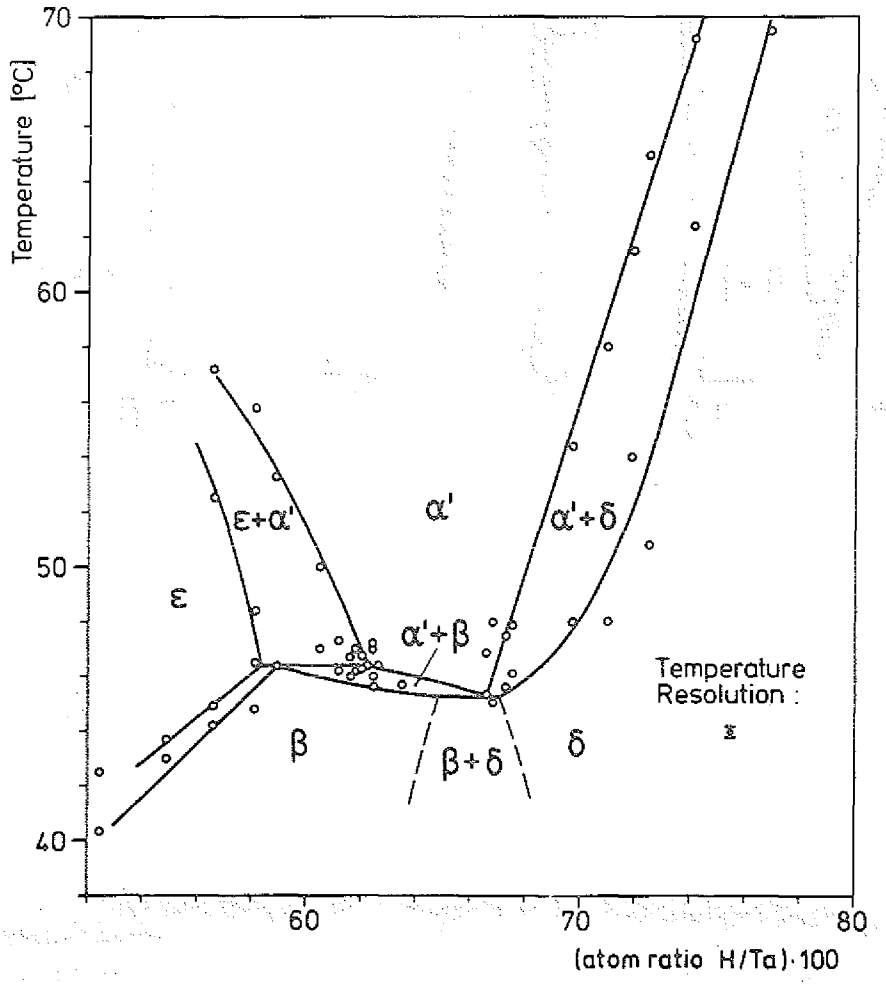

Fig.23. Partial Ta-H phase diagram [72] established with very low heating rates and precise temperature and concentration control.

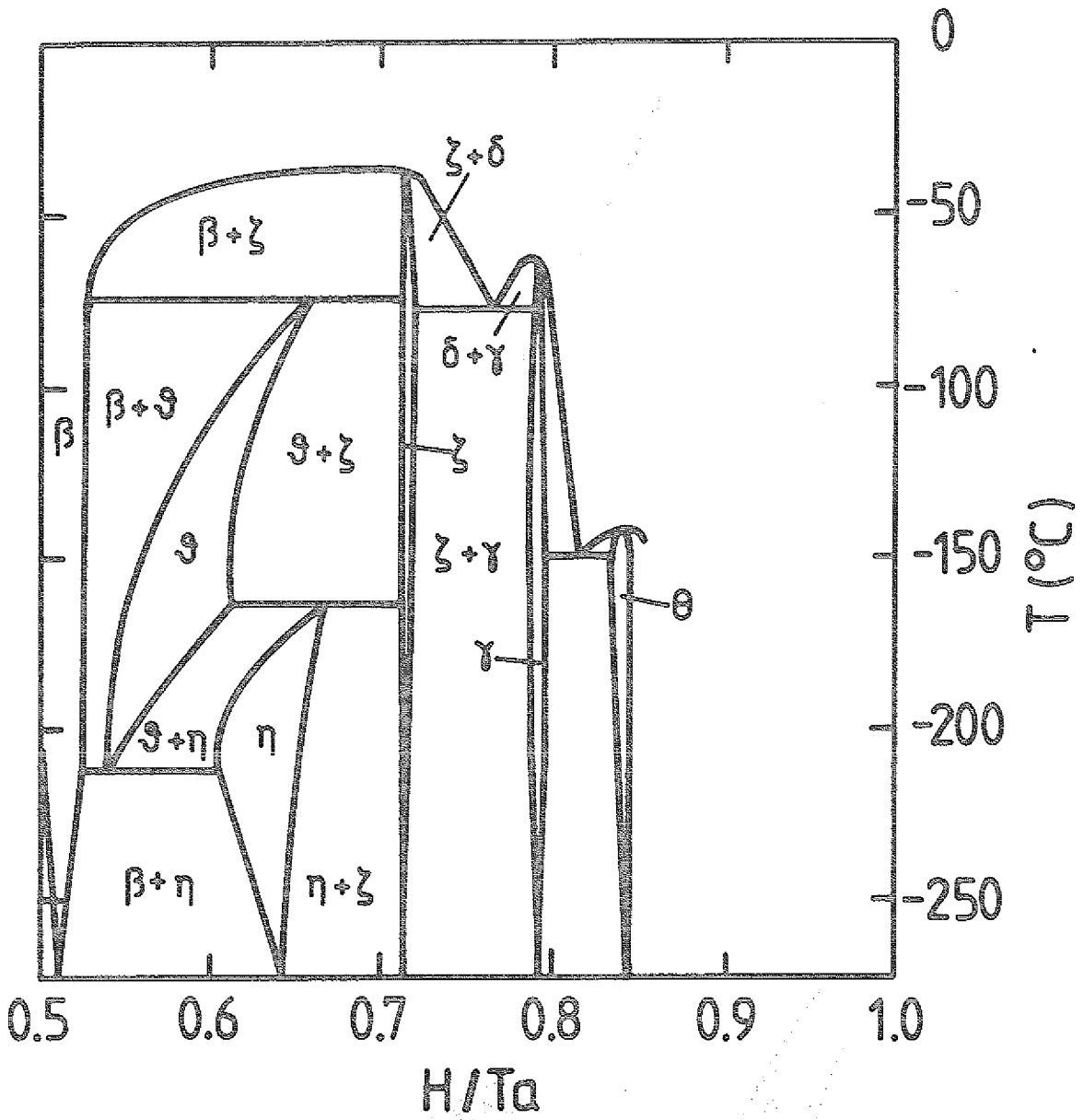

Fig.24. Low temperature Ta-H phase diagram, adapted after [18, 70].

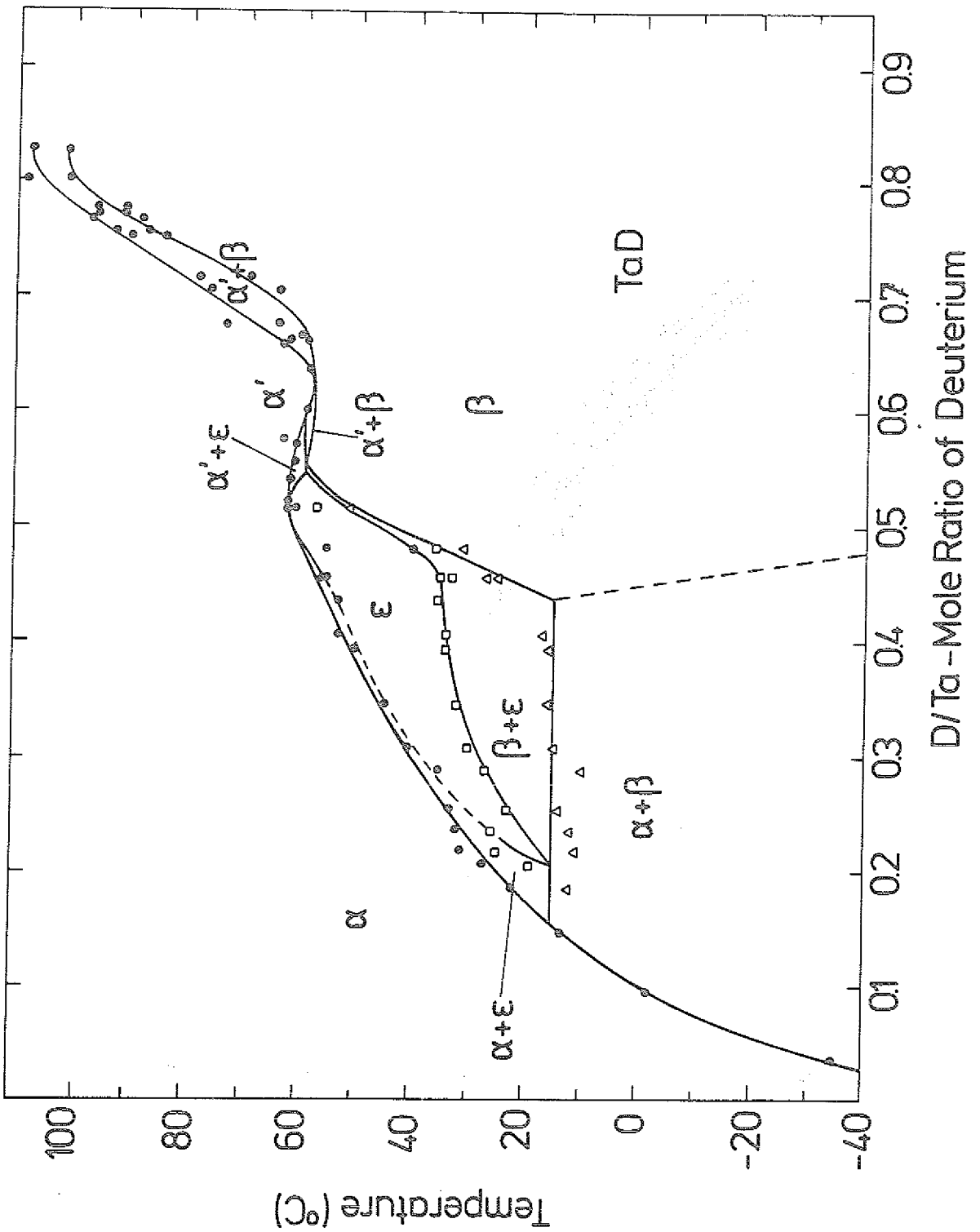

Fig.25. The Ta-D phase diagram [73]. Low temperature transitions are not shown. No difference is made between β and δ.

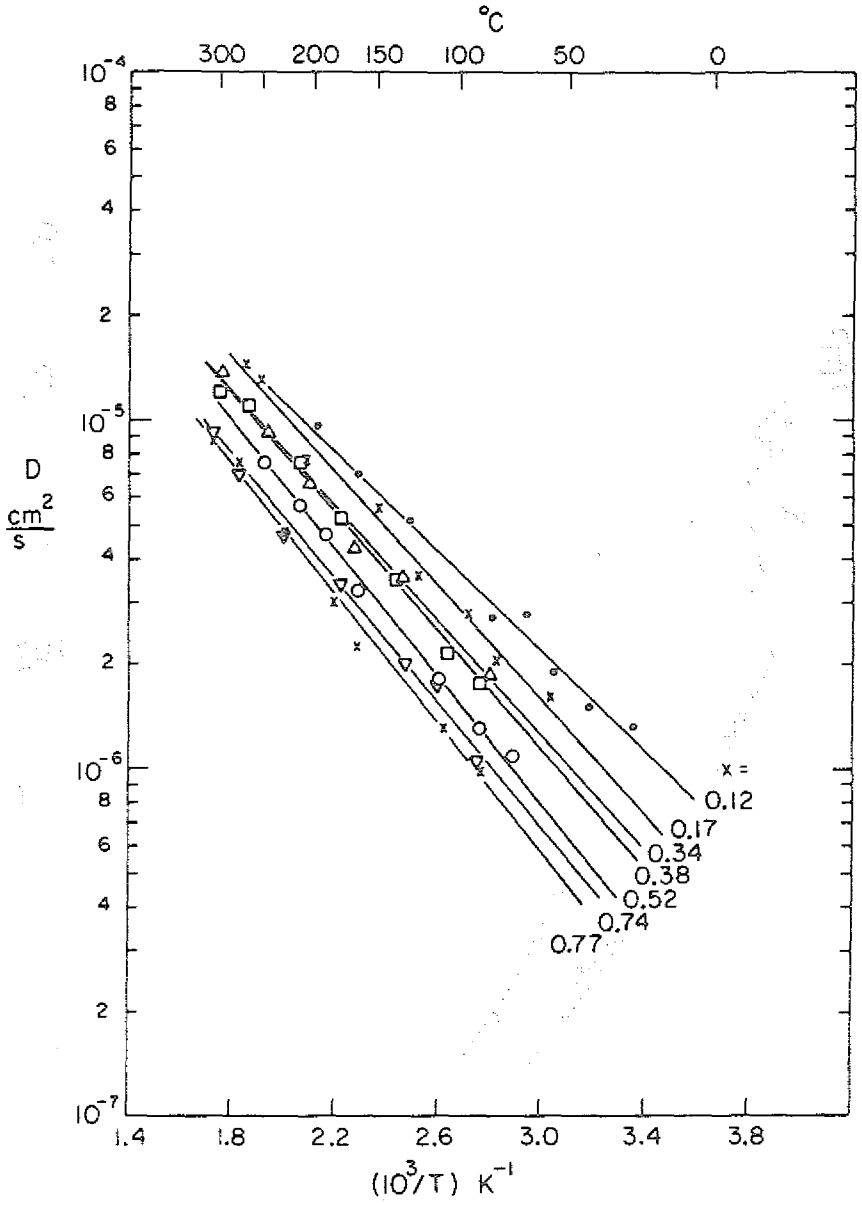

Fig.26 . NMR derived, concentration dependent diffusivities of H in Ta [76].

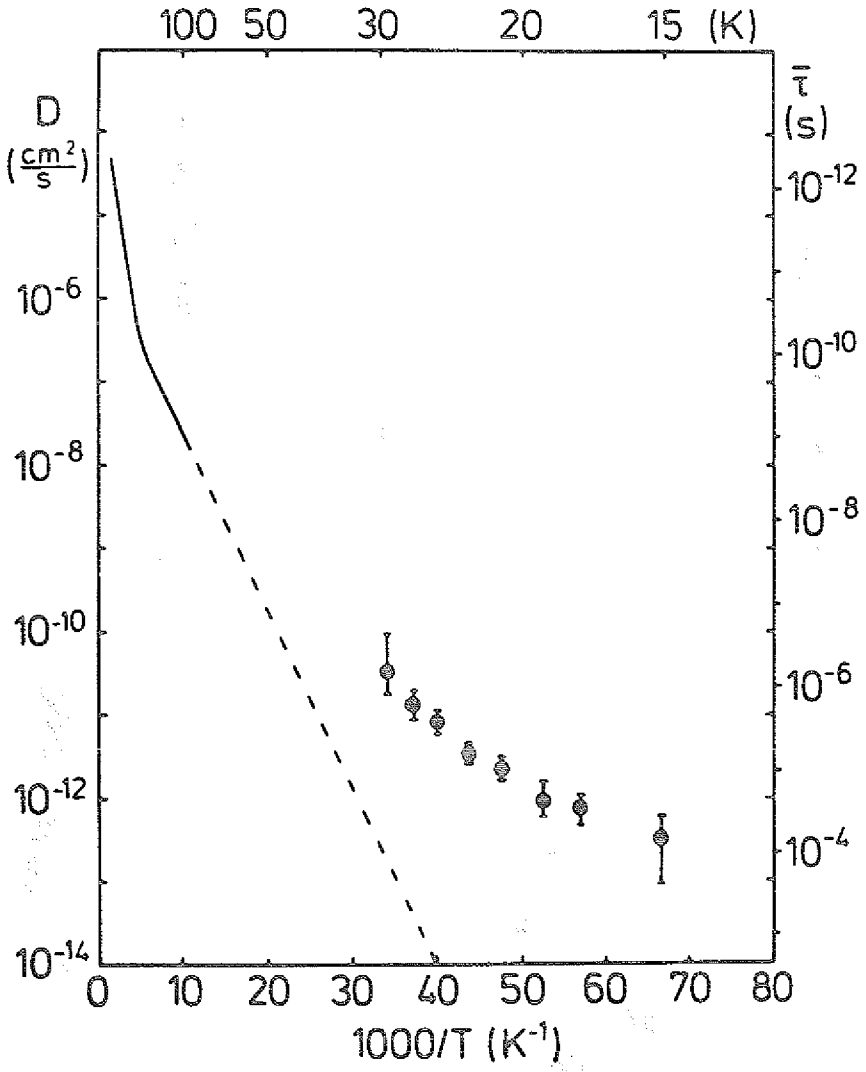

Fig. 27. Diffusivity of H in Ta for T<30 K as obtained with a nuclear technique after [78]. The extrapolation of the high-temperature data is depicted.

Fig. 28. Gorsky type diffusivities of H in the alloy $TaH_{0.52}$ [79]. Depending on temperature this alloy is in phase α, β or ϵ.

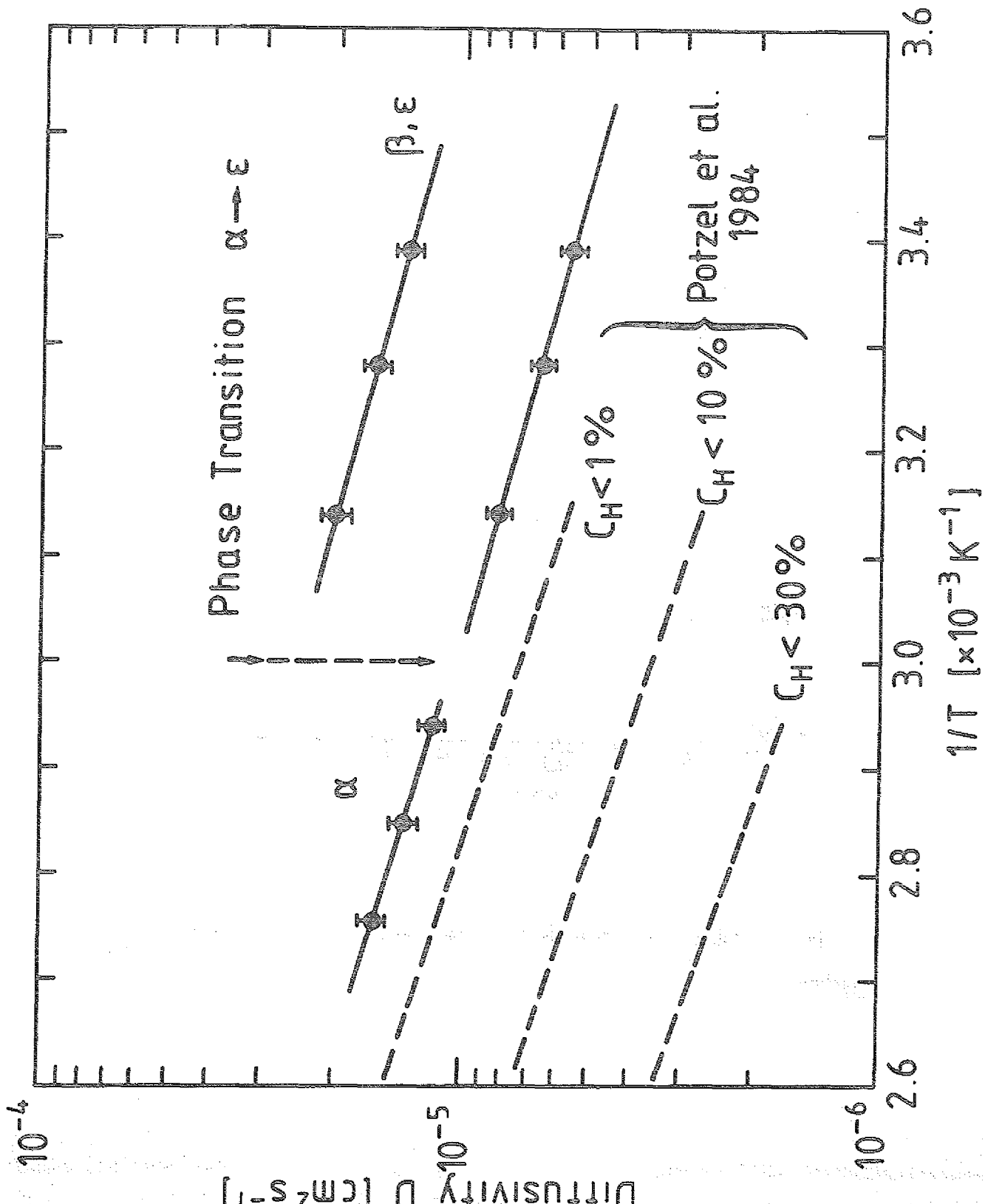

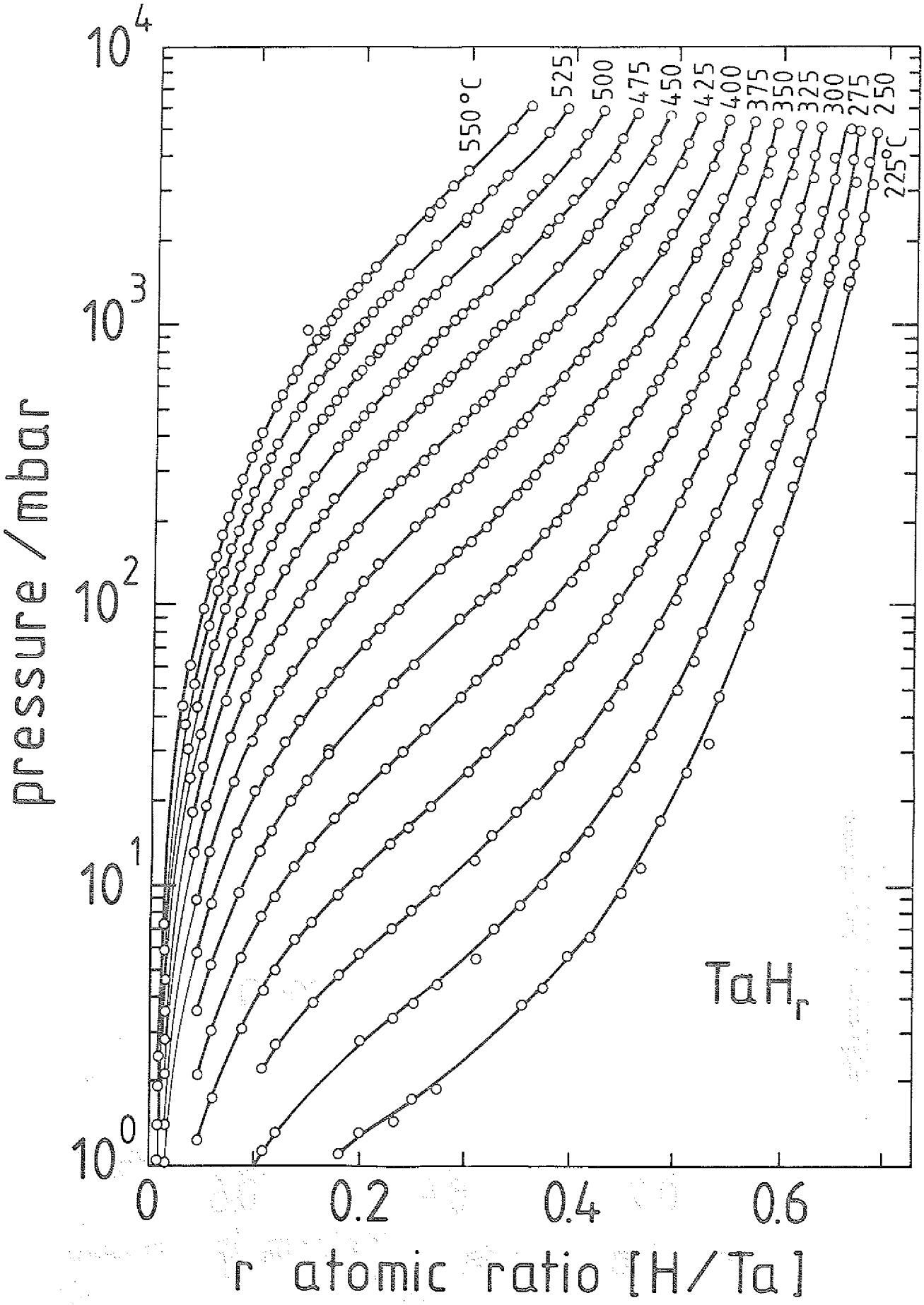

Fig.29. General p-c-T behavior of H in Ta [49].

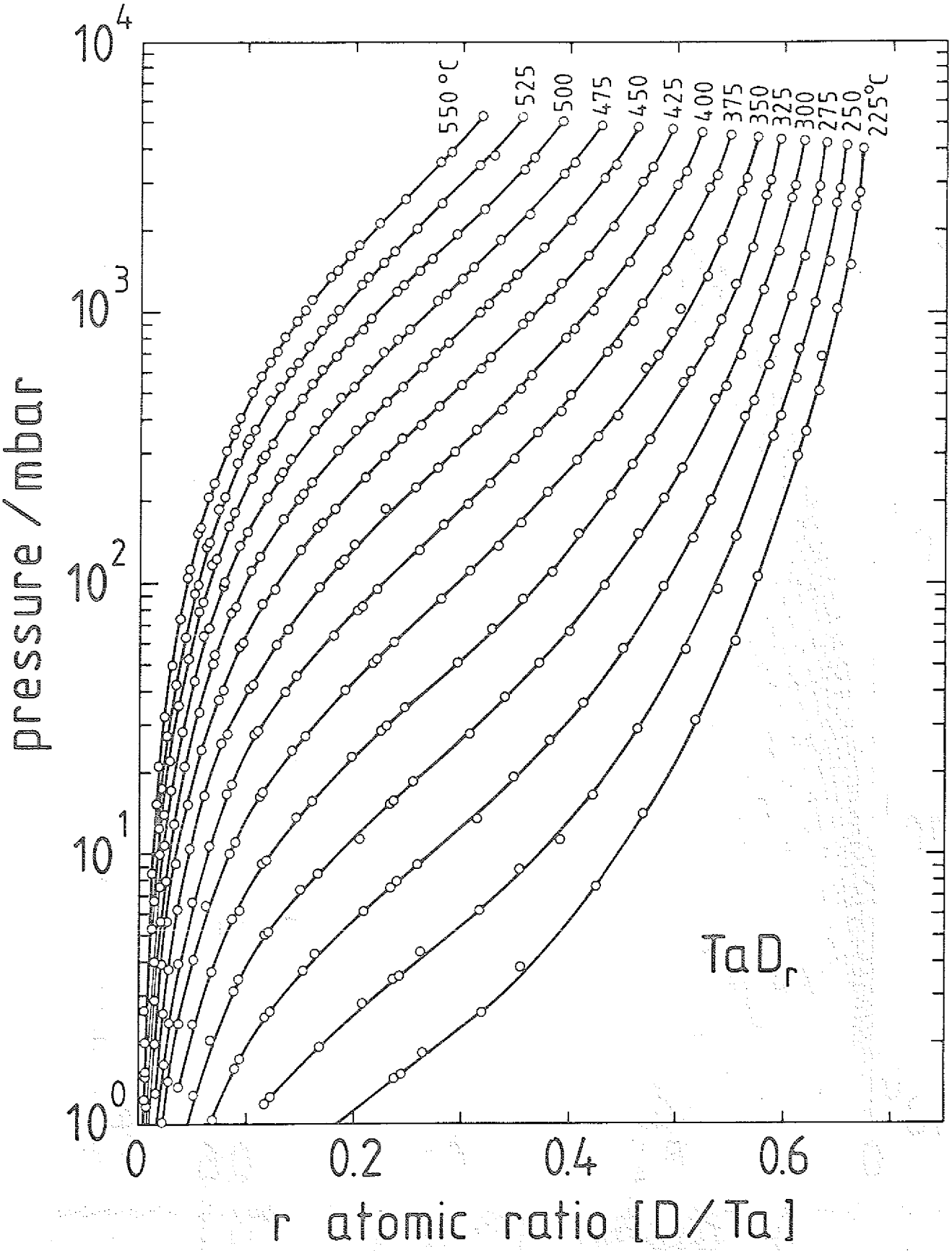

Fig.30. General p-c-T behavior of D in Ta [49].

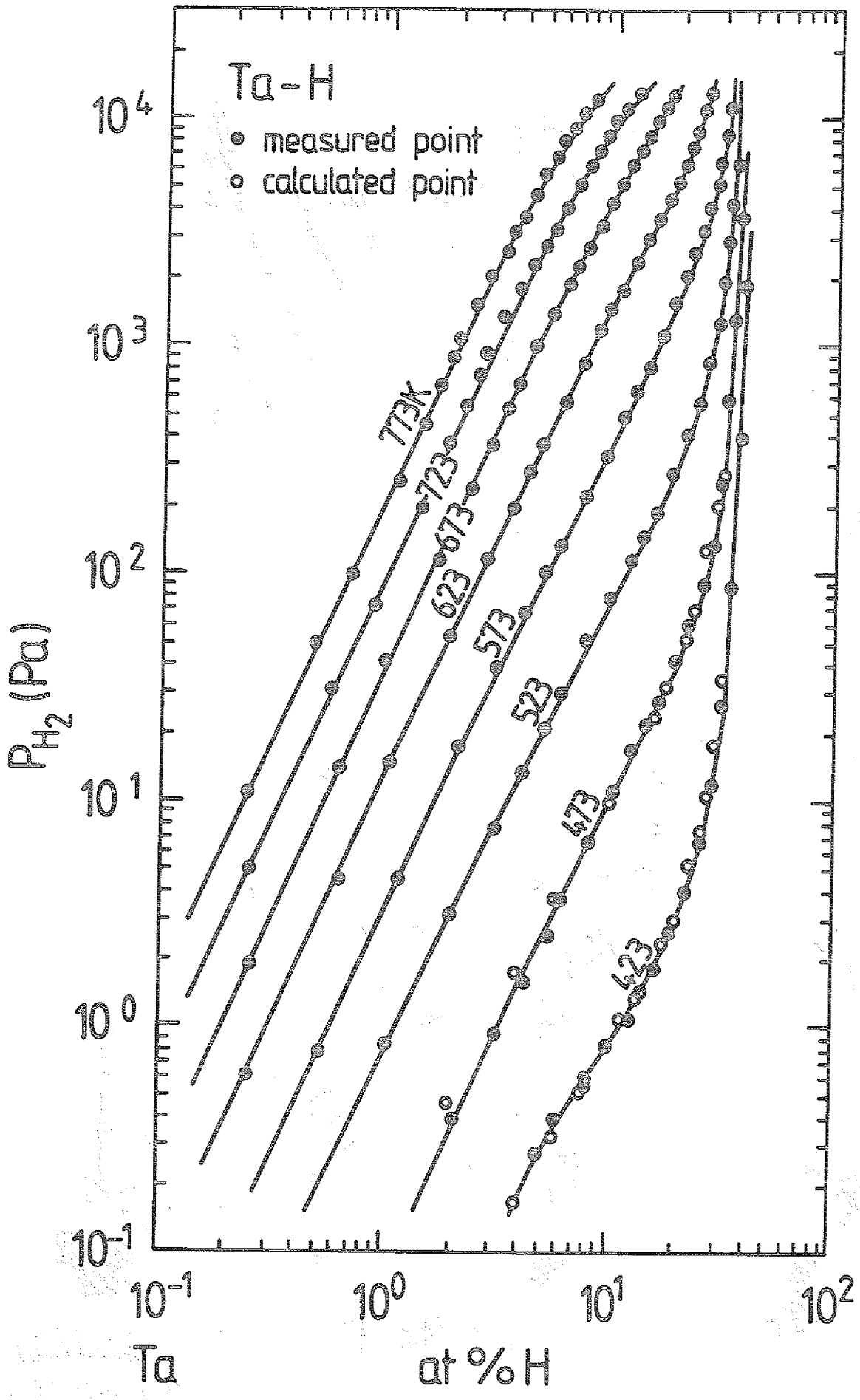

Fig. 31. p-c-T-curves for H and D in Ta [50].

(a) log p versus at.% - isotope H

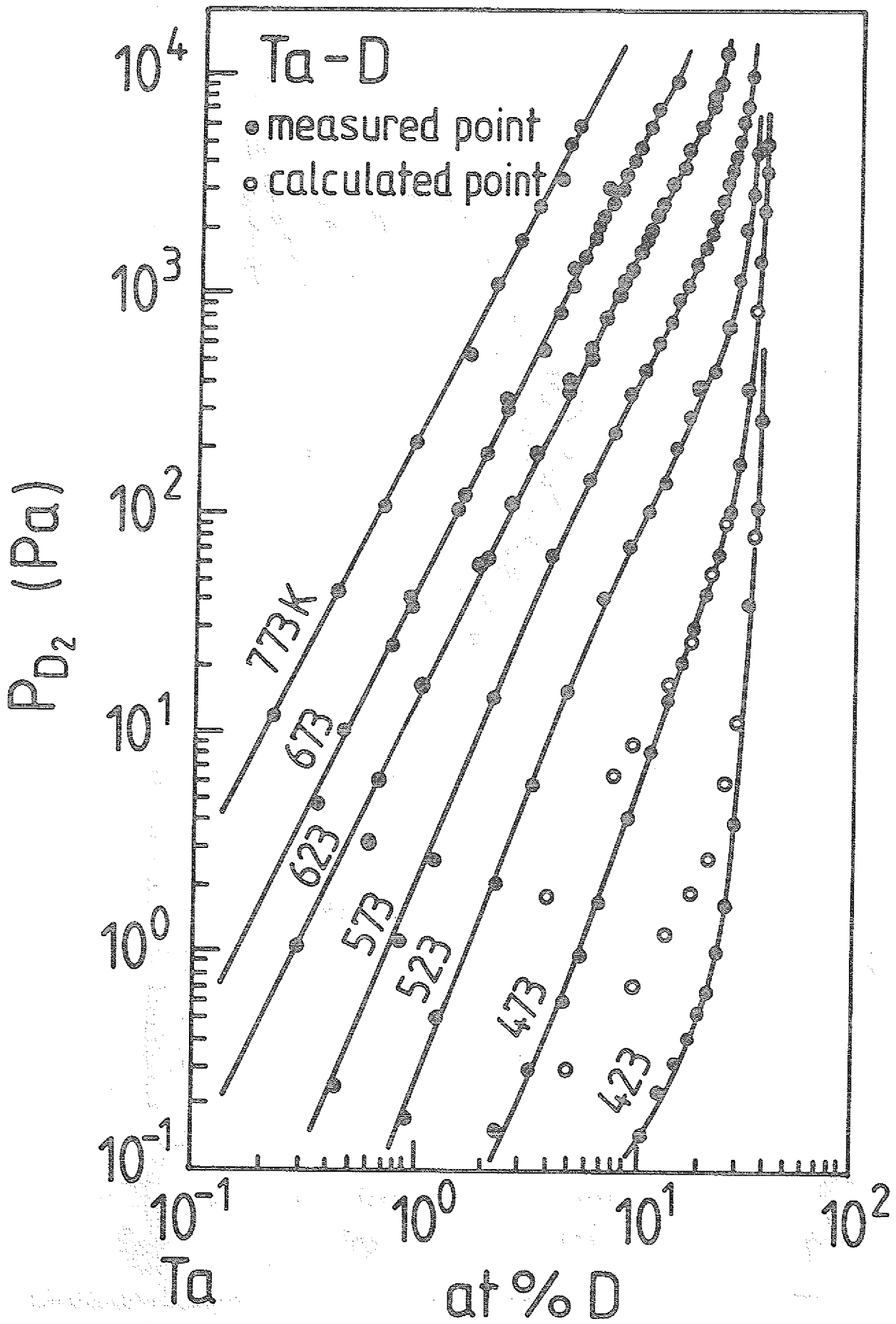

Fig. 31 (b) log p versus at.% - isotope D

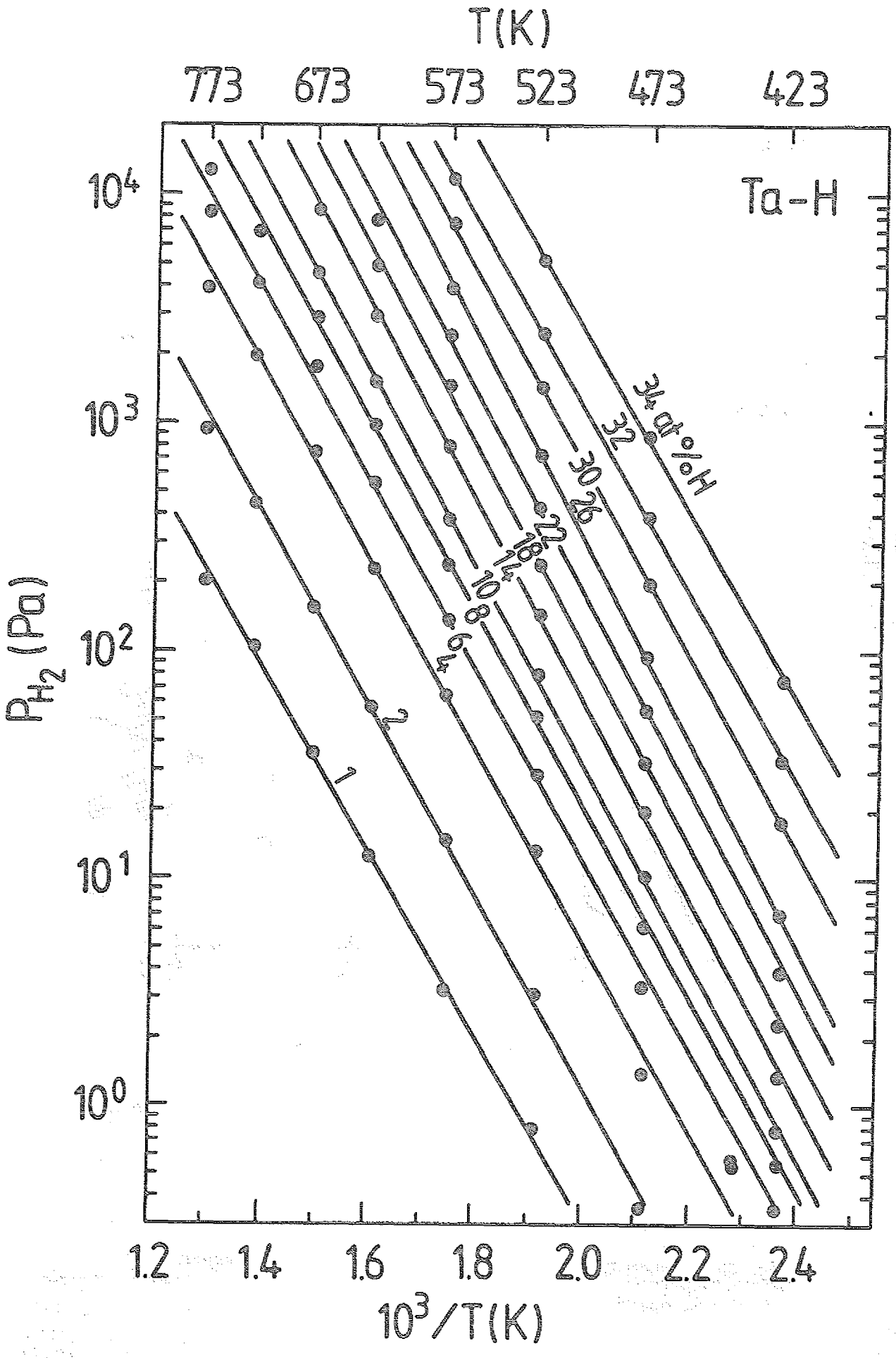

Fig. 32. p-c-T-curves for H in Ta [50]. log p vs. 1/T representation.

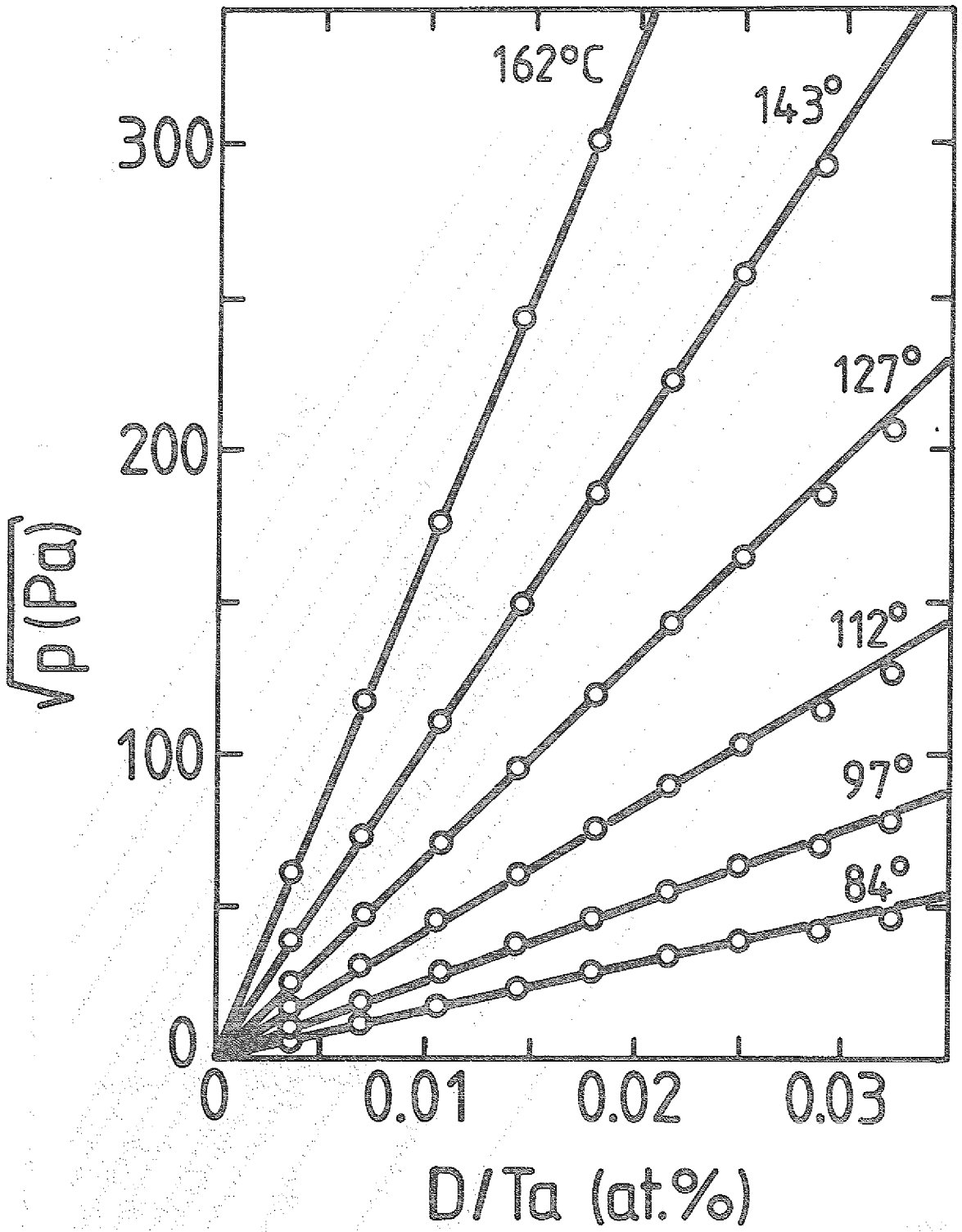

Fig. 33. Sieverts type curves for D in Ta [80]. We do not expect a considerable isotope effect.

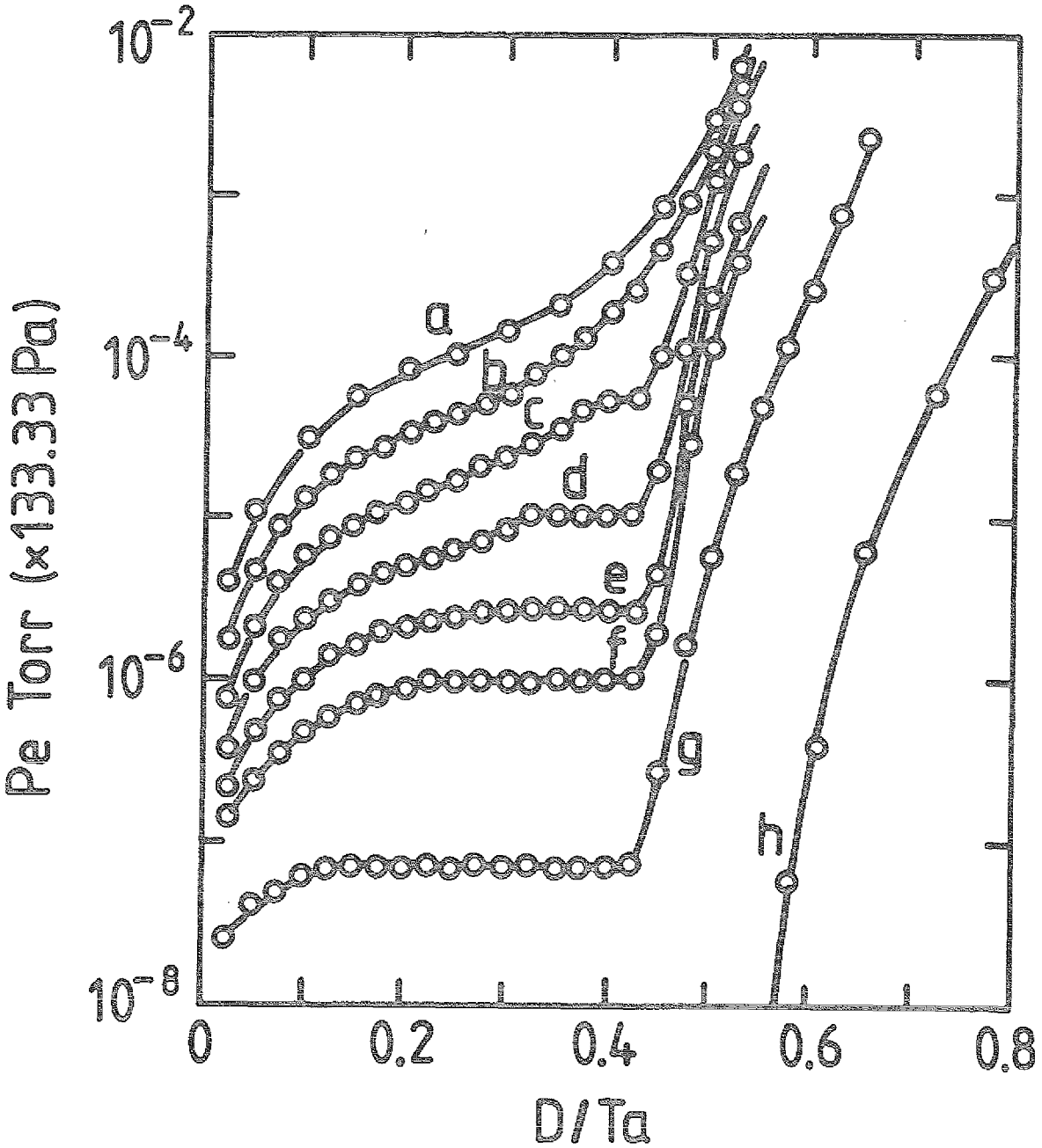

Fig. 34: p-c-T data in the two-phase region (α + ordered phase)
a: 70 °C, b: 60 °C, c: 50 °C, d: 40 °C
e: 30 °C, f: 22.5 °C, g: 0 °C, h: -78 °C

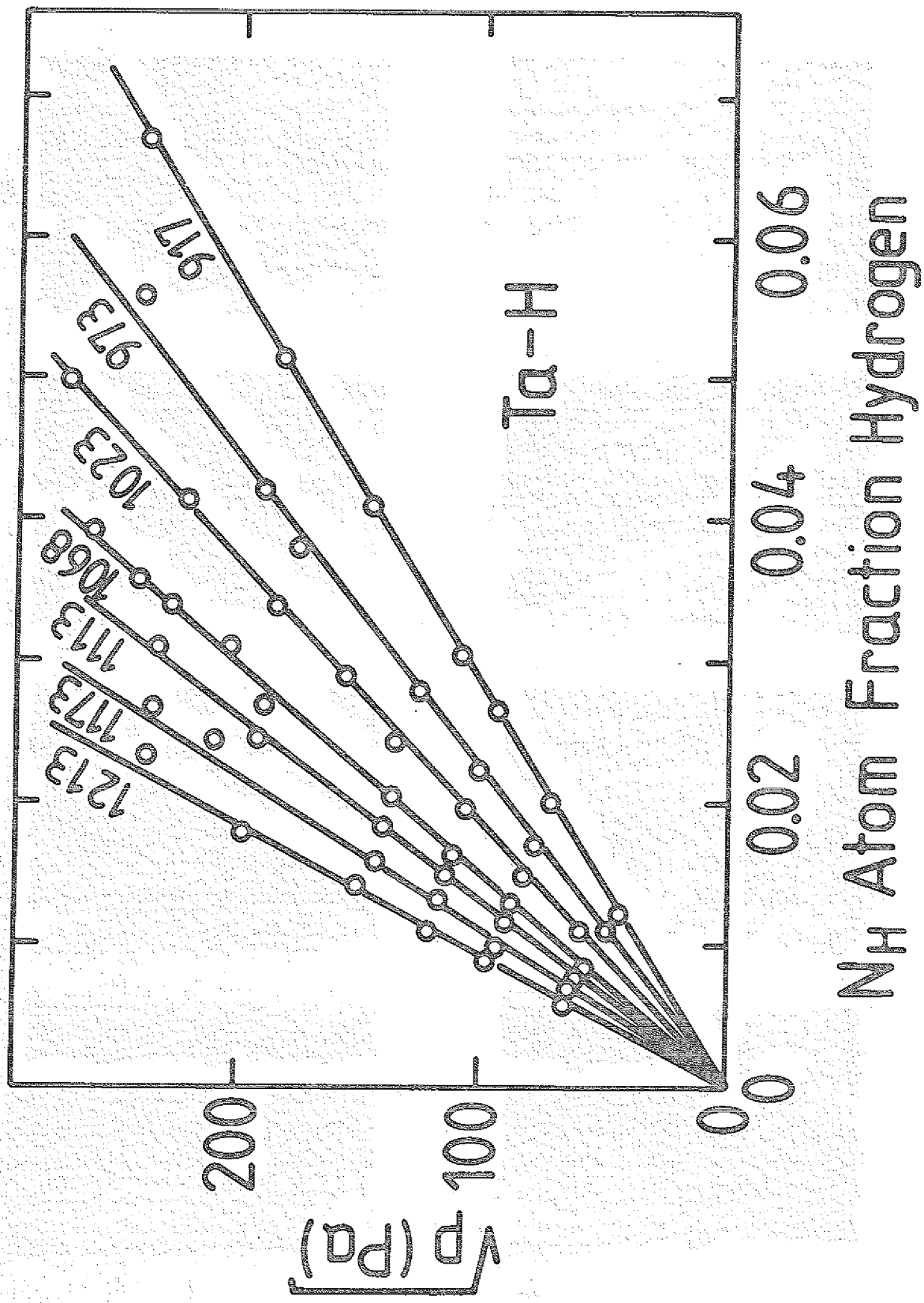

Fig. 35. Sieverts type curves for H in Ta extending to rather high temperatures [81].

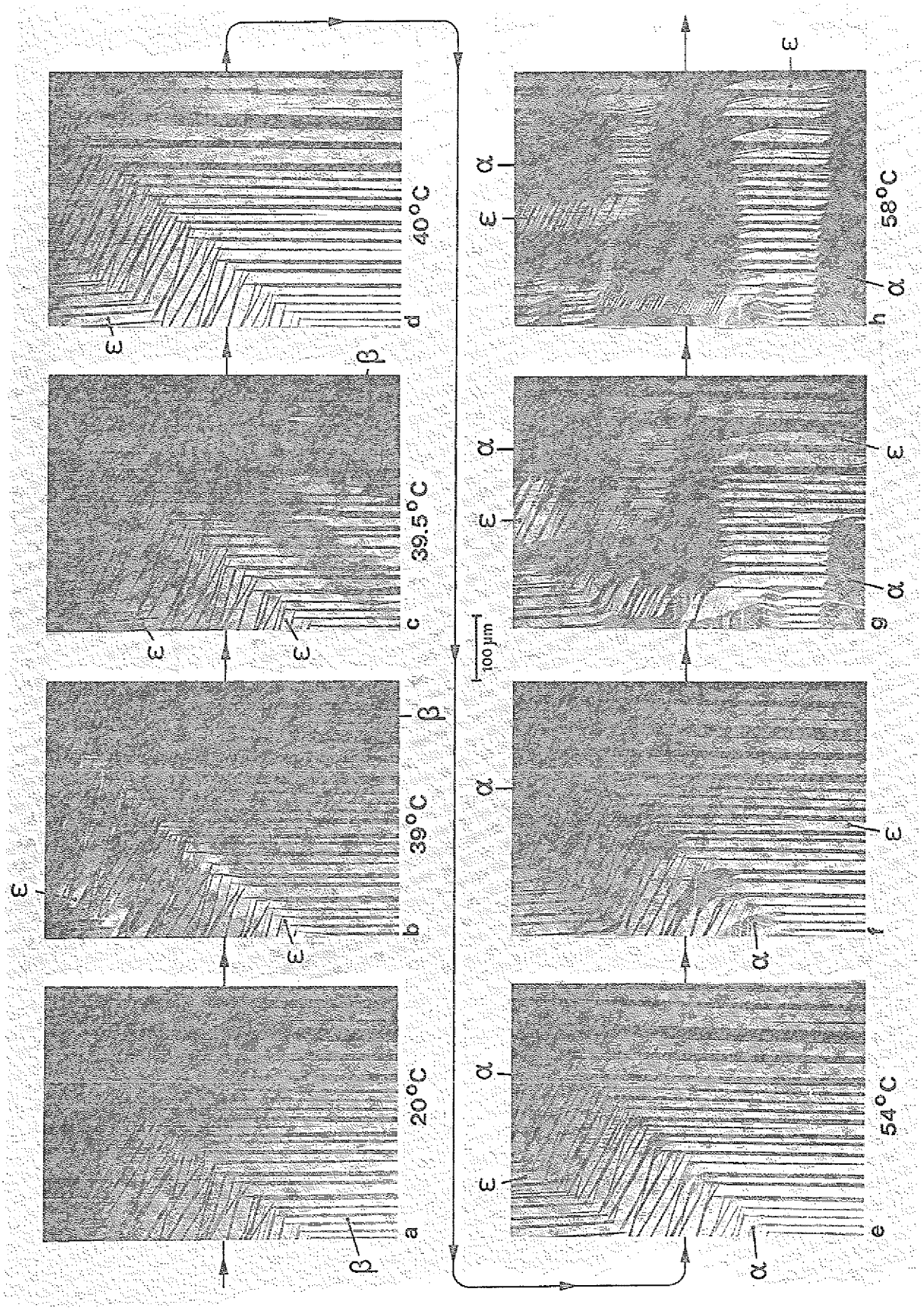

Fig. 36. Series of optical micrographs depicting in polarized light the β to ϵ to α transformation [2]. Phase ϵ appears much brighter than β. Striped regions are domains of the ordered phases. These domains are not present in the α- phase.

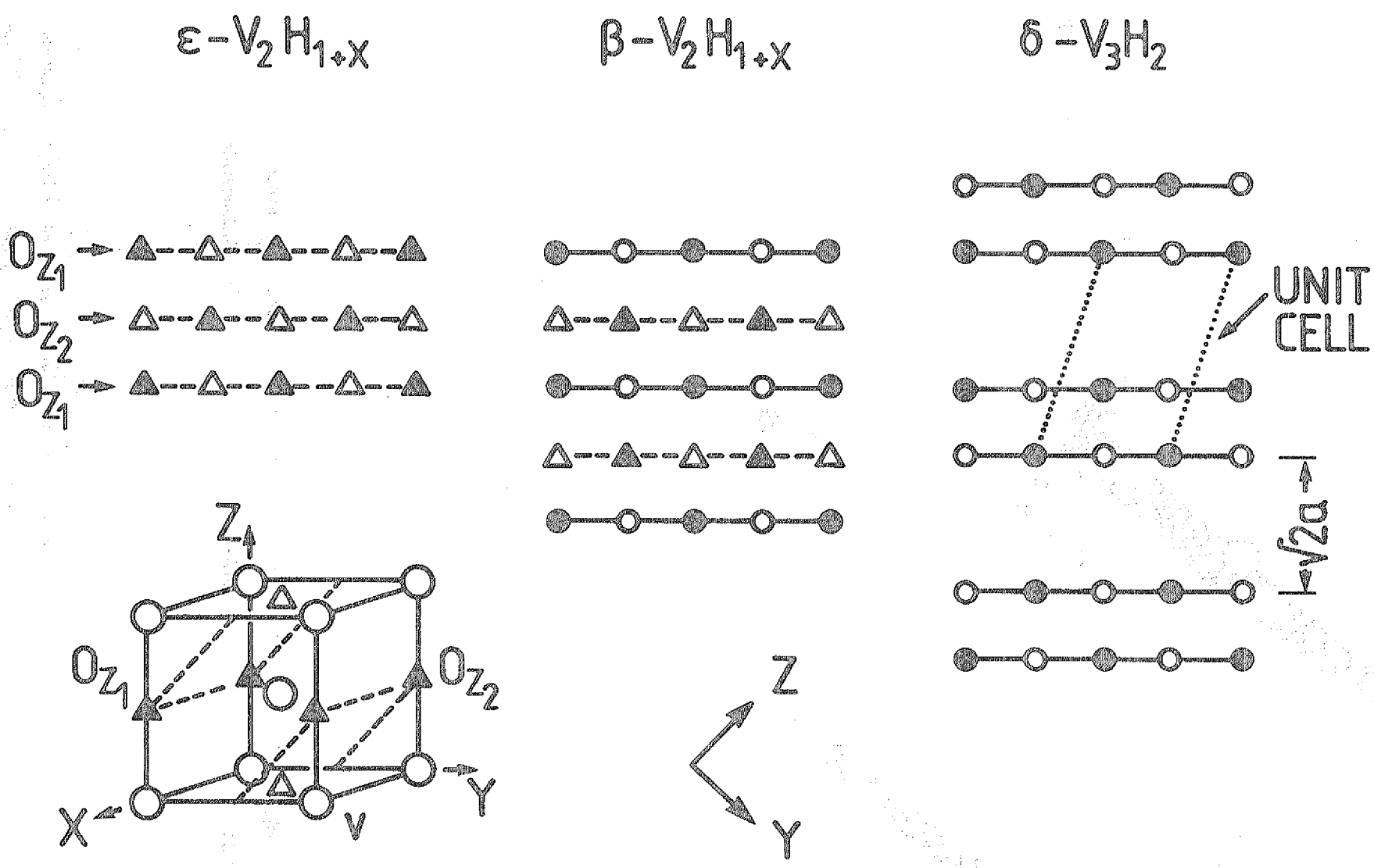

Fig. 37. The structures of hyperstoichiometric β, ϵ and δ-VH after [67, 68] as projected on (100)-plane. Full and open triangles indicate partly filled o_z- sites at x=0 and 1/2, respectively. Full and open small circles denote hydrogen atoms on the o_z sites of x=0 and 1/2, respectively.

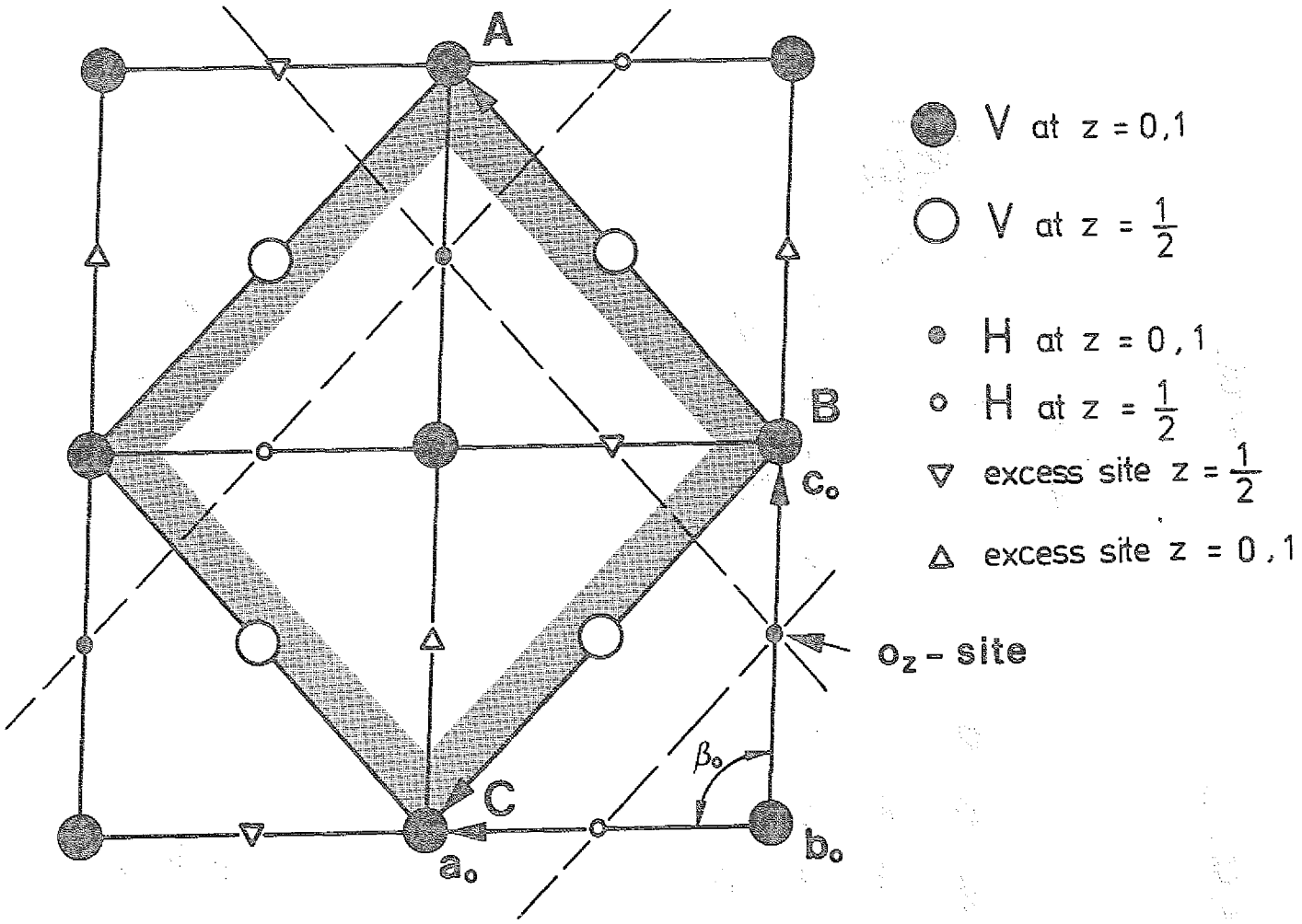

Fig.38. The monoclinic structure of the VH or VD β-phase. Most of the hydrogen atoms occupy octahedral sites. For more details, see deuteride Section.

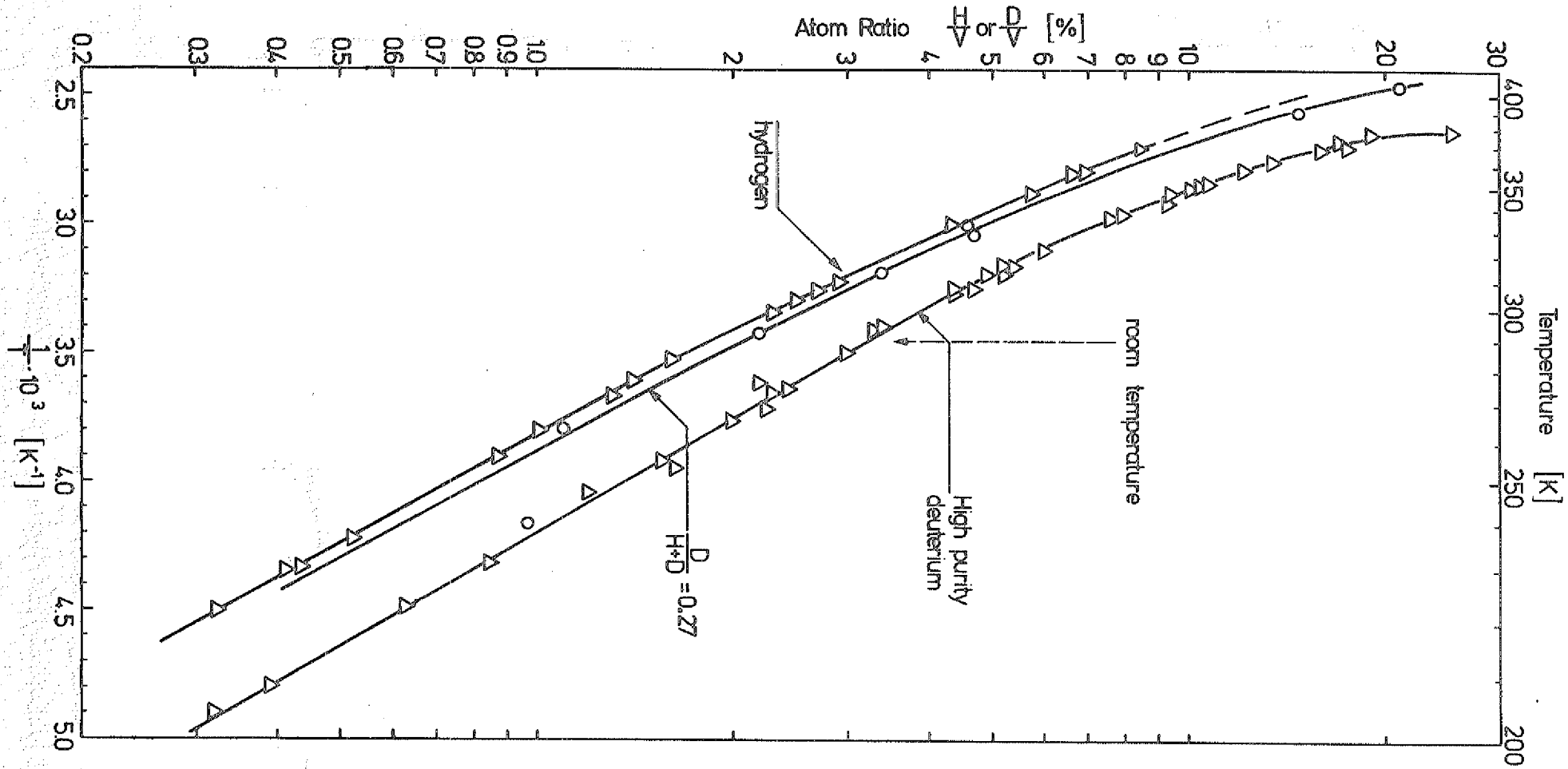

Fig. 39. Solvus for the VH and VD and a mixed system [96].

VH-solvus: $\Delta H = 0.1413 \pm 0.005$ eV and $c_o = 5.10 \pm 0.50$.

VD-solvus: $\Delta H = 0.135 \pm 0.004$ eV and $c_o = 7.00 \pm 0.70$. These enthalpies are the energies required to transfer one H atom from the ordered to the α phase.

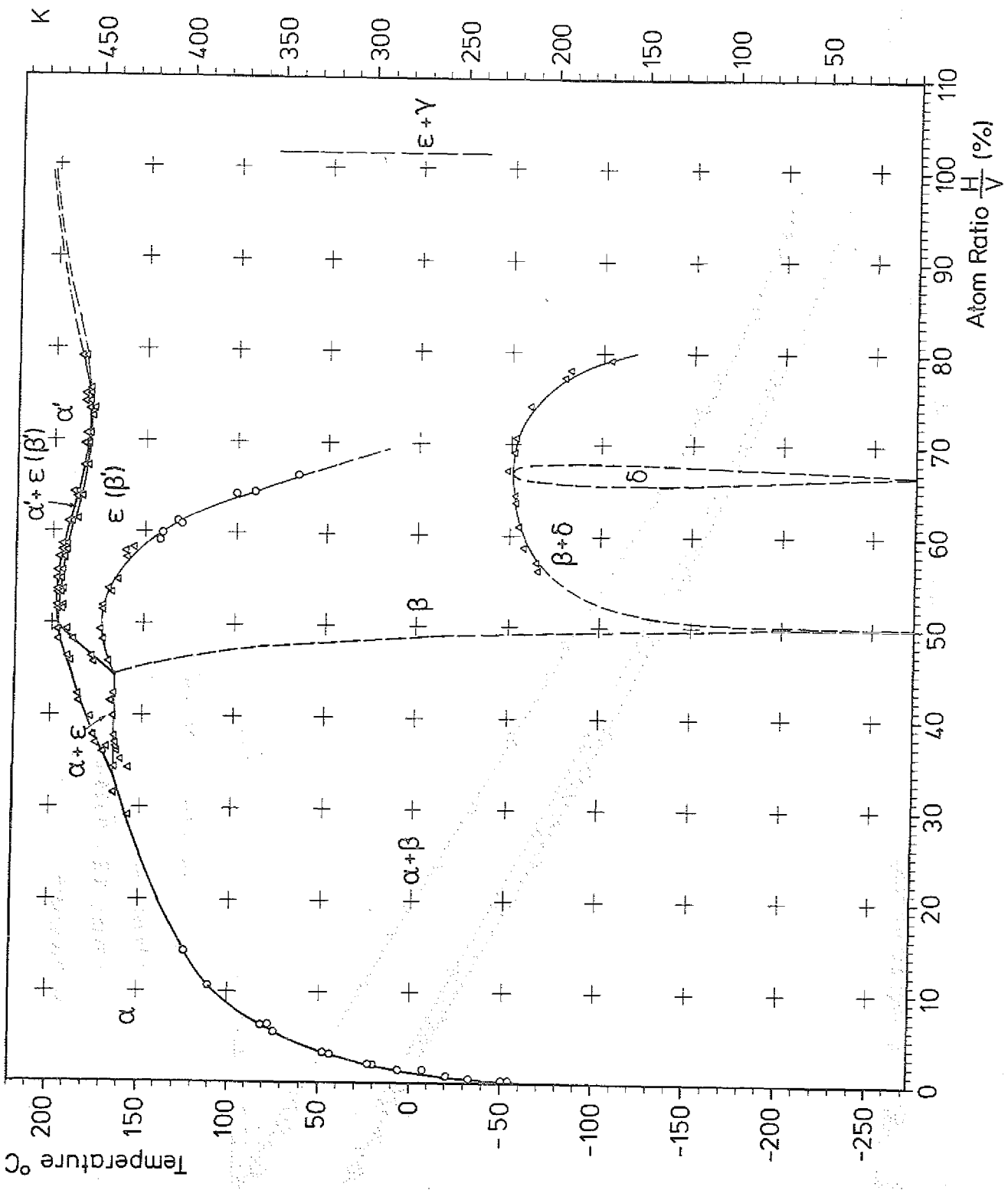

Fig. 40. V-H phase diagram derived from DTA data [4].The β to ϵ transition is of second order; there is a $(\beta + \delta)$ two-phase region.

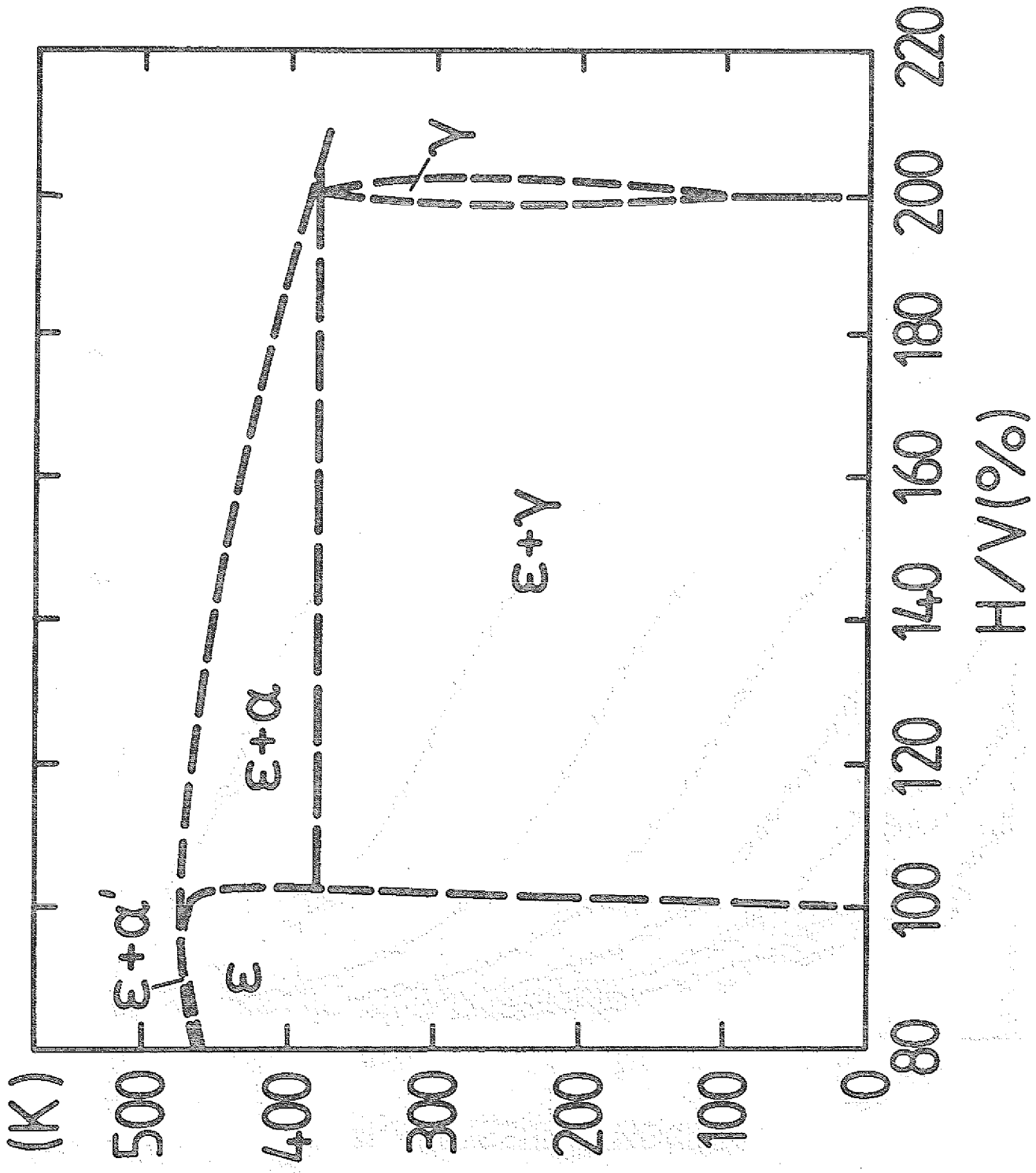

Fig. 41. Partial high-concentration diagram covering the range from c= 0.80 to 2.0 [97].

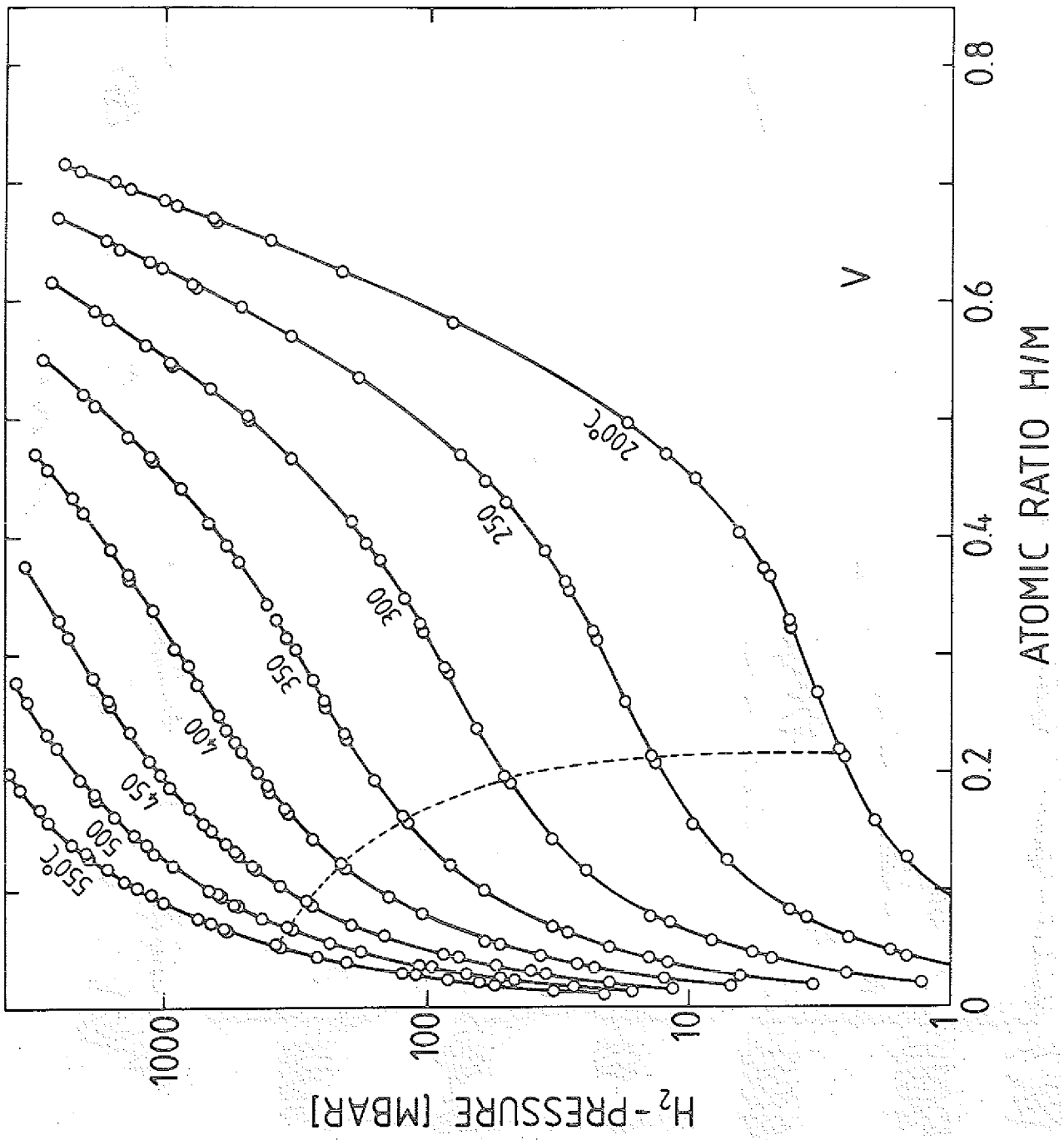

Fig. 42. General p-c-T-curves for H in V [102].

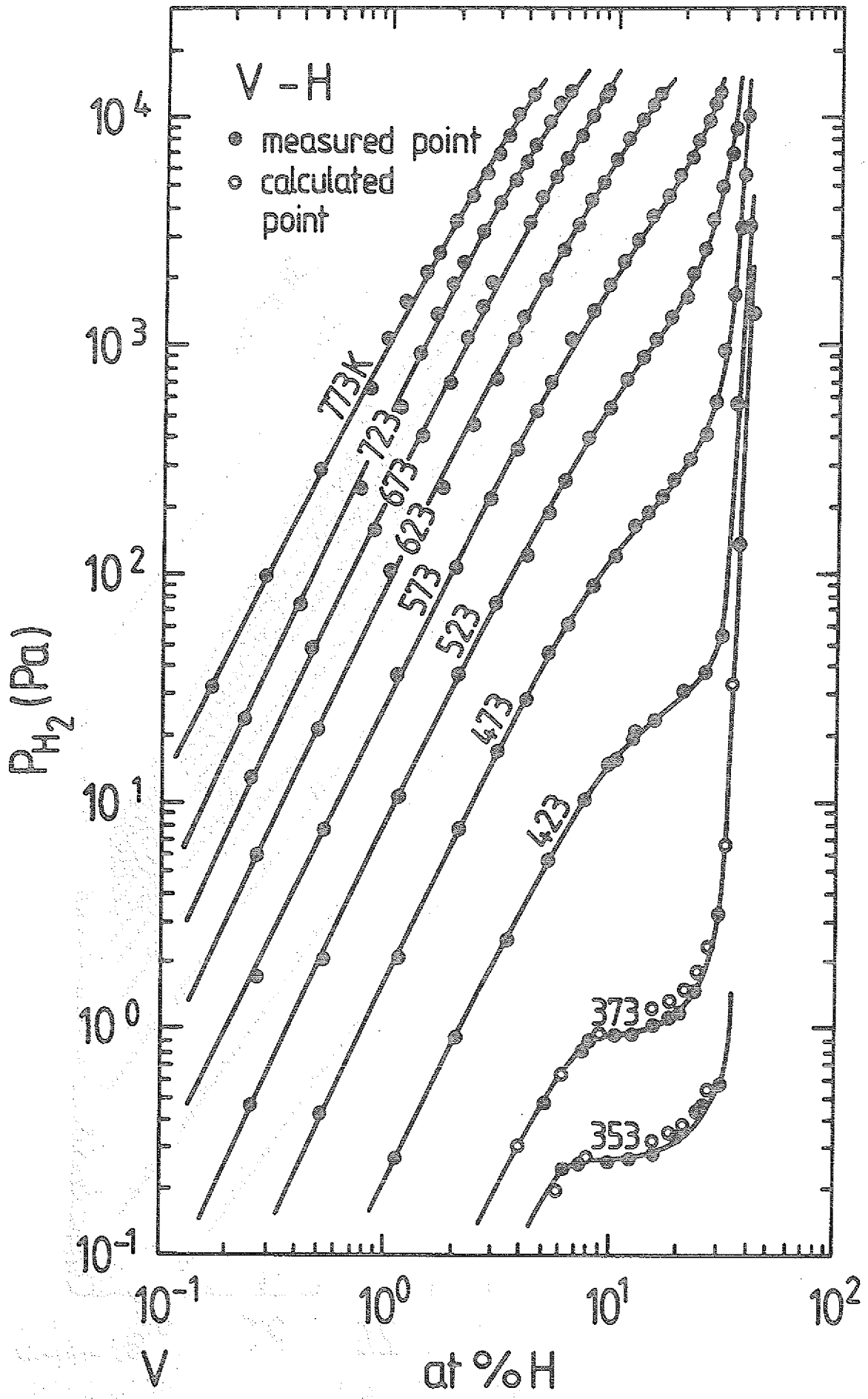

Fig. 43. p-c-T-curves for H in V [50].

(a)log p vs. at.%,

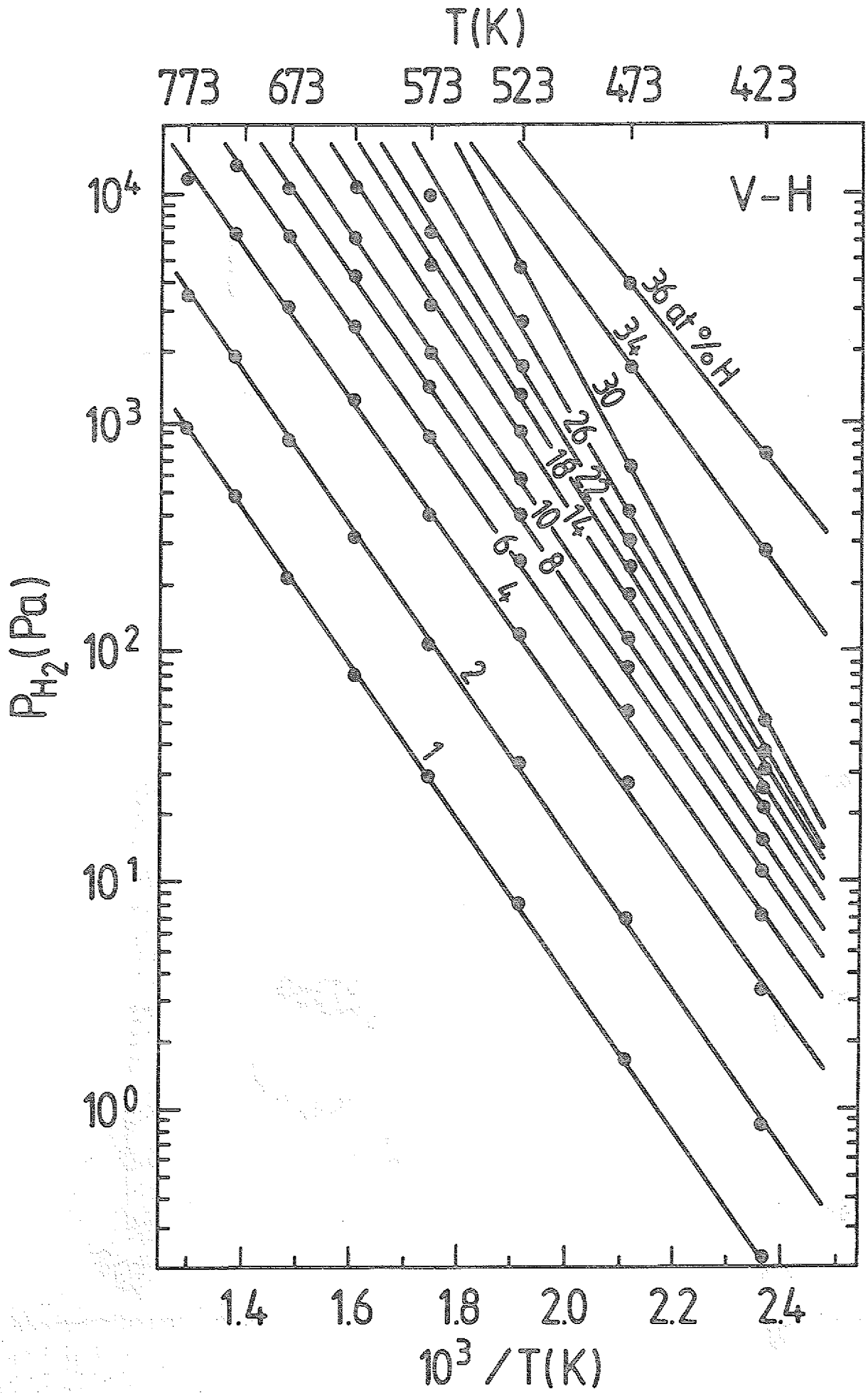

Fig. 43 (b) log p versus 1/T.

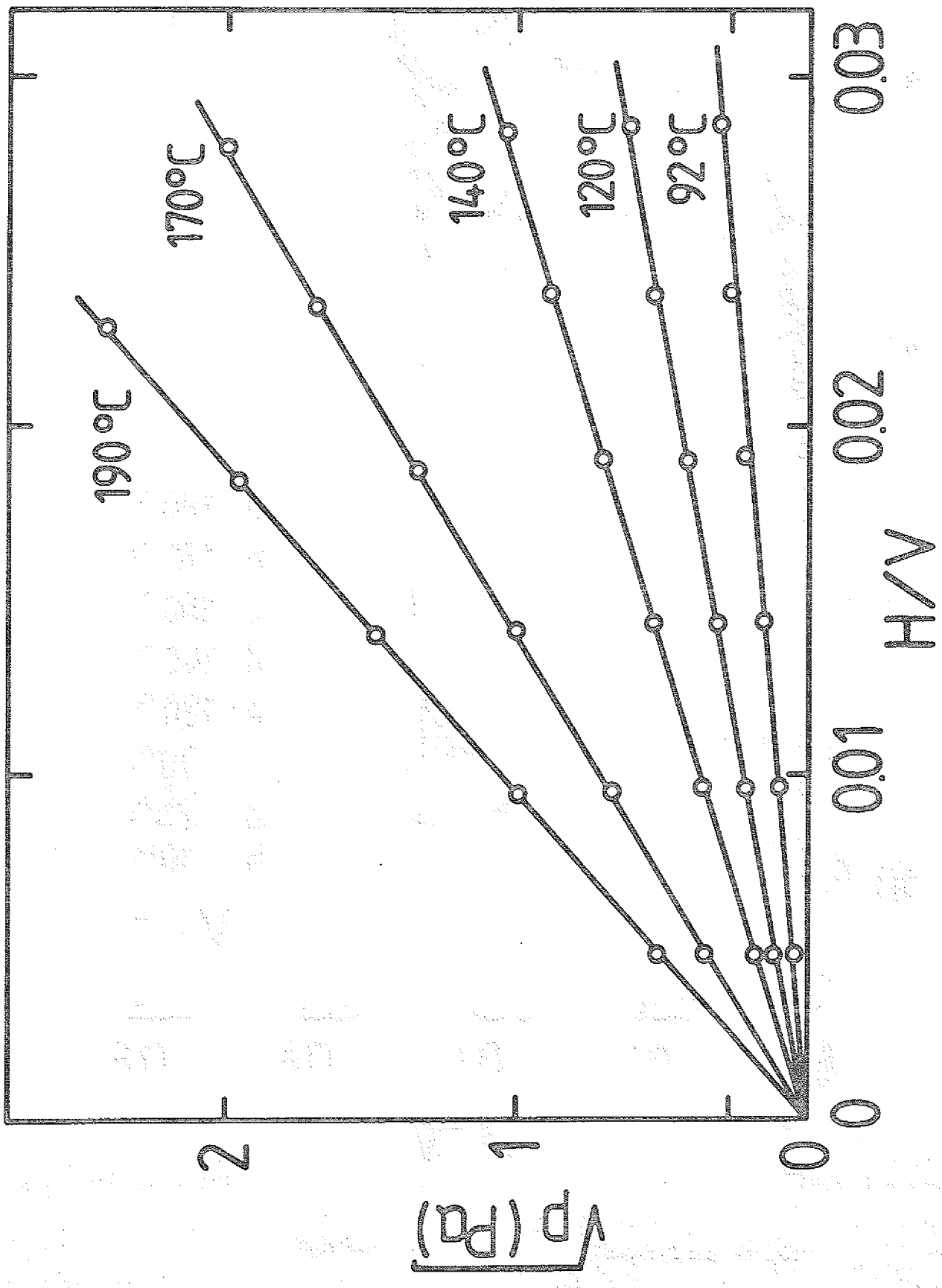

Fig. 44. Sieverts curves for H in V [103].

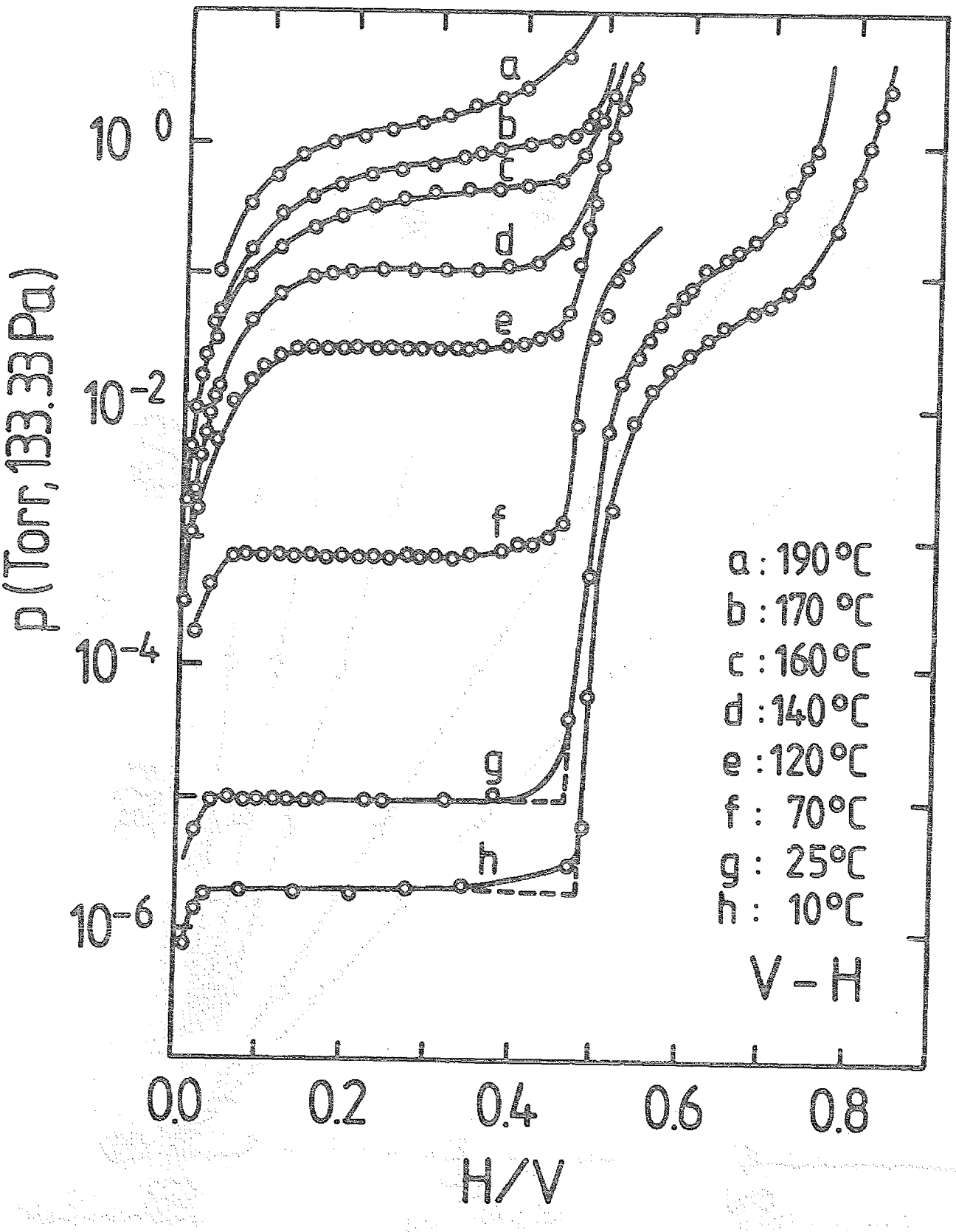

Fig. 45. p-c-T-curves for the $(\alpha+\beta)$-phase region [103].

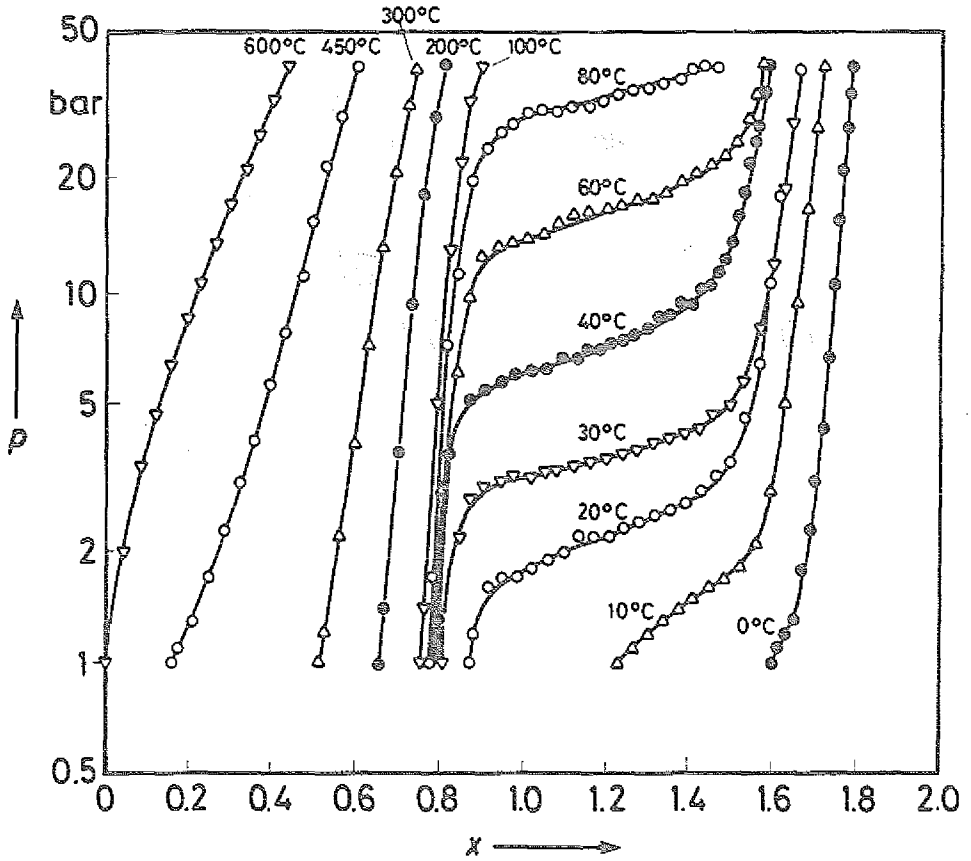

Fig. 46. p-c-T-curves for the VH – VH_2-equilibrium [104].

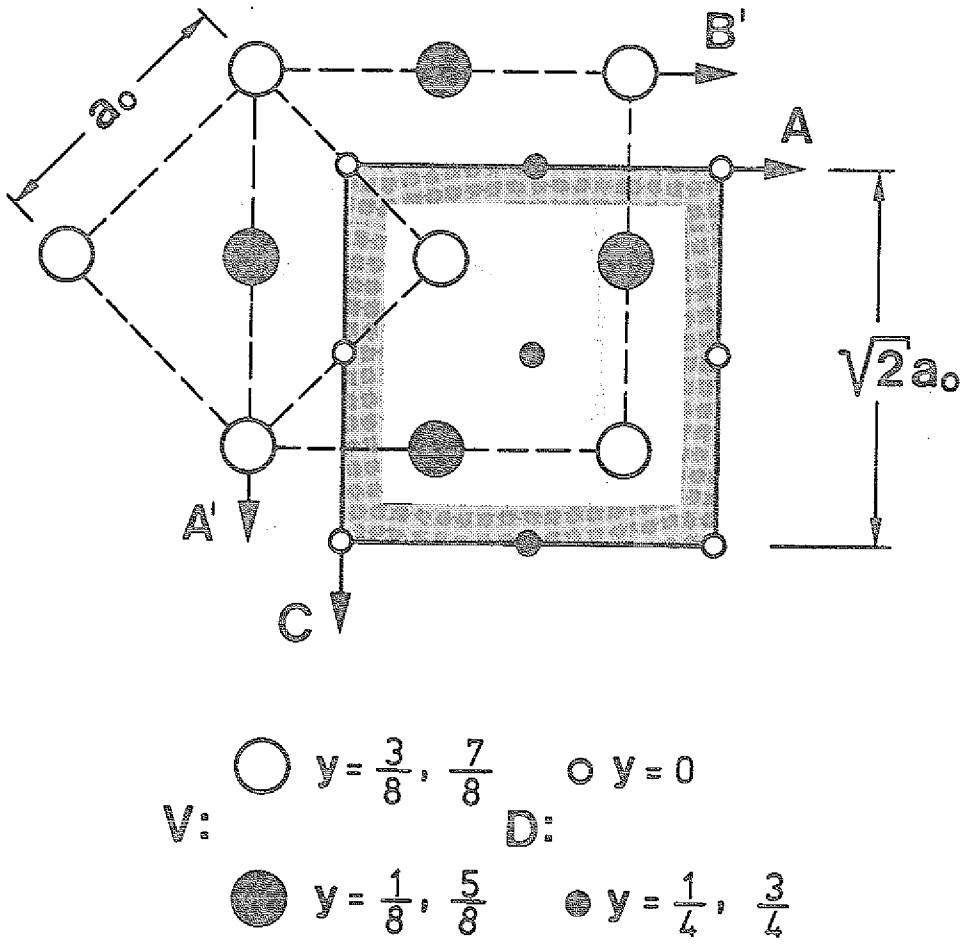

Fig. 47. The structure of γ-VD [115, 116].

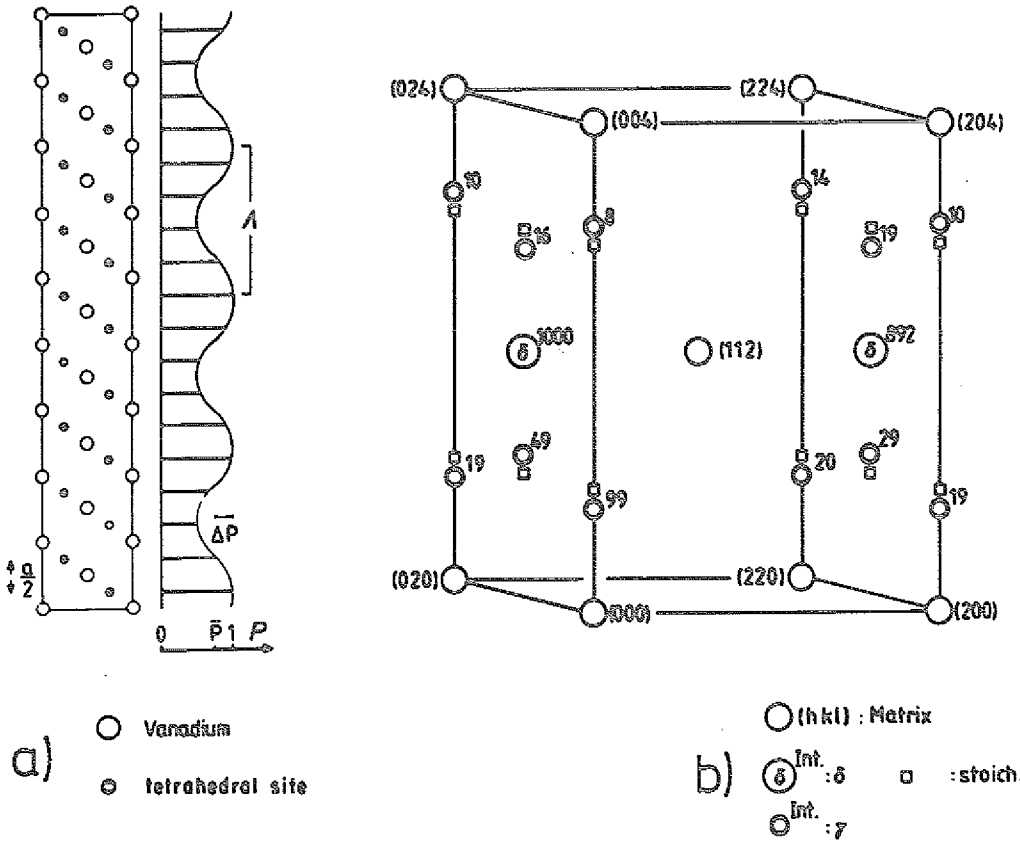

Fig. 48. Incommensurate density modulations in hypostoichiometric γ-VD .

(a) sinusoidal deuterium density modulation. The indicated tetrahedral sites are occupied according to the sinusoidal distribution function P.

(b) calculated reciprocal lattice using model in (a). Excellent agreement with the experiment is obtained. Superlattice reflections are only observed at positions denoted by δ and γ.

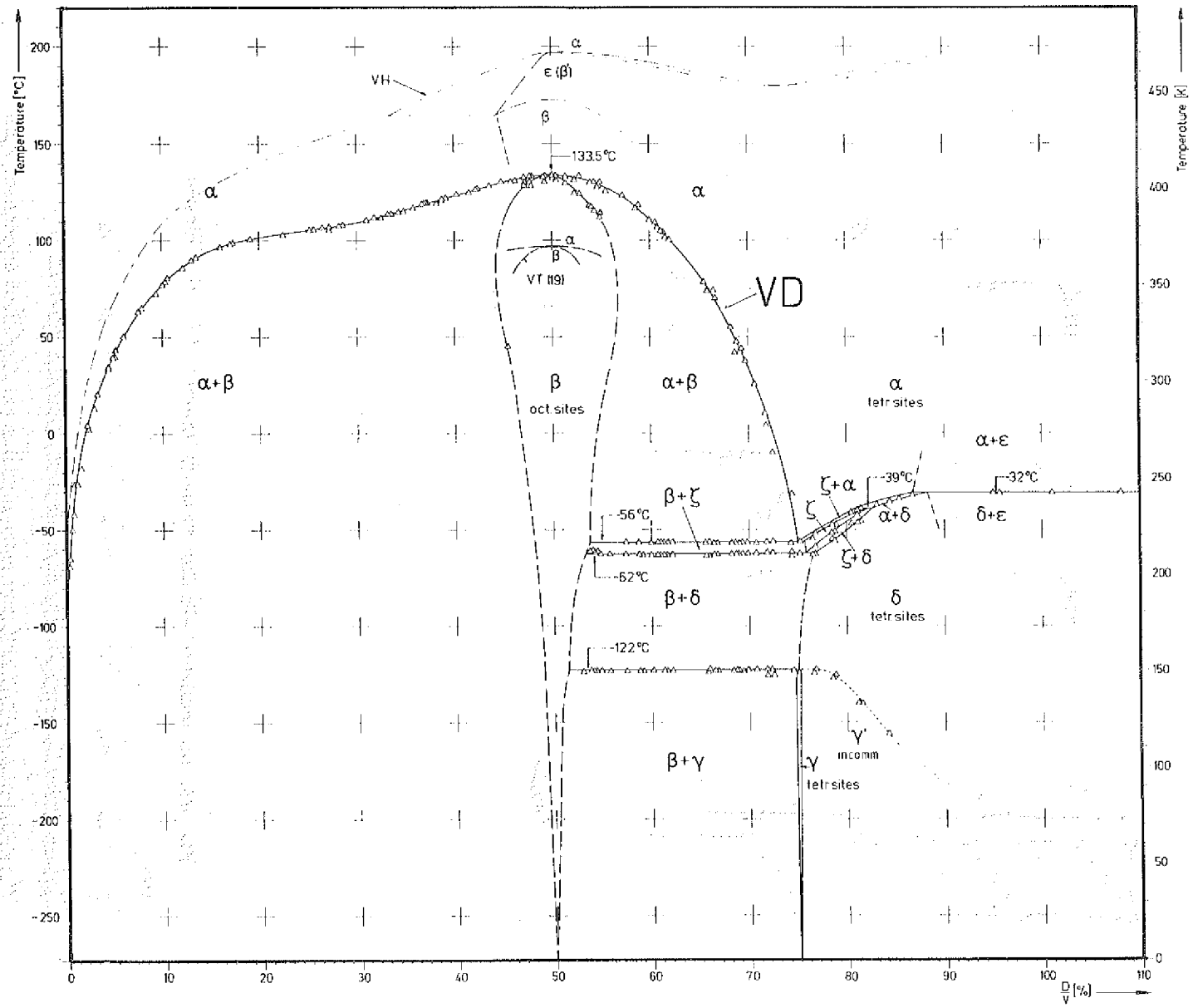

Fig. 49 . V-D phase diagram [4].

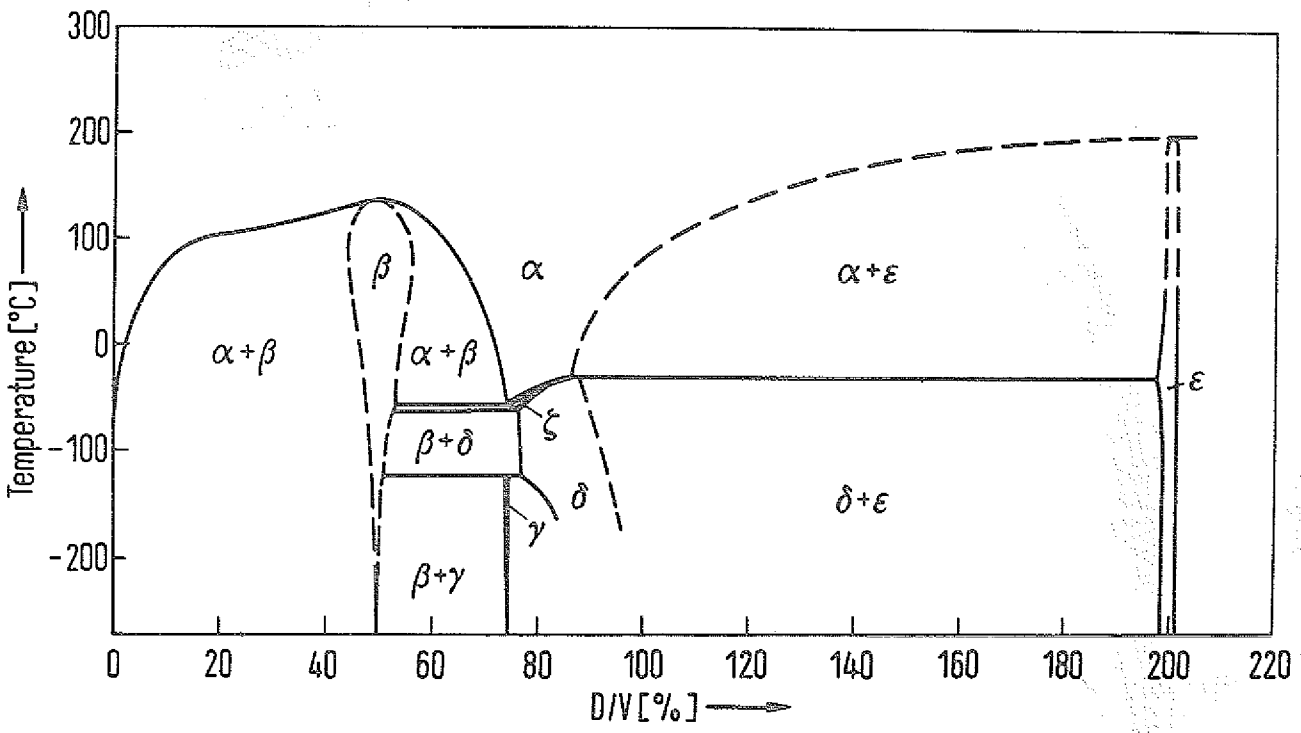

Fig. 50. Schematic, rather hypothetical phase diagram for D in V up to c=2.0 [97].

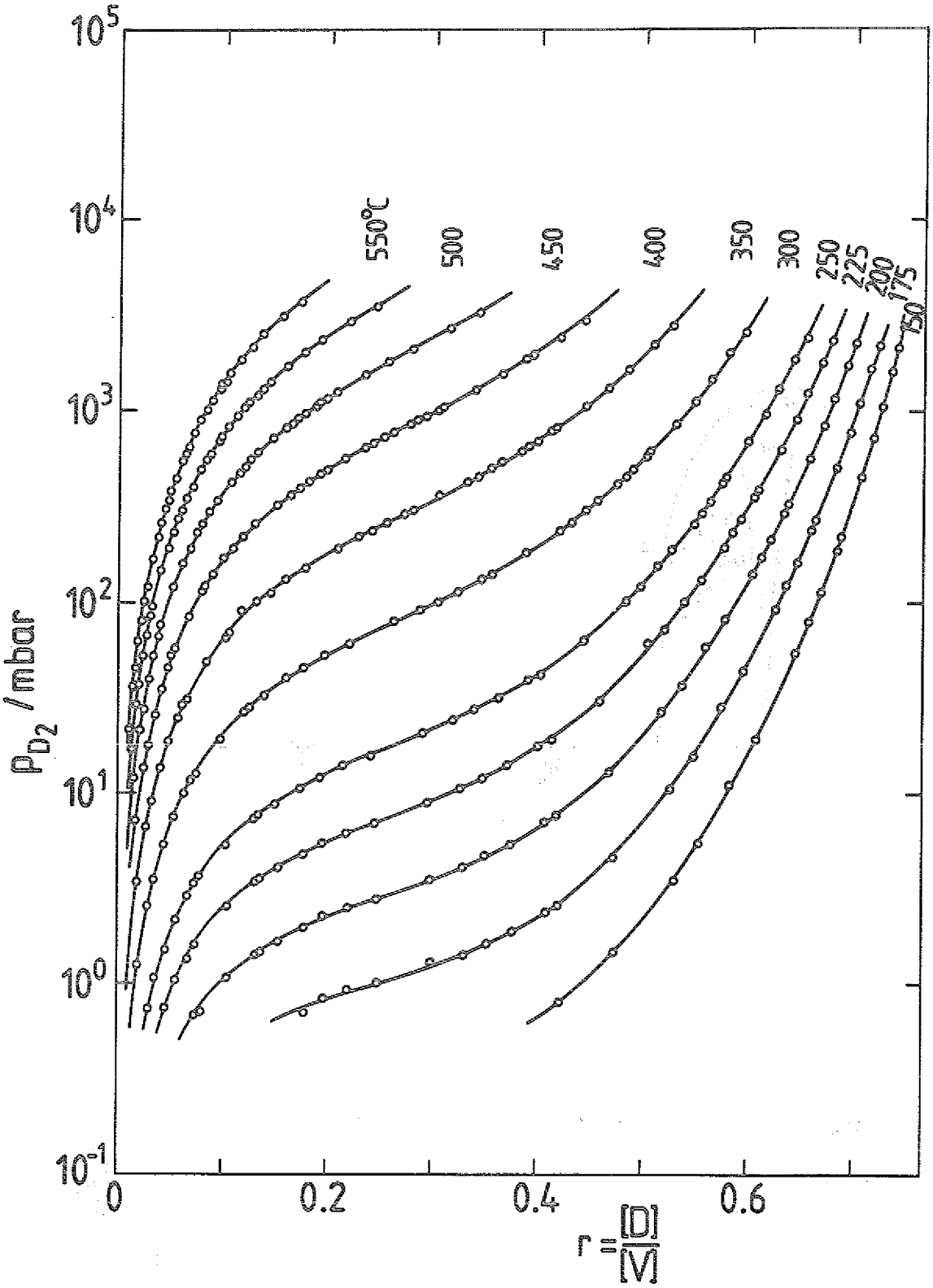

Fig. 51. p-c-T-data for deuterium in V

(a) Data by Meuffels [102]

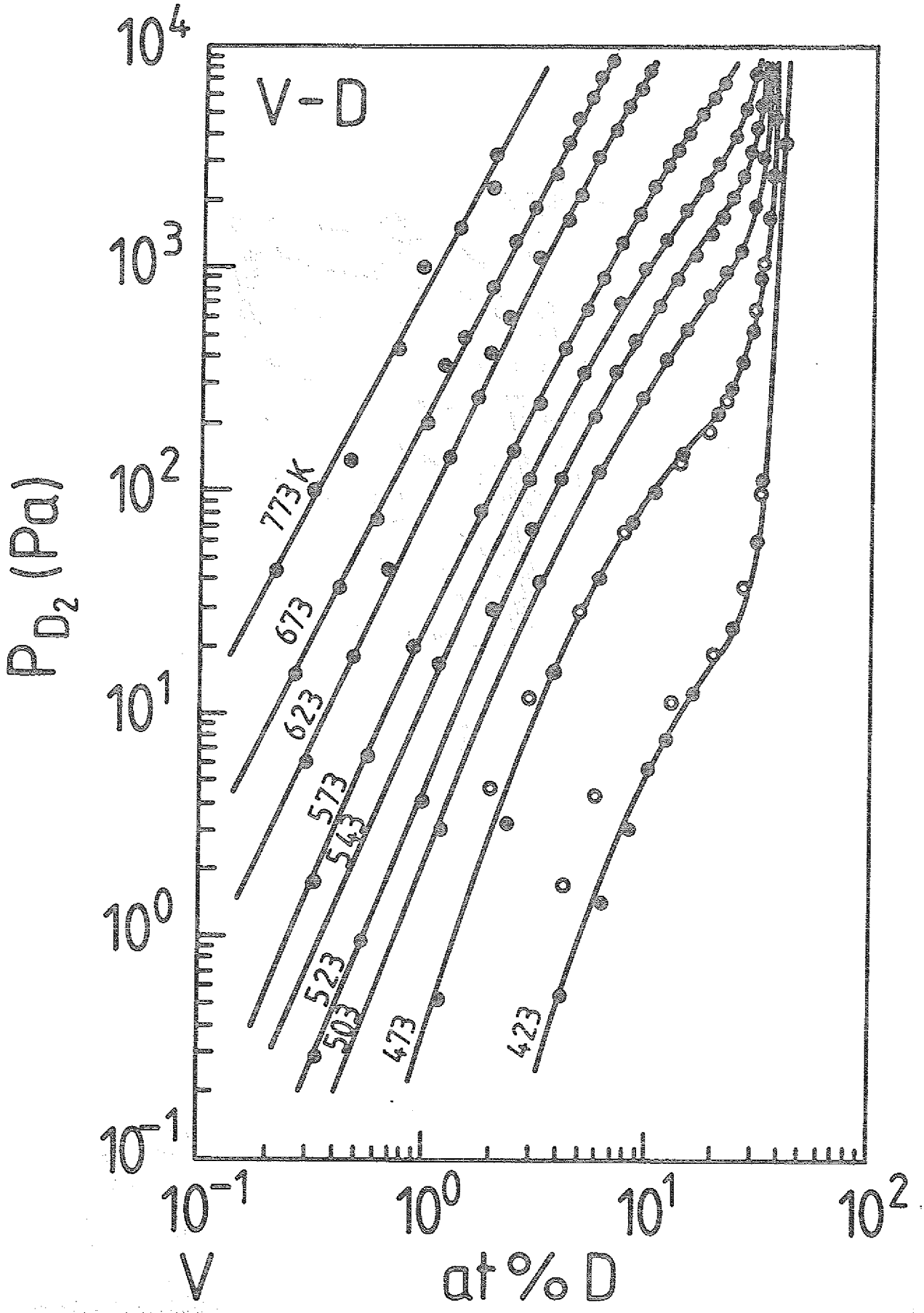

Fig. 51 (b) Data by Fujita et al. [50]

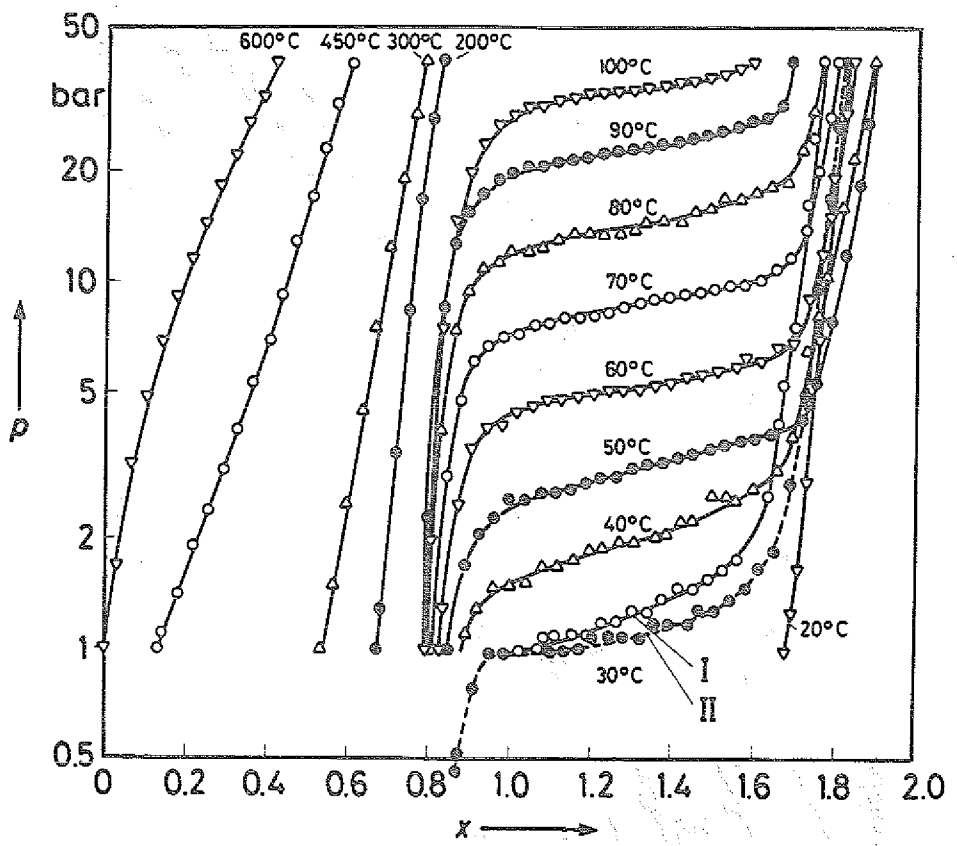

Fig. 52. The VD – VD_2 equilibrium: p-c-T data after Rummel [104].